HEAT TRANSFER AT TURN PORTION OF ROTATING MULTI-PASS INTERNAL COOLING CHANNELS OF GAS TURBINE BLADES

A Dissertation

by

HAO-WEI WU

Submitted to the Office of Graduate and Professional Studies of
Texas A&M University
in partial fulfillment of the requirements for the degree of

DOCTOR OF PHILOSOPHY

Chair of Committee,	Je-Chin Han
Committee Members,	David Staack
	Sy-Bor Wen
	Hamn-Ching Chen
Head of Department,	Andreas A. Polycarpou

December 2015

Major Subject: Mechanical Engineering

ABSTRACT

Three test sections are investigated in the study. One is a three-passage channel with hub turn, another is two-passage channel with tip turn, and the other is a four-passage serpentine channel. The test section with hub turn is a three-passage internal cooling channel with a 180° U-bend at the hub turn portion. The flow is radially inward at the second passage, while it is radially outward at the third passage after the U-bend. Measurement was conducted at the second and the third passages. Aspect ratio of the second passage is 2:1 (AR=2:1), and the third passage is wedge-shaped with side wall slot ejections. Study of heat transfer begins with smooth channel surface. Roughened surface with rib turbulators and pin-fin array is also tested. Tests are conducted for both cases of with and without turning vane at the turn portion. Range of Reynolds numbers is from 10,000 to 40,000, and the corresponding rotation number is from 0 to 0.32.

The test section with tip turn is a two-passage rectangular channel with aspect ratio of 2:1, and two 90° sharp turn at tip. Tests are only conducted with roughened surface. Straight ribs are placed on leading and trailing surfaces of both passages with P/e = 8, e/D_h = 0.1, α = 45°. Ribs are in staggered arrangement between leading and trailing surfaces. With and without vane conditions are both studied. Range of rotation number studied is from 0 to 0.42

The serpentine channel has geometry more close to real engine blades. The aspect ratio of each passage is increasing from leading edge to trailing, while the orientation angle of passage is decreasing. Broken ribs are attached to the leading and trailing

surface of the channel and heat transfer is studied. Heat transfer data is compared with previous geometry of straight ribs on the same test section. Rotation numbers studied are 0 and 0.23.

Nu/Nus to rotation number correlation is found on every surface for all geometries of all three test sections. Rotation effect on leading and trailing surfaces is different depending on the flow direction, which is consistent with previous studies. Heat transfer enhancement at tip turn and hub turn are reported. The effect of turning vane is also shown.

DEDICATION

To my family, especially my parents and my wife, for their endless and unconditional love, support, and encouragement.

ACKNOWLEDGEMENTS

I would like to express my appreciation to my academic advisor, Dr. Je-Chin Han, for giving me the opportunity to work and learn with him in the area of gas turbine blade cooling. He guided me with his valuable experience and knowledge in this area through my whole academic life. I would also like to thank Dr. David Staack, Dr. Sy-Bor Wen, and Dr. Hamn-Ching Chen for their time and support serving as my committee members, and giving me suggestions on my research and dissertation. I also appreciate all the company and encouragement from my labmates who always gave me helpful advice and solutions.

I would also like to appreciate the sponsorship from Solar Turbines Inc. on the project of internal cooling channel with hub turn and trailing edge ejections. Thanks to Dr. Moon and Dr. Zhang for their support and advises.

Last but not the least, I would like to thank Siemens for the sponsorship on the rotating serpentine channel. Thanks to Dr. Lee and Dr. Azad for their help on the project.

NOMENCLATURE

A	projected surface area of a copper plate segment
A_j	cross sectional area of the slot
AR	channel aspect ratio, W:H
Bo_x	local buoyancy parameter, $(\Delta\rho/\rho)_x Ro^2 (R_x/D_h)$
C_D	discharge coefficient
D_h	channel hydraulic diameter
e	rib height
f	friction factor
f_o	fully-developed friction factor in non-rotating, smooth pipe
H	channel height
h	regionally averaged heat transfer coefficient
k	thermal conductivity of the coolant
L	length of the heated portion of the test section
L_e	length of the unheated portion of the inlet part
$\dot{m}_j$	mass flow rate through the j^{th} slot
$\dot{m}_n$	mass flow rate radially at the exit of the n^{th} region
$\dot{m}_{xn}$	local mass flow rate at the n^{th} region
Nu	regionally averaged Nusselt number

Nu_o	Nusselt number for fully-developed turbulent flow in non-rotating smooth pipe
Nu_s	regionally averaged Nusselt number under stationary condition
P	rib spacing
P_i	pressure at the inlet of the test section
P_o	pressure at the outlet of the test section
P_{in}	pressure at the inlet of the slot
P_{exit}	pressure at the exit of the slot
Pr	Prandtl number of the coolant
Q_{net}	net heat transfer
Q_{loss}	external heat loss
R	mean radius of rotation (from the center of rotation to center of heated channel)
R_x	local radius of rotation (from the center of rotation to local region within heated channel)
Re_x	local Reynolds number
Re_i	Reynolds number at the inlet of the test section
Ro_i	inlet Rotation number, $\Omega D_h/V_i$
Ro_x	local Rotation number, $\Omega D_h/V_x$
Ro	Rotation number, $\Omega D_h/V$
$T_{w,x}$	regionally averaged wall temperature

$T_{b,x}$	local coolant bulk temperature
$T_{f,x}$	local film temperature
V	bulk velocity of the coolant in the streamwise direction
V_i	bulk velocity of the coolant at the inlet of the test section
V_x	bulk velocity of the coolant at the local region
W	channel width
β	angle of channel orientation with respect to the axis of rotation
	viscosity of the coolant
ρ	density of the coolant
ρ_{in}	inlet coolant-to-wall density ratio, $(T_w-T_{bi})/T_w$
ρ_x	local coolant-to-wall density ratio, $(T_w-T_{bx})/T_w$
	rotational speed

TABLE OF CONTENTS

Page

LIST OF FIGURES

Page

1. INTRODUCTION

Gas turbines are widely used in the world today. Reaching higher turbine efficiency has pushed designers to increase the inlet temperature of the gas turbines. Higher inlet temperatures and the resultant higher thermal loadings require novice cooling technologies to keep the turbine blades from the possible failure under extremely hot mainstream air.

A diversity of internal cooling techniques were studied and summarized by Han et al. [1]. The internal cooling enhancement technique applied to the channel would be varied according to its' location in the blade, since channels at different zones will have different aspect ratios (AR), and encounter with different thermal loadings. The aspect ratio is defined as the ratio of the channel width (W) to the channel height (H) (AR=W/H). Typically, at the blade trailing edge, AR=4:1 is often used for the modeling, as seen in Figure 1.

1.1 Rotation Effect

Rotation number (Ro), which is described as the ratio of the Coriolis force to flow inertia force, is presented when evaluating the effect of rotation. Rotation has great effect on heat transfer, and thus many researchers devoted themselves to study the rotation effect, such as Wagner et al. [2, 3], and Han et al. [4]. Valued data of rotation effect on heat transfer enhancement in smooth channels under rotating condition were provided. Effects on leading surface and trailing surface with both radially inward and outward flow were also shown. Taslim et al. [5] investigated heat transfer of rib-roughened walls

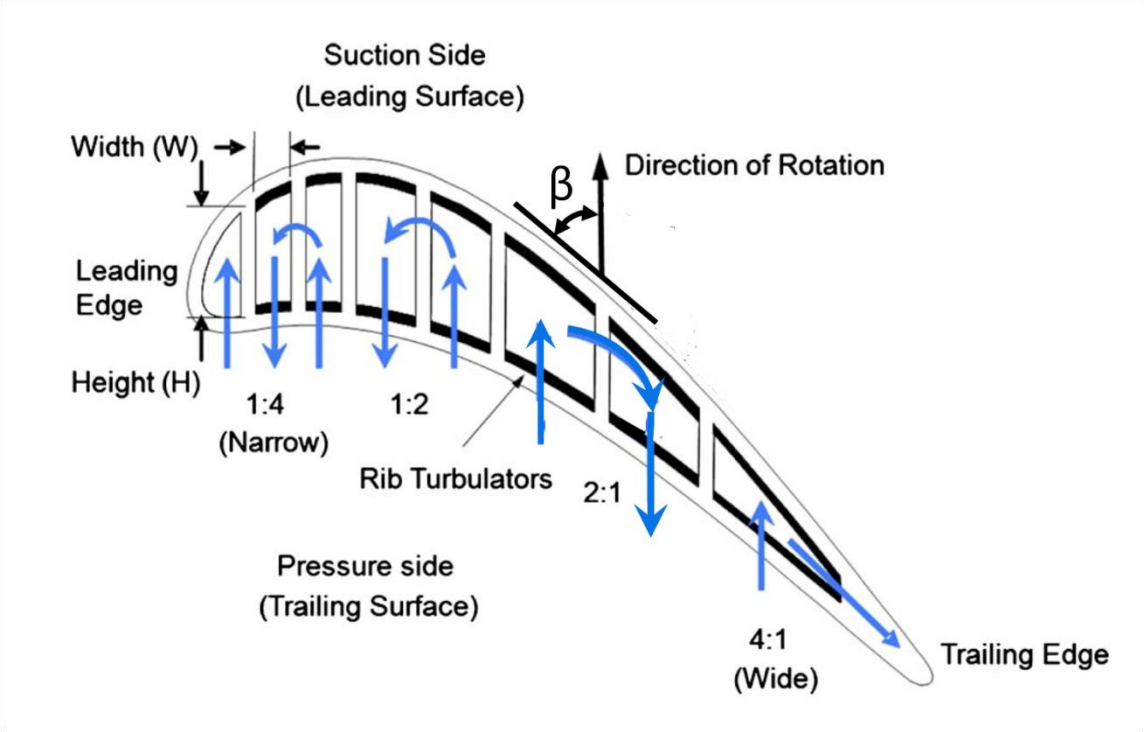

Figure 1 The various aspect ratios of gas turbine blade internal cooling channels

with radially outward flow under rotating condition using liquid crystal technique. Dutta et al. [6] conducted CFD simulations to study the heat transfer on both leading and trailing surfaces of a rotating square channel with radially outward flow. Generally, it could be concluded from previous studies that, heat transfer is greatly affected by rotation. For radially inward flow, heat transfer is enhanced at leading surface, and decreased at trailing surface; for radially outward flow, heat transfer is decreased at leading surface, and enhanced at trailing surface. Recent work including Lei et al. [7,8], Rallabandi et al. [9] also have good agreement on the rotating effect with previous studies.

1.2 Channel Orientation Effect

Figure 1 shows the rotation direction and the corresponding channel orientation angle (β). For consistency, the orientation is based on the first passage only in this study. Due to the blade shape and the channel location, the leading and the trailing surfaces of the internal cooling channel can not always be perpendicular to the direction of rotation ($\beta = 90^{o}$). From Parsons et al. [10] and Johnson et al. [11], it is concluded that the channel orientation angle has significant impacts on the heat transfer coefficient at leading or trailing surface. The difference of heat transfer between leading and trailing surface caused by rotation could be larger with a channel orientation angle at 90^{o} in comparison to 135^{o} Case. In recent years, Huh et al. [12] investigated channel orientation effect in a two-pass smooth and ribbed rectangular channel with $\beta = 90^{o}$ and 135^{o}. Qiu et al. [13] studied β angle effect on smooth surface of a wedge-shaped channel with lateral ejection with $\beta = 90^{o}$ to 180^{o}. Li et al. [14] investigated channel orientation effect in rotating smooth square U-duct with $\beta = 45^{o}$ to 135^{o}. Moreover, in a numerical study conducted by Srinvasan et al. [15] in a rotating smooth wedge-shaped cooling channel ($\beta = 90^{o}$ to 180^{o}), it was confirmed that heat transfer difference between leading and trailing surfaces due to the rotation can be deducted by changing the channel orientation angel compared to reference case($\beta = 90^{o}$).

1.3 Turn Effect

Turning portions are inevitable if there is more than one flow passage. However, flow behavior will be complicated after passing through the turning portion. Depending

on the geometry of the turn, there may be separation, recirculation or turn-induced secondary flow produced at the turn. Changes in flow behavior results in change in heat transfer behavior. More studies were found under stationary condition. Results from Han et al. [16] showed that an 180^o sharp turn can greatly enhance the heat transfer at the area around the turn for both smooth and ribbed cannels. Schabacker et al. [17] and Son et al. [18] studied flow behaviors at ribbed channels with an 180^o sharp turn using PIV technique. Complicated flow behaviors such as the dominating phenomenon of rib induced effects after the turn were observed. It was concluded that the characteristics of secondary flows plays a key role on the heat transfer enhancements for both smooth and ribbed channels. Saha et al. [19] investigated heat transfer at turning portion in a smooth channel with three kinds of turn geometries under stationary condition, and the result is compared with numerical simulation. Flow behavior was also carried out with CFD. By reducing the turn-induced flow with modified turn shapes, the pressure drop through the turn can be reduced. With certain shape of turn, the pressure drop can be reduced without decreasing heat transfer coefficient.

1.4 Turning Vane Effect

Due to the complexities of the turn-induced secondary flow at the turn portion, as well as the separation and recirculation of mainstream, large pressure loss may occur after flow passing through the turn and entering the following passage. In order to reduce the pressure drop and smooth out the turn effects, turning vanes are used. Several researchers devoted themselves into the studies of the turning vane effects. Luo and

Razinsky [20] performed a numerical study on turning vane effect for smooth surface with 180^o turns. Schüler et al. [21] studied turning vane effect on pressure loss and heat transfer of a ribbed channel. Many key factors of the turning vane effects including shape of the turn, as well as location, dimension, and the shape of the turning vane were studied in previous works. Reductions of pressure loss and flow separation were reported, and the amount of this reduction was correlated in regards to the key factors stated above (Ref. [20, 21]). Lei et al. [7, 8] conducted an investigation on heat transfer at hub turn portion with a channel that had an upstream and downstream rectangular passage (AR=2:1) connected by an 180^o U bend under rotating condition. It was concluded that, in the turn portion, presence of turning vane reduced the heat transfer enhancement due to rotation. Chu et al. [22] performed a numerical simulation of flow and heat transfer in a rotating channel with turning vane in hub portion. Reduction on pressure drop at turn portion with presence of turning vane is observed. It is also concluded that the changes of heat transfer due to rotation at turn portion and after-turn area is decreased by the presence of turning vane.

1.5 Effect of Pin-fins

Pin-fins are often used in channels close to the trailing edge of a blade. An array of pin-fins is preferred rather than just a single one. By increasing the total area and inducing turbulence, pin-fins result in heat transfer enhancement. Also, their arrangement is an important element for optimizing the heat transfer enhancement. Chyu et al. [23] reported the staggered arrangement generated a more turbulent flow field, and

its overall heat transfer and pressure drop increased in comparison to the in-line arrangement. Rallabandi et al. [24] investigated heat transfer in a wedge-shaped pin-fin channel with slot ejection under rotating condition. Full conduction pin-fins array was studied, as well as partial conducting pin-fins. Heat transfer coefficients at different regions of channel were reported. Full conduction pin-fin array was shown to have better overall heat transfer coefficient. Krueckels et al. [25] studied pin-fin array in a trailing edge passage using transient liquid crystal technique, and the results were compared with numerical simulation. Different shapes of pin-fin and array geometries were investigated in the study.

1.6 Slot Ejection at Trailing Edge

Limited by the geometry of a turbine blade, and the concerns of cooling strategies, there are often ejections at the trailing edge of a turbine blade. To provide more protection for the blade, the coolant at the trailing edge is extracted from the passage either through discrete holes or through slots. Taslim et al. [26] investigated heat transfer of a trapezoidal (wedge-shaped) channel with trailing-edge ejection. The results suggested that the average heat transfer coefficients were consistent with the Dittus–Boelter correlation in a smooth, wedge-shaped channel. This finding was further confirmed by Hwang and Lu [27]. Besides, it was also concluded that an increase in the ejection rate has the benefit of increasing the heat transfer coefficients on the narrow side of the channel, while paying the cost of reducing the heat transfer coefficients on the wide side of the channel. Liu et al. [28] performed a study on heat transfer in trailing

edge channel with tapered ribs and slot ejection under rotating conditions. It is concluded that local heat transfer coefficient is higher in narrow region due to slot ejection. Heat transfer decreased at wide region due to reduced slot ejection effect. Tapered ribs enhanced heat transfer at ribbed surface, but still lower than the region with ejection. Also from [28], it is reported that rotation does not have significant effect on pressure drop through ejection slots.

1.7 Entrance Effect

Due to the limitation on geometry of the turbine blade, the coolant may not always travel through a constant cross-section channel. Entrance effect on heat transfer was therefore studied. In Wright et al. [29], it was concluded that the entrance effect is significant even with ribbed surface. The heat transfer is higher with a sudden and partial contraction entrance than that with a fully developed entrance, and the influence starting from the entrance to 4 hydraulic diameter of the channel [29].

1.8 Objectives

Due to lack of information, and frequently thermal damage at hub turn portion in real industrial applications been reported, study of heat transfer at turn portion under high rotation number condition is necessary. The purpose of this study is to fill up the gap of knowledge at this area. Heat transfer at tip turn is very different from that at hub turn. Thus tip turn test section is also included in the study. The aspect ratio of the rectangular tip turn passages is the same with that of the second passage of hub turn

channel. The configuration of pin-fin array and slot ejection is an industrial application of Solar Turbines Incorporated. Detailed study and documentation with similar configurations are valued for future application reference. Most of the open literature focusing on heat transfer in turning region was performed in non-rotating condition. A very small number of studies have been in rotating conditions and their attention has often been on the tip turn region. Therefore, limited researches have been conducted to discuss the heat transfer characteristics of the hub turn portion, up to now. Moreover, the combination of the aforementioned considerations with a wedge-shaped channel, pin-fin arrays, and slot ejections at the trailing edge, and also with a multi-passage ribbed roughened channel has never been seen before in the literature. Therefore, this study investigates heat transfer in the hub turn portion , as well as in the tip turn portion, along with ribs and pin-fin arrays and slot ejections for both with and without turning vane scenarios. Rotation number varies from 0 to 0.32 for the hub turn channel, and 0 to 0.42 for the tip turn channel.

Further study on the four-passage serpentine channel with tip and hub turn is to continue on improvement of heat transfer, and also on development of optimal turbulator configuration along the passage. The rotation numbers studied are 0 and 0.23 for the serpentine channel.

The objectives of the current study are to:

1. Investigate the effect on heat transfer at all walls of the passage, and turn portion with smooth channel surface under both stationary and rotating conditions.
2. Investigate the effect on heat transfer at all walls of the passage, and turn portion

with roughened channel surface under both stationary and rotating conditions.

3. Study the effect of the turning vane on heat transfer at all walls of turn region in both stationary and rotating conditions.
4. Compare two channel orientation angles for the effect of the channel orientation angle on heat transfer at all surfaces of the turn region, as well as the passages of the roughened channel in rotation condition.
5. Determine the effect of rotation number on heat transfer at all surfaces of the turn region as well as the passages.

2. HUB TURN CHANNEL*

2.1 Experimental Setup

2.1.1 Rotating Facility

Study of the heat transfer in a rotating cooling channel with hub turn is performed in a rotating facility as shown in **Figure 2 [28]**. An electric motor controlled by a frequency controller is used to drive the shaft. The rotational speed goes from 0 – 400 rpm. A 100 channel slip-ring serves as an interface to transfer the signals from the rotating test section to the data acquisition system. Distance from the axis of rotation to the center of test section is approximately 65 cm. The compressed coolant air coming from compressor first goes through a regulator, which provides the air loop a constant upstream pressure. Following the regulator is an orifice meter with 2 in outer pipe, and a 1 in orifice plate. An incline manometer is used to measure the pressure difference through the orifice meter. After the orifice meter, air goes into the bottom of the rig through the rotary union and then into the hollow shaft. After travelling through the hub, the air then goes into a rubber hose that connect to the air inlet of test section, which is inside the pressure vessel. Air is heated when passes through the heated test section. Another rubber hose is connected to the outside of the base plate of pressure vessel as a flow exit. The other end of the exit rubber hose is a copper tubing that goes in the

*Reprinted with permission from "Heat Transfer in a Rib and Pin Roughened Rotating Multi-Pass Channel with Hub Turning Vane and Trailing-Edge Slot Ejection" by H. W. Wu, H. Zirakzadeh, J. C. Han, L. Zhang, and H. K. Moon, 2015. ASME Turbo Expo 2015: Turbine Technical Conference and Exposition, Volume 5: Heat Transfer, Paper No. GT2015-42418, pp. V05AT11A007; 14 pages, Copyright 2015 by ASME.

rotating shaft under the slip ring. The copper tubing goes straight up to the top of the shaft and connects to the second rotary union at the top of the shaft. A needle valve is attached to the pipe after the top rotary union to adjust the back pressure of the flow loop. Flow rates are controlled by adjusting the back pressure and the corresponding pressure difference through orifice meter while keeping the upstream pressure constant.The typical rotation numbers for the aircraft engine are in the range of 0 to 0.25. In the laboratory environment, rotating speed is low comparing to the air craft engines. One way to achieve the desired range of rotation numbers with the applicable Reynolds numbers is to run the inlet air at higher pressures. With the coolant air pressurized, the density increases while the velocity decreases at a given mass flow rate (Reynolds number). Decreasing in velocity results in increasing in rotation numbers. In the current study, the air is pressurized about 5 times of the atmospheric pressure. Highest rotation number reached is 0.42.

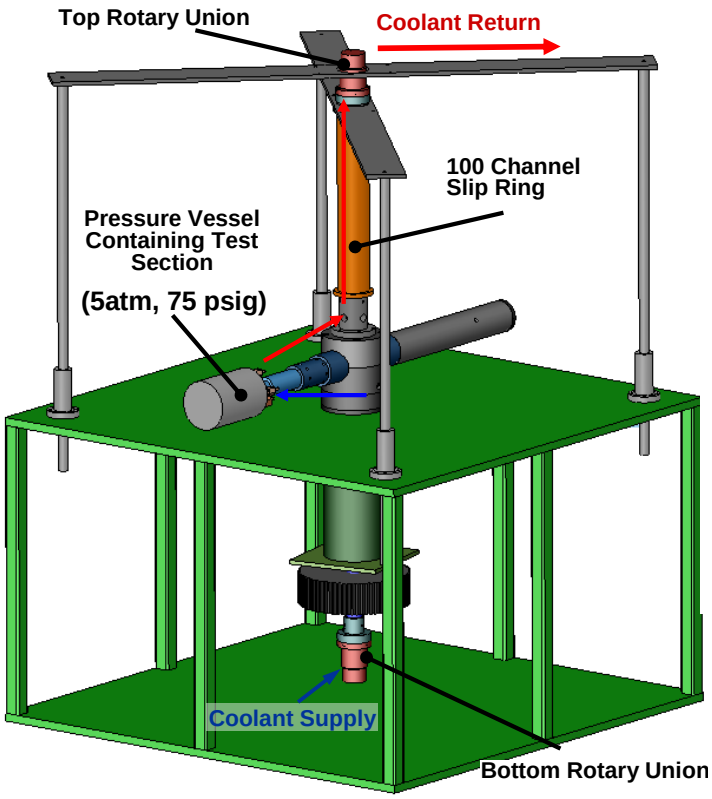

Figure 2 Rotating Facility for hub turn channel [28]

2.2 Test Section Geometry

2.2.1 Smooth Surface

The geometry of the three-pass channel with a 180^o U bend in the hub portion and slot ejection is shown in **Figure 3 & 4**. First passage was square and served as flow inlet. It was not heated during tests. Second and third passages were connected by an 180^o U-bend hub turn. Aspect ratio of the second passage is 2:1 (AR = 2:1). Half way through the turn, the cross section area of the channel gradually starts to change so that at the entrance of the third passage, it becomes wedge-shaped with a narrow outer wall, as shown in **Figure 3 (b)**. There are totally eight slots for ejection on the side wall. Each slot has a rectangular shape with half circle edges at the short sides. Dimensions of slots are 1.8 mm in height, and 8.5 mm in width. The radius of the half circle at the short sides of slots is 0.75 mm. As shown in **Figure 3 (a)**, air passes through the pressure vessel and the rubber hose and then expands into the squared cross-section of the first passage.

After the 180^o sharp turn at the end of the first passage, flow goes into the second passage which has 2:1 aspect ratio, and becomes radially inward. Next, flow passes through the hub turn portion, where the passage gradually becomes wedge-shaped, and then enters the wedge-shaped third passage in a radially outward direction. The flow later ejects out of the test section through slots at the side wall of the third passage. The experimental heated surfaces, including leading surface, trailing surface, inner divider walls and side walls are placed in the second and the third passages. Surfaces at the hub turn region were also heated. Dimensions of the second and the third passages are shown in **Figure 4**. The height of the second passage is 12.70 mm and the width is 25.66 mm.

The height of the inner wall and the side wall of the third passage is 11.74 mm and 5.69 mm, respectively. The body of test section was made of SLS PA nylon, which has a low thermal conductivity, and was used to support the copper plates and heaters. A strip of insulating silicon glue (k=0.15 W/mK) with 1.59 mm in length was applied between adjacent copper plates to prevent conduction among different regions, and also help create a smooth contact surface between them. Conduction effect between adjacent copper plates is small and negligible.

A prefabricated Kapton heater is placed at each surface beneath the copper plates to heat up the flow. As it is shown in **Figure 3 (b)**, in the second passage, a total of four heaters were used for inner divider wall, side wall, leading and trailing surfaces. Tip side wall is not heated. In the hub turn region, three heaters were applied on the surfaces i.e. hub wall, leading and trailing surfaces. In the third passage, only three heaters were used, since there were ejection slots on the side wall, and the tip is not heated. Therefore, only inner divider, leading and trailing surfaces were heated in this passage. All surfaces were heated to target wall temperature during tests. To reduce contact resistance between the heaters and the copper plates, thermal conductive paste (k=0.7 W/mK) was applied at the gap. The hydraulic diameter of the second passage (D_{h2}) was 16.9 mm. The distance between rotation axis and center of the test section (R) was 660.4 mm, and R /D_{h2}~39. Biot numbers of the copper plates were calculated. The largest Biot number in the study is less than 0.025. Lumped capacitance method is applied to determine the local wall temperature along the channel. Thus the passage can be divided into several regions

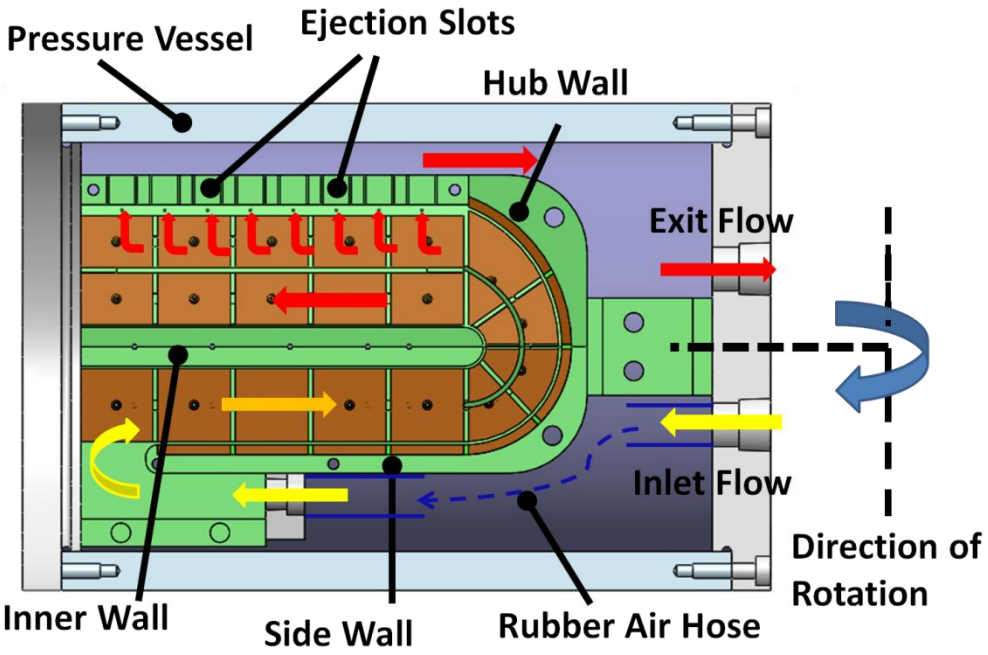

(a)

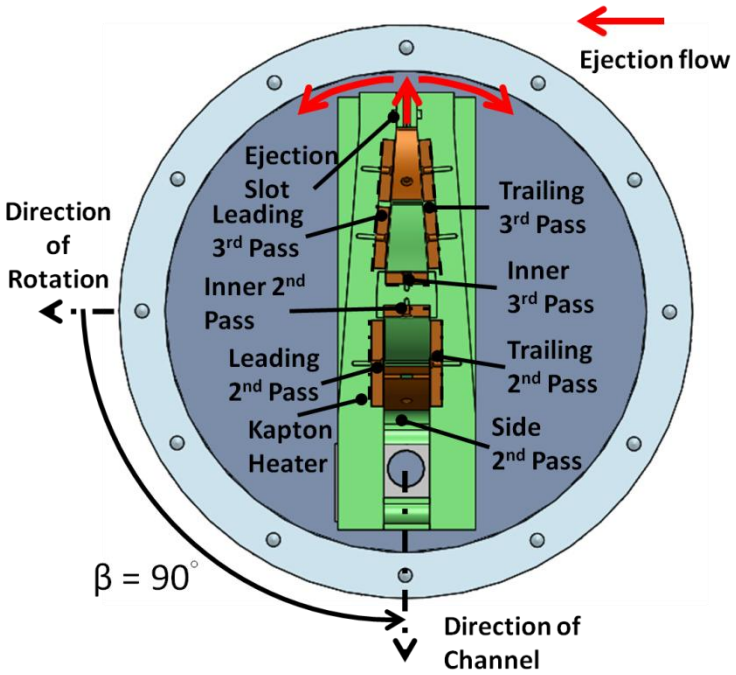

(b)

Figure 3 Schematic of test section inside pressure vessel (a) Side view (b) Axial view

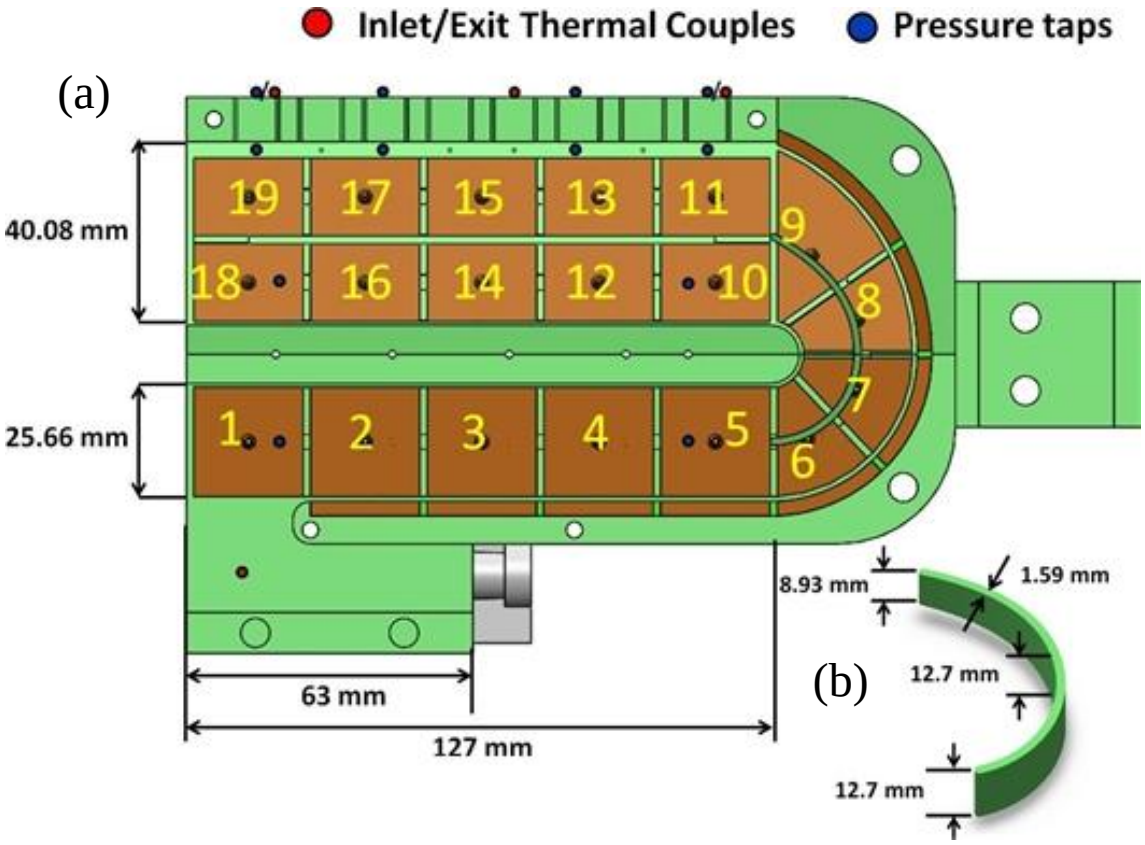

Figure 4 Dimensions of (a) Test section and the numbering sequence of regions, and (b) Turning Vane.

based on the copper plate covered area. Nineteen heated regions in total in the test section along streamwise direction are as shown in **Figure 4**. Each of the second and third passage is consisted of five regions, except for the side wall. Side wall in the second passage had four regions. For the hub turn portion, each surface was divided into four zones. The overall length for the second or third passage was 127.0 mm and for the unheated first passage was 62.0 mm. In the hub turn portion, the radius of divider wall in the second passage was 6.35 mm (Rin =0.25W) and hub wall radius in the second passage was equal to 35.24 mm (Rout=1.37W). The height of the turning vane was equal to the height of the passage. The thickness of turning vane was 1.59 mm. Shape of the turning vane in the second passage was a quarter-circle with the radius of 18.5 mm. For the later half of the turn portion, the shape of the turning vane at this side was constructed along the center line of the flow passage. Inlet temperature and ejection temperature were monitored by thermocouples.

The thickness of all copper plates was 3.175 mm. In the second passage, the copper plates on the leading and trailing surfaces were square with dimension of 23.81 mm x 23.81 mm while the divider wall copper plates were rectangular with measure of 23.81 mm x 12.70 mm. In the third passage, the copper plates on the leading and trailing surfaces were rectangular with dimension of 23.81 mm x 17 mm while the divider wall copper plates were rectangular with measure of 23.81 mm x 11.74 mm. For the first half of hub turn region, the copper plates were identically fan-shaped on trailing and leading surface, and they were identically arc-shaped on the hub wall. For the second half of the turn portion, the divider between the two copper plates within this area had an

intersection with the centerline of the flow passage at the center point of the passage centerline. The copper plates were then made to the corresponding shapes. Blind holes with diameter of 1.59 mm, were drilled in depth at 1.72 mm on the backside of each copper plate to embed the thermocouples with highly conductive epoxy. Temperature was measured in every region on every heated surface. As a result, a total of 56 temperature measurements were made from the copper plates. Two different β angles of 90^o and 45^o were studied as they are close to the condition of a real turbine blade.

2.2.2 Roughened Surface

With an AR=2:1, the second passage is roughed by squared copper ribs (P/e=8, e/Dh=0.1, α = 45°). Copper ribs of the same configuration, as in the second passage, are placed at inner half of the third passage, and pin-fin arrays made also with copper are embedded at the outer half of the third passage along with slot ejections at the side wall. Squared copper ribs were placed on the leading and trailing surfaces of the second passage and the inner half of the third passage. The height of the rib (e) is 1.59 mm, and e/D_h is 0.1. The ratio of rib pitch (P) to rib height (e) is P/e=8. The ribs on the leading and trailing walls are parallel to each other but in staggered arrangement, and the attack angle (α) is 45^o to the mainstream flow. Full length copper Pin-fins with diameter of 3mm was installed at the outer half of the third passage forming an array as shown in **Figure 5** and **Figure 6**. Soft Buna-N/PVC foam insulations at the middle of the pin-fins are added to reduce conductions.

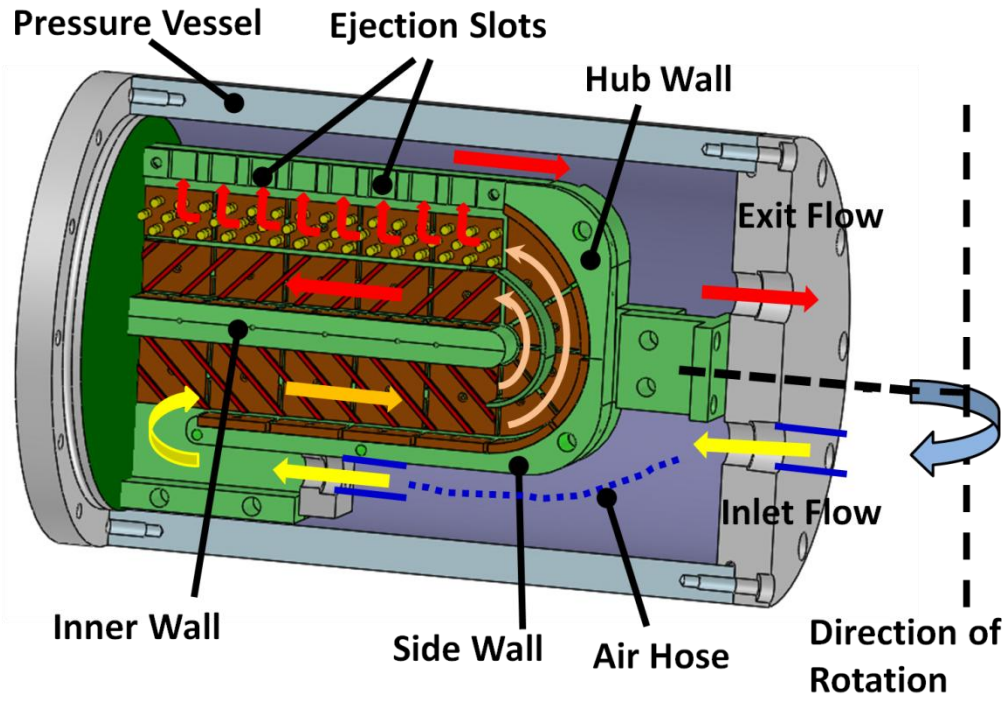

(a)

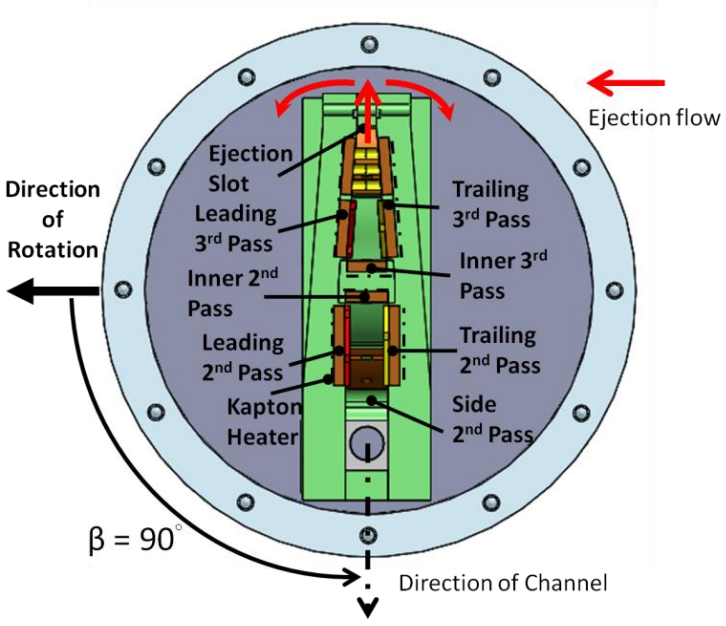

(b)

Figure 5 Test section inside the pressure vessel

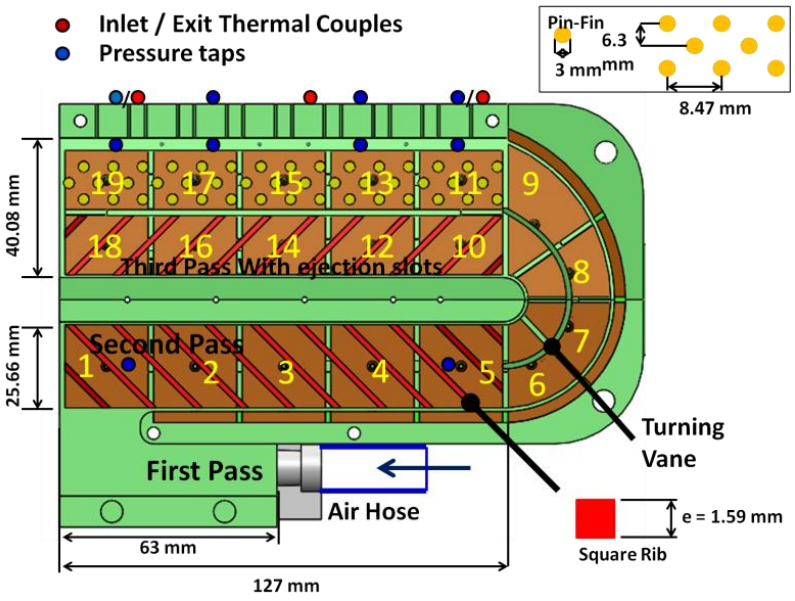

Figure 6 Dimension of Test Section

2.2.3 Pressure Measurement

Ejection affects the calculation of bulk air temperature, as well as local Reynolds number at the location of the ejection slot, since flow losses part of its mass in this zone. Mass flow rate at each slot is needed to calculate bulk air temperature and the local Reynolds number. In order to obtain the mass flow rate at each ejection slot, pressure drop between the upstream and downstream of the slot was measured. Pressure taps were installed at the inlet and outlet of each ejection slot as depicted in **Figure 4 & 6**, and an inclined manometer was used for the pressure measurement.

For the cooling air, the inlet pressure is kept at 68 psig, while the outlet pressure varies from 68 to 55 psig depending on Reynolds numbers.

2.3 Data Reduction

2.3.1 Pressure Measurement

The pressure difference between the upstream and downstream of ejection slots was measured through pressure taps and an inclined manometer in order to obtain mass flow rate passing through them. Rallabandi et al [24] showed that the velocity of ejection jet at each slot, V_i, can be estimated using Eq. (1). An empirical parameter, which is called discharge coefficient, C_D, is added into the calculation for the balance of the mass flow rate. Assuming the discharge coefficient, $C_{D,}$ through each slot is identical, pressure difference for slot i is ΔP_i:

$$\overline{\frac{2\Delta P_i}{\rho C_D}} = V_i \qquad (1)$$

Also, mass balance requires:

$$\sum_{i=1}^{8} \rho V_i A_s = m \quad (2)$$

C_D could be obtained by solving (1) and (2) simultaneously. Therefore, velocity through each slot as well as a unique discharge coefficient for every Reynolds number could be found, and the mass flow rate through each slot was obtained. Local Reynolds number can be estimated using Eq. (3) and the known local mass flow rate m_x and perimeter P_m:

$$Re_x = \frac{4m_x}{\mu P_m} \quad (3)$$

Figure 7 shows the calculated discharge coefficients under different Reynolds numbers at each slot location, as well as the corresponding local Reynolds number in the third passage. Pressure data was taken under stationary condition, while the test section is not heated. Results from measurement for smooth surface is similar to the roughened surface. Only results from roughened surface are shown for simplicity.

2.3.2 Heat Transfer Measurement

Regionally averaged heat transfer coefficient (h) at various locations within a rotating duct was investigated in this study. Wall temperature at region 3 and 14 were kept uniform at 65℃ throughout all the tests. Eq. (4) and (5) are for calculations of the regionally averaged heat transfer coefficient and the net heat transfer rate respectively.

$$h = \frac{Q_n}{A_P(\mathrm{T_{w,x}} - \mathrm{T_{b,x}})} \quad (4)$$

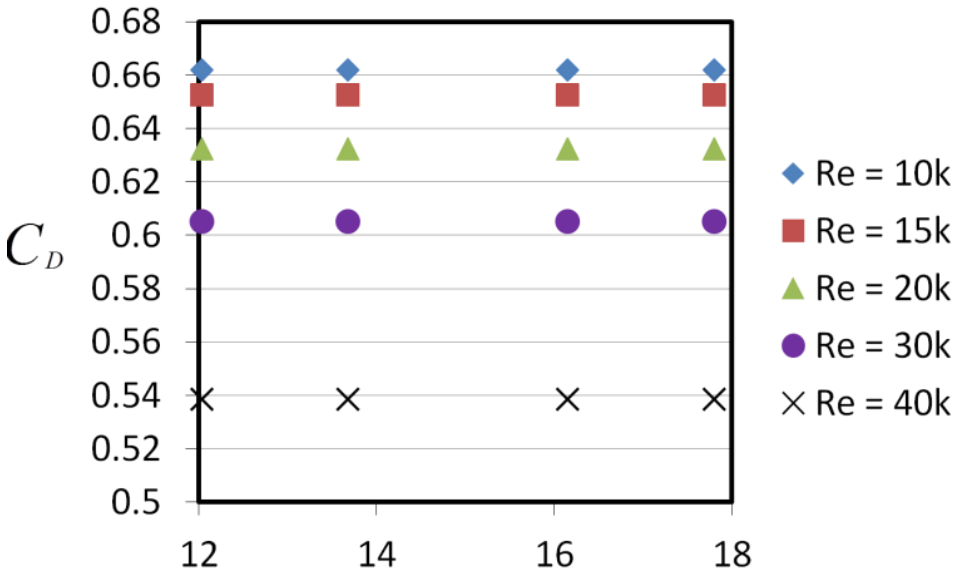

(a)

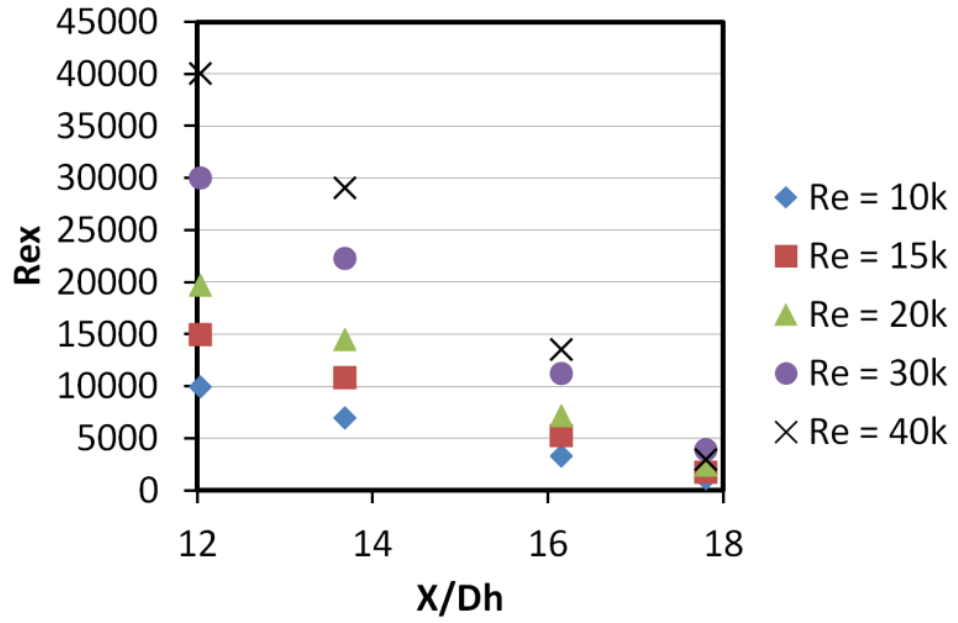

(b)

Figure 7 (a) Discharge Coefficients under different Reynolds numbers for stationary with turning vane cases. (b) Local Reynolds number distribution at stationary cases from Re = 10,000 to 40,000 with turning vane at each measured ejection slot position

$$Q_n = \frac{V^2}{R_H}\left(\frac{A_P}{A_{htr}}\right) - Q_l \quad (5)$$

First the resistance of the heater (R_H) was measured using a multi-meter. Then, the heater was installed into the test section and the applied voltage (V) was measured as well. In this study, it is assumed that the heat flux provided by the heater is uniform. Thus, the heat input to a copper plate is equal to the power input to each heater multiplied by the ratio of the projected area (A_p) to the total heater area (A_{htr}). Heat loss calibration tests at two different wall temperature conditions were performed for each rotational speed, as well as stationary case without presence of any flow. Thus, the external heat losses (Q_l) escaping from the test section during the experiment was obtained. The heat loss of test section through conduction was measured to be at 2~6% of the net heat input provided to each heated surface. Detailed heat loss calibration was described in Lei et al. [8].

The local regional wall temperature ($T_{w,x}$) could be directly obtained using the thermocouple embedded in the blind hole on the backside of each copper plate. The temperature of each copper plate was considered to be uniform since copper has a very high thermal conductivity. Temperature at the inlet and outlet of the test section were also measured by thermocouples. With information provided above, the local bulk air temperature at any location in the test section could be calculated using linear interpolation. Another method to determine the bulk air temperature was by performing energy balance along the channel.

Temperature distribution is shown in **Figure 8.** Interpolated bulk temperature is used for the calculation of heat transfer coefficient. In this study, the Dittus-Boelter/McAdams correlation for heating ($T_{w,x} > T_{b,x}$) was utilized to provide a basis of

comparison on Nusselt number. Therefore, Nusselt number for fully developed turbulent flow through a smooth stationary pipe (Nu_o) was determined by this correlation. As a result, the heat transfer enhancement (Nu/Nu_o ratio) was given as:

$$\frac{Nu}{Nu_o} = \frac{(\frac{hD_h}{k})}{(0.023Re^{0.8}Pr^{0.4})} \quad (6)$$

where heat transfer coefficient (h) is calculated by Eq. (4). All air properties are based on the channel averaged bulk air temperature with a Prandtl number (Pr) for air of 0.711.

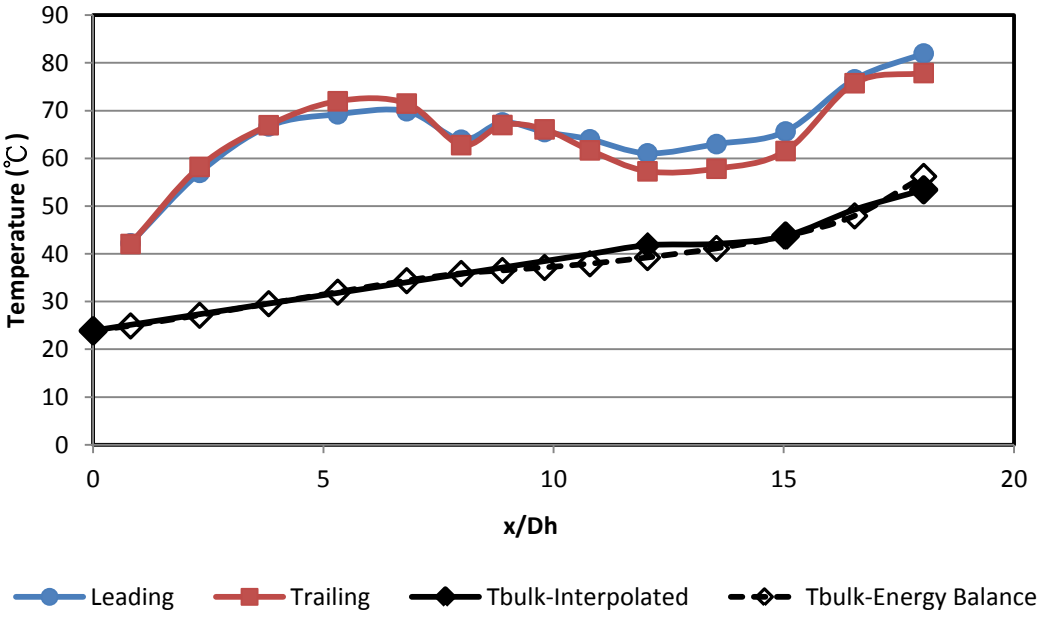

Figure 8 Temperature distribution along Leading and Trailing surfaces and bulk air temperature for Re=20k stationary without turning vane and β=90°

2.3.3 Experimental Uncertainty

Uncertainty analysis performed in this study was based on the method described in Kline and McClintock [30]. Air properties were calculated locally at every region based on the local bulk mean temperature with information provided by NIST. Some of the parameters mentioned above, such as Reynolds number and Rotation number were re-calculated regionally. A difference of less than 5% was shown in the comparison between the regionally re-calculated values and the channel-averaged ones. The uncertainty from the temperature measuring instrumentation is estimated to be 0.5℃. At lowest Reynolds number (*Re*=10,000), the maximum uncertainty of the *Re* is approximately 10% and the maximum uncertainty of the Nu is estimated as 12.5%.

2.3.4 Flow Field Behavior

Lei et al.[7], and Rallabandi et al. [24] presented an investigation of the secondary flow induced by ribs and pin-fin arrays. Coletti et al. [31, 32] investigated flow behaviors in a rib-roughened channel using PIV technique. Flow over rib-roughened wall is shown. Conceptual views depicting the most notable mainstream and secondary flow characteristics in a smooth or ribbed channel are shown in **Figure 9 & 10**. Based on measured heat transfer coefficient distributions, conjecture of flow behavior is provided as following: After entering the test section through the hose with circular cross-section, mainstream air expanded rapidly in the first passage. Because of the short distance of the first passage, the flow was still under developing conditions when it entered the sharp

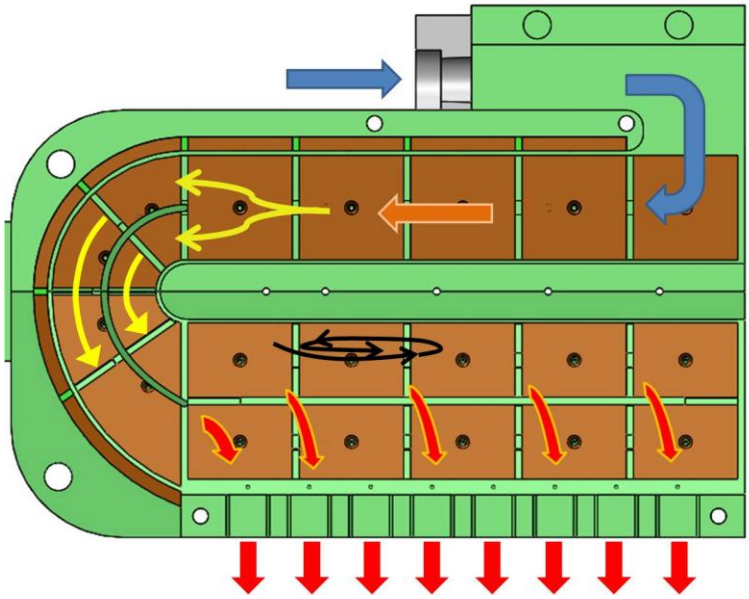

(a)

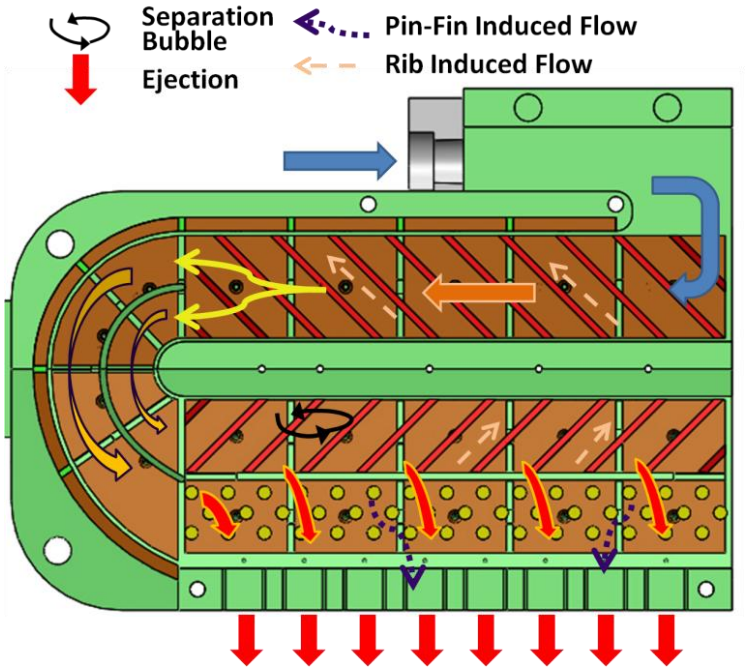

(b)

Figure 9 Conceptual view of mainstream flow with turning vane (a) Smooth and (b) Roughened Surface

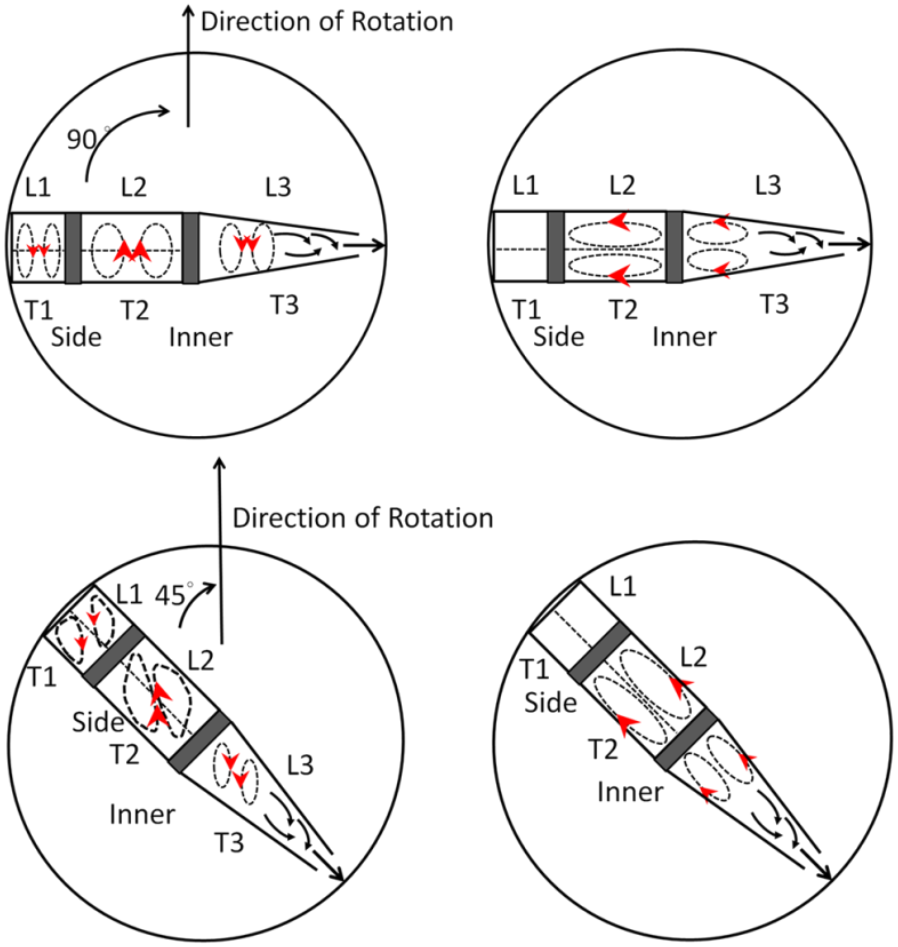

(a) (b)

Figure 10 Illustration of secondary flow induced by (a) Rotation, and (b) Angled ribs for both channel angle β=90° and 45°

turn. Then, air went into the heated second passage and thermal boundary layer started to develop as wall temperatures increased. At leading and trailing surfaces, air flowed along the angled ribs from inner wall to the side wall and went back to the center portion of the channel, passing the rib from the top, forming a pair of vortex, as shown in **10(b)**. Then, in the hub turn region, considering the case without turning vane, the mainstream velocity was higher near the inner divider wall where flow started to separate after its' mid-point. The secondary dean vortices were generated at this moment in the cross-section planes perpendicular to the mainstream pushing the mainstream core toward the hub wall, and into the wedged shape portion. After the 180^{o} U-bend in the third passage, the flow is pushed toward side wall by the combining effects of recirculation bubble near inner wall, and the pressure drop induced by first ejection slot on the outer side wall. Less flow at the inner side of the third passage is expected. As flow goes into the third passage, dean vortex vanished very quickly and rib-induced vortices, as well as vortices generated by the pin-fins dominated in the roughened third passage . Air flowed along the angled ribs from center of the passage to the inner wall. However, with slot ejection on the side, flow lost mass gradually when it went deep into the passage, and the local Reynolds number decreased. Before it ejected from the slots, air must pass through the pin-fin array, and thus vortex would be induced. Eventually, flow hit the end wall and the entire flow exited through the last ejection slot. Considering the case with turning vane, flow in the first or second passages was not much affected by the turning vane since they were at upstream of the hub turn region. However, the flow behavior in the turn region and after the turn was greatly affected. First, the passage was divided into

two parts in the turn region i.e. the inner passage and the outer passage separated by the turning vane. Luo and Razinsky [20] had concluded that dean vortices would be generated in both regions. Therefore, it could be predicted that dean vortices were generated but in smaller sizes compared with case without turning vane, at both regions. A smaller vortex results in a weaker secondary flow, and lower pressure gradient between the inner divider wall and the hub wall. Moreover, flow separation near the inner divider wall was suppressed by the turning vane, and the size of the recirculation zone in the third passage was largely decreased. Consequently, the difference in velocity between the inner wall and side wall was reduced, and there was less push on the flow towards the side wall compared to the case of without turning vane. Consequently, more flow was travelling in the inner half of the third passage for the case of with turning vane.

Rotation and rotation-induced buoyancy forces were also important to the heat transfer enhancement in the roughened channel. **Figure 10** illustrates the secondary flows with channel orientation angle of 90^o and 45^o. A pair of vortex was induced by the Coriolis force. It favored the trailing surface in radially outward passages, while it favored the leading surface in radially inward passages for the orientation angle (β) of 90^o. If the channel was tilted ($\beta=45^o$), as shown in **Figure 10(a)**, with radially outward flow, the pair of vortices impinged on the trailing surface and the inner divider wall. With radially inward flow, this impingement happened on the leading surface and the inner divider wall in the passage. The heat transfer may be enhanced by the combination of these complex flow behaviors, or it may be reduced.

The ratio of the Coriolis force to the inertial force is defined as rotation number

(Ro). It is used to evaluate the effect of rotation, and as shown in Eq. (7).

$$_{o} = \frac{\Omega D_h}{U_b} \tag{7}$$

The corresponding rotation number Ro at each tested Reynolds number and rotational speed are shown in **Figure 11**. In the current test section, the highest rotation number of 0.32 was achieved at Reynolds number of 10,000 and rotation speed of 300 rpm.

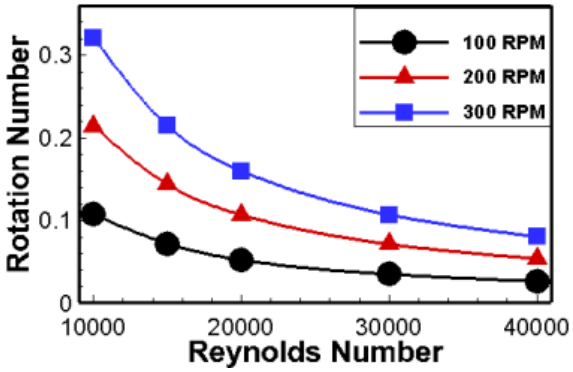

Figure 11 (a) Rotation number at varies Reynolds numbers and different rotation speeds

2.3.5 Vane Conduction Effect Correction

Although the turning vane was made of SLS Nylon PA with the thermal conductivity of 0.7 W/(m K), heat was still conducted between the leading surface and trailing surface through the vane, and transferred away by air convection when the turning vane was applied at the turn portion. To accurately calculate the heat transfer coefficient on the leading and trailing surfaces, heat conducted by the vane must be deducted. The turning vane could be treated as two constant cross-section fins extending from both leading and trailing surfaces until they met at the mid-plane of the vane.

Insulated boundary condition at the mid-plane was assumed, and temperature measured from the leading and trailing surfaces was considered as the base temperature of the fin. Heat conduction in the turn portion could then be calculated region by region on both leading and trailing surfaces using Eq. (8):

$$Q_f = (kA_c hP_v)^{0.5}\left(\mathrm{T_{w,x}} - \mathrm{T_{b,x}}\right)\tanh\left(L\left(\frac{hP_v}{kA_c}\right)^{-0.5}\right) \quad (8)$$

where k is the thermal conductivity of the vane material, L, $P_{v,}$ and Ac are height, perimeter and cross-section area of the vane, respectively. It was assumed that the heat transfer coefficient h on the vane surface was of the same level as that on the hub wall in each region. Temperature difference refers to that of between local surface temperature and the local bulk air temperature. The actual heat transfer Q_a on leading or trailing surface with vane is shown as in Eq. (9), and this number is used to calculate the heat transfer coefficient in Eq. (4).

$$\mathrm{Q}_a = \mathrm{Q_n} - \mathrm{Q_f} \quad (9)$$

This correction procedure was applied to every case with turning vane for all the Reynolds numbers and rotation speeds. It was observed that the highest conduction effect by vane occurred at Re=10,000 and RPM=300, accompanied with the largest disparity of Nu/Nu_o of 15%. The streamwise distribution of Nu/Nu_o before and after correction at Re=10,000 in rotating conditions (RPM=300) is shown in **Figure 12**.

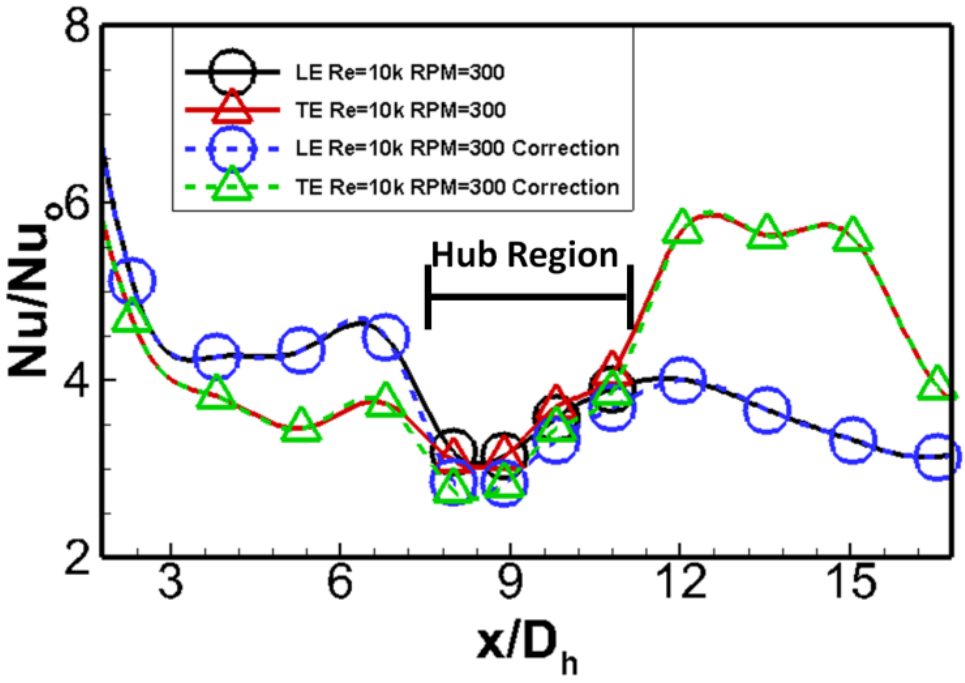

Figure 12 Effect of conduction by turning vane on streamwise Nu ratio (Nu/Nu_o) on leading and trailing surfaces at Re=10k, rpm=300, and β=90

2.4 Discussion of Results – Smooth Surface

2.4.1 HTE (Nu ratio) Distribution In the Third Passage

Figure 13 illustrates the Nusselt number ratio distribution in the third passage. In this figure, regions 10, 12, 14, and 16 are categorized as 'inner half' of the passage while 'outer half' includes regions 11, 13, 15, and 17.

Consider stationary ($\beta=90^o$) without vane case (**Figure 13 (A)**), HTE values obtained at outer half are always higher than those at inner half. Since the pressure level cross the ejection slot is relative lower than the ones around the inner half neighborhood, thus the flow has a tendency to rush through the slots and results in more mass flow to pass by the outer half than inner half. The HTE shirks monotonically as the main flow travels through the passage. Since the main flow continuously suffers from mass losses by flow discharging across the ejection slot configuration. Fewer and fewer mass remains in the passage as the flow travels downstream. The elevated HTE at the first two regions in inner half with turning vane (**Figure 13 (B)**) diminishes the gap between the inner and outer halves. The turning vane guides the flow through the 180^o turn and helps to distribute more evenly on both inner and outer halves of the third passages. However, in the last two regions, the vane effect fades since this neighborhood is far away from the vane.

Rotation effect in the third passage (radial outward flow) is evident when comparing **Figure 13 (A)** and **(C)**. HTE in both inner and outer halves on trailing surfaces increases meanwhile a reverse trend is found at leading surface outer half. This conclusion coincides with previous literature associated with rotation effect studies.

Rotation effect in leading surface inner half is minimal. This is again due to the pressure difference cross the slot discharge configuration. The HTE distribution in this neighborhood is dominated by the coolant mass flow; since it is already too low and the effect of rotation vanishes. Comparing **Figure 13 (C)** and **(D)**, the presence of turning vane reduces HTE difference between outer and inner halves on both leading and trailing surfaces. Since the guide vane helps the circulating flow to distribute more uniformly on both sides of vane intrusion. Compare **Figure 13 (C)** and **(E)**, it is obvious that all the HT distribution decreases remarkably. The effect of changing channel angle orientation from $\beta=90^{o}$ to 45^{o} significantly hinders HT in the third passage. Since in $\beta=45^{o}$ case, the secondary flow introduced by rotation impinges the outer wall and the trailing surface simultaneously. Combine with the pressure gradient across ejection slots, the secondary flow component towards outer wall further pushes the flow to evacuate from the third passage. Thus HT in $\beta= 45^{o}$ case is greatly reduced compares with $\beta=90^{o}$. Turning vane effect can be observed by comparing **Figure 13 (E)** and **(F)**. HTE at all documented area slightly increases with turning vane. At regions 10 and 11 neighborhood, the HTE gap between inner and outer halves is cut down. However, this phenomenon diminishes at the rest of the passage. Since less mass flow remains in the passage compares with $\beta=90^{o}$ case, thus the turning vane impacted area is even more restricted when $\beta= 45^{o}$.

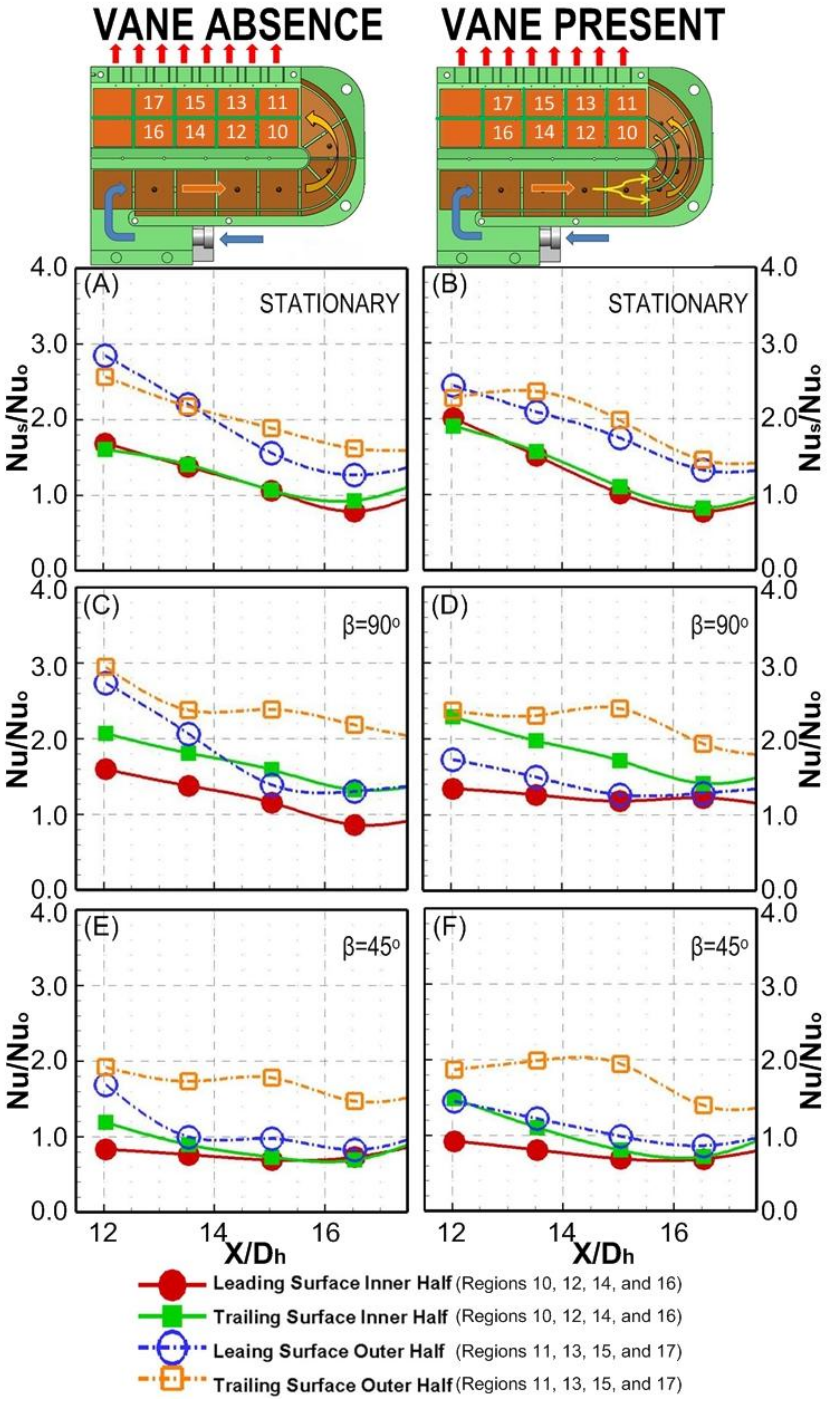

Figure 13 HTE (Nu ratio) distribution in the third passage: (A) stationary, Re = 20k; (B) Ro = 1.6, Re = 20k, β=90°; (C) Ro = 1.6, Re = 20k, β=45°

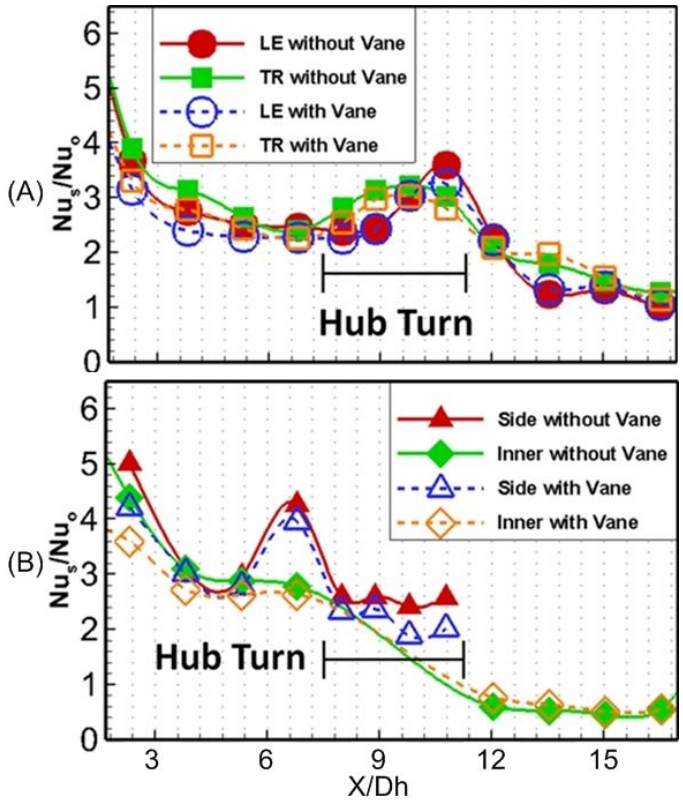

Figure 14 Effect of turning vane on stationary streamwise Nu ratio (Nu_s/Nu_o) distributions at Re=20k for (a) Leading and trailing surfaces. (b) Side and inner walls.

2.4.2 Streamwise HTE Distribution-Stationary Results

Figure 14 displays the heat transfer enhancement (Nu/Nuo) streamwise distribution at stationary Re=20000 condition for both with and without turning vane case. It serves as the example to demonstrate the heat transfer patterns of the radial inward flow in second passage, 180° U-band hub turn, and then radial outward flow with slot ejection in third passage. Data recorded from almost all regions are reported in the figure except regions 1 (channel inlet), 18, and 19 (channel end) due to extreme flow behavior difference. In the third passage, streamwise data are actually reported as pairs. For the two regions that share the same streamwise location (x/D_h), averaged values of both regions [region pairs (10, 11), (12, 13), (14, 15), and (16, 17)] are averaged and documented to represent the final data for aforementioned position. According to the data extracted from region 1 and 2, an obvious entrance effect is concluded and it dominates the flow pattern at the channel entrance. Due to the mass flow bleeds through ejection slots in the third passage and located next to the close end, flow behavior in region 18 and 19 neighborhood is very different from other parts of the channel. Cross reference with the results reported by Lei et al. [7], **Figure 14 (A)** depicts a similar HT trend at the second passage. However, the values are 15~20% less.

One possible reason is due to entrance condition difference. In [7], the mainstream supply fitting is not aligned with the squared first passage perfectly since 37% of the fitting opening is blocked by the test model. The entrance flow in [7] has to squeeze through the remaining asymmetric gap and then expand in the First passage. As illustrated in **Figure 3 (A)**, the current test section is redesigned to guaranty no blockage

occurs at the junction portion. Flow in this study can enter the first passage directly without any obstruction. The difference in flow exit configuration scheme for both studies may also contribute to the HT enhancement contrast. Since the flow channel in [7] does not have the ejection slot configuration design adjacent to the 180° U-band hub turn. The back pressure experienced at the second passage of both test models is different and thus can significantly impact the HT phenomenon.

The mainstream enters second passage (x/Dh=0∼8) after the sharp tip turn. As shown in **Figure 14(A)**, in the second passage, HT enhancements on both leading and trailing surfaces are very close due to flow symmetry in stationary channel. HT on all walls decreases along the streamwise direction in the second passage due to the entrance effect. Contributed by elevated turbulent mixing, HT starts to increase again after region 5 (x/Dh≈6.8). The turning vane marginally affects the HT data around the region 5 neighborhood (hub turn upstream).

In the hub turn regions (x/Dh = 8∼10.5) the general trend is the HT increases on both leading and trailing surface as the flow travels through the hub turn. This is due to the channel turn introduced turbulent mixing and the secondary flow. Compare the with-vane and no-vane cases, the turning vane slightly impedes the HT at the trailing surface, however the cut back level decreases as the flow travels along the turn. Leading surface HT is nearly not effected by the turning vane. The turning vane substantially impedes the hub wall HT and the cut back can be up to 15%. This is due to the turning vane dwindle the scale and strength of the secondary vortex and impedes turbulent mixing.

The mainstream is guided into the third passage (x/Dh = 10.5~18) after the hub turn. The HT enhancement decreases on both leading and trailing surfaces. In addition to the entrance effect, the wear down in streamwise mass flow rate can also contribute to this phenomena. On the other hand, the HT enhancement on inner divider wall is quite uniform. It is worthy to point out that the value is actually lower than Dittus-Boelter/McAdams correlation. This low HT region corresponds to the recirculation bubble in the flow behavior. The turning vane lightly boosts HT (up to 7%) on both leading and trailing surface. However, the elevated level reduces as the flow travels downstream. Similar trend can also apply to the inner divider wall; however, the gain is limit.

2.4.3 Streamwise HTE Distribution-Rotating Results

The streamwise HT enhancement (Nu/Nuo) in a 90° channel orientation angle (β) smooth channel under rotation (Ω =300 rpm, Ro=0.16) at Re=20000 condition for both with and without turning vane case are documented in **Figure 15.** It serves as the example to explain the HT variation of the flow circulating through the test model.

In radial inward flow (second passage, x/Dh =0~8), rotation benefits and impedes HT on the leading and trailing surfaces respectively. A reverse trend is also concluded for radial outward flow (third passage, x/Dh =10.5~18). This results from the rotation introduced Coriolis force impacts mainstream core as described in previous section. Meanwhile the rotation effect on both inner divider and outer side walls of radial inward flow is marginal. However, it benefits HT at the third passage inner divider wall and the

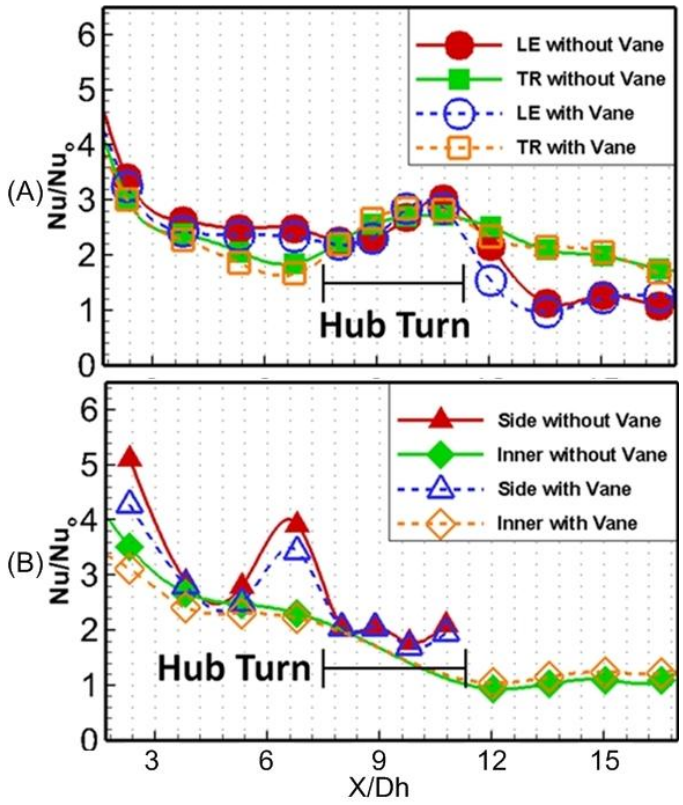

Figure 15 Effect of the turning vane on streamwise Nu ratio (Nu/Nu_o) distributions under rotating conditions (rpm=300, Ro=0.16) at Re=20k, and β=90° for (A) leading and trailing surfaces. (B) Side and inner walls.

increased level becomes comparable with empirical correlations. The effect of turning vane is diverse in the second and third passages. It slightly reduces and increases HT on all interested surfaces in the second and third passage respectively. On both leading and trailing surfaces, the cut down is more obvious as the mainstream travels through the second passage. A maximum reduce as large as 10% is observed at region 5 ($x/Dh \approx 6.8$) on outer side wall. In the hub turn regions (x/Dh = 8~10.5) of leading and trailing surfaces, the HT performance almost falls into same level. Compare with stationary (**Figures 14**) results, one can find the rotation effect slightly suppresses HT. However, this HT cut back is most severe (near to 11%) at the hub turn side wall. The turning vane effect is diluted in the hub turn area under rotation. The HT benefits gained from its presence are small, this proves that rotation effect is the dominate factor for HT of hub turn regions.

2.4.4 Streamwise HTE Distribution- Channel Orientation Results

The internal cooling channel design is largely confined by the blade profile. In many occasions the associated passages may have an orientation other than perpendicular (β=90°) to rotation direction. The streamwise HT enhancement (Nu/Nuo) results for both 45° and 90° channel orientation angles (β) are illustrated in **Figure 19**. In light of fair comparison, flow parameters (Re=20000, Ro=0.16) are kept identical compare with stationary and rotation case studies in previous sections; smooth channel with turning vane is the only configuration variant studied. **Figure 16** serves as a framework to explain the HT variation of the flow circulating through the test model.

In radial inward flow, (second passage, x/Dh =0∼8) as the channel orientation changes from 90° to 45°, a small HT reduce is observed on the leading, trailing as well as the inner divider wall surfaces. The HT difference between leading and trailing surfaces slightly propagates while the flow travels to downstream. Meanwhile, the outer side wall HT experiences a miniature gain. As the channel orientation alters to 45° (**Figure 5(B)**), rotation-induced secondary flow simultaneously impinges onto leading surface and side wall rather than leading surface alone (for β=90°). The weakened and reinforced vortex impingement on leading surface and sidewall are responsible for the HT behavior change. As shown in **Figure 10**, the channel orientation angle effect on HT is almost negligible in the hub turn regions (x/Dh = 8∼10.5). Consider the radial outward flow in the third passage (x/Dh =10.5∼18), the HT on all interested surfaces are dramatically impacted by the channel orientation. The significant HT setback is as large as 60%, 33%, and 25% in the inner divider wall, trailing, and leading surfaces respectively. Particularly at the inner divider wall, the orientation effect worsens the HT to only 50% of the empirical correlation value. This is due to the combine effect of slot ejection and rotation-induced secondary flow as shown in **Figure 8(B)**. The secondary flow impinges onto trailing surface and side wall rather than trailing surface directly (for β=90°). The vortex component impinges towards the sidewall can further push more mainstream to (3^{rd} passage mid region near inner wall, **Figure 20**), and region 15(3^{rd} passage mid region adjacent to ejection slots, **Figure 21**.

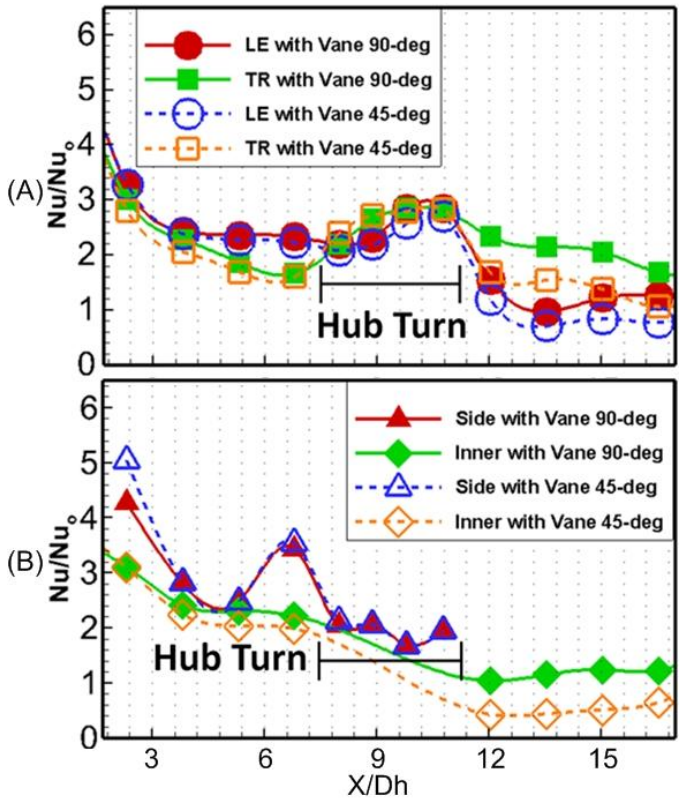

Figure 16 Effect of channel orientation (β=90° and 45°) on streamwise Nu ratio (Nu/Nu_o) distributions under rotating conditions (rpm=300, Ro=0.16) at Re=20k for (A) Leading and trailing surfaces. (B) Side and inner walls.

2.4.5 2ND Passage Flow Developed Zone

Region 4 (**Figure 18**) Nu/Nu_s –Ro data, is used to represent the second passage (radial inward flow) right before the hub turn neighborhood. In the 90^o channel orientation case, the HTE trend confirms with typical rotation involved radial inward flow passage results. Since the HTE on leading surface increases with rotation number, meanwhile on trailing surface, it first decreases up to 20% then slightly increases starting Ro equals 0.15. The rotation effect in HTE on side and inner walls follow similar direction as observed on leading and trailing surfaces respectively. The impact from turning vane existence is almost negligible, since this region is located 2.5 D_h upstream the vane stagnation and the flow is less likely effected by the its intrusion.

In 45^o channel orientation cases, similar Ro-HT trend are found on leading and trailing surfaces as well as on side wall. On leading surface and side wall, shuffle channel orientation angle from 90^o to 45^o slightly elevates HT, yet, a small contraction is experienced beyond Ro equals 0.21. The rotation introduced HT reduction on trailing surface is also alleviated despite the increase is impeded to Ro equals 2.0 and the magnitude is lower. The contrast is most significant on the inner surface. Instead of an increasing beyond Ro equals 0.2 as concluded in 90^o case, the HTE declines monotonically through the studied Ro range. The cut back is as large as 30%. The presents of vane concludes a negative role in terms of HT in 45^o channel orientation. It overturns the Ro-HT trend on leading surface from slightly increase to decrease. Meanwhile HT in both trailing surface and side wall are further decreased with turning vane.

2.4.6 25~50% of Hub Turn Zone

As illustrated in **figure 18** (region 7), it is clear that the HTE generally declines with rotation number in all three surfaces regardless turning vane presence and channel orientation angle. Consider the 90^o channel orientation vane absence case, starting from Ro equals 0.21, the decreasing HT trend levels out on leading surface meanwhile slightly reverse on both trailing and hub wall surfaces. However, with turning vane presence, the HTE trends on all three surfaces drops monotonically.

Regardless vane presence, HTE ratio strictly decreases with rotation in 45^o channel orientation angle cases. Consider the case without turning vane, on leading surface, the HT difference compared with 90^o case is first limited. Than the HT trend kept decline even after Ro equals 0.21, and the cut back (compare with $\beta=90^o$ no vane case) is around 15% around Ro equals 0.32. Changing channel orientation angle to 45^o is slightly beneficial to HT on trailing and hub wall surfaces. Although the values at both Ro lower and upper boundaries are almost identical with 90^o case, it is clear that HT is higher in$\beta=45^o$ across the studied Ro range. Turning vane is advantageous on trailing surface HT. The Ro-HT trend tend to level out beyond Ro equals 0.21, and the gain is as large as 15% (for both $\beta=90^o$ with vane and $\beta=45^o$ no vane cases as base line) at Ro equals 0.32. Nonetheless, turning vane effect on leading and hub wall surfaces is minimal for $\beta=45^o$ cases.

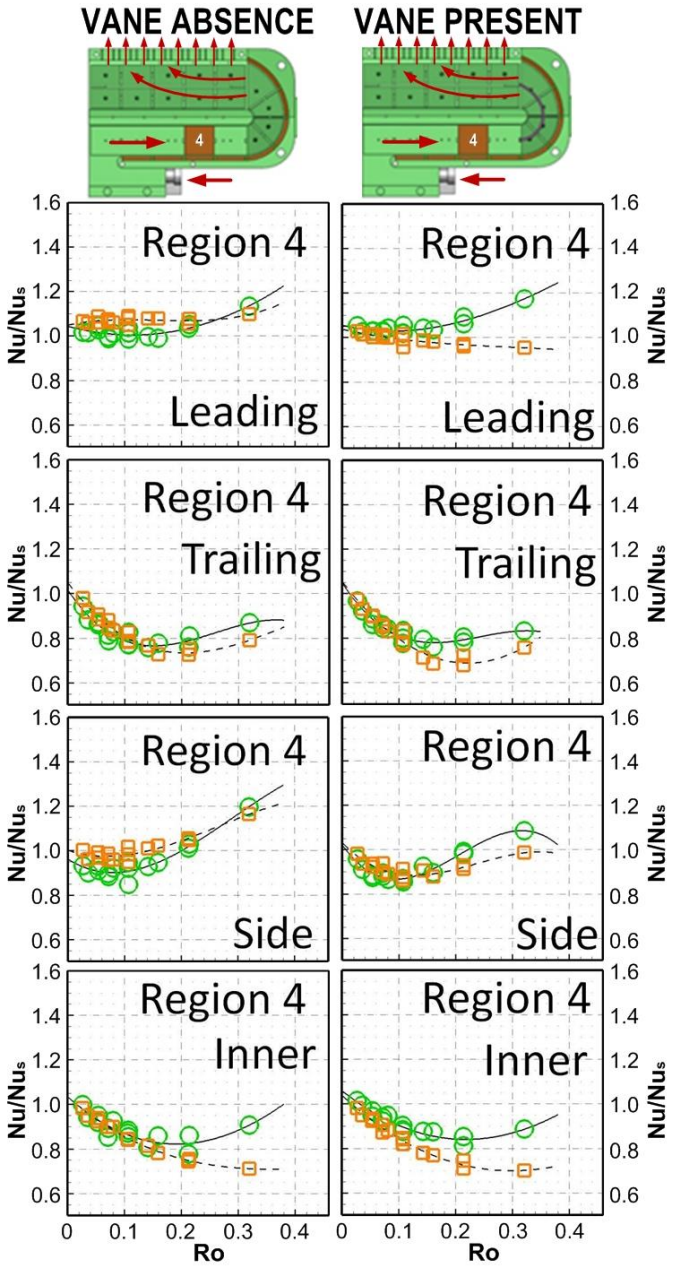

Figure 17 Nu ratio (Nu/Nu_s) distribution as a function of rotation number (Ro) on all surfaces for β=90° (○) and 45° (□) at regions #4 for cases (a) vane absence (b) vane present

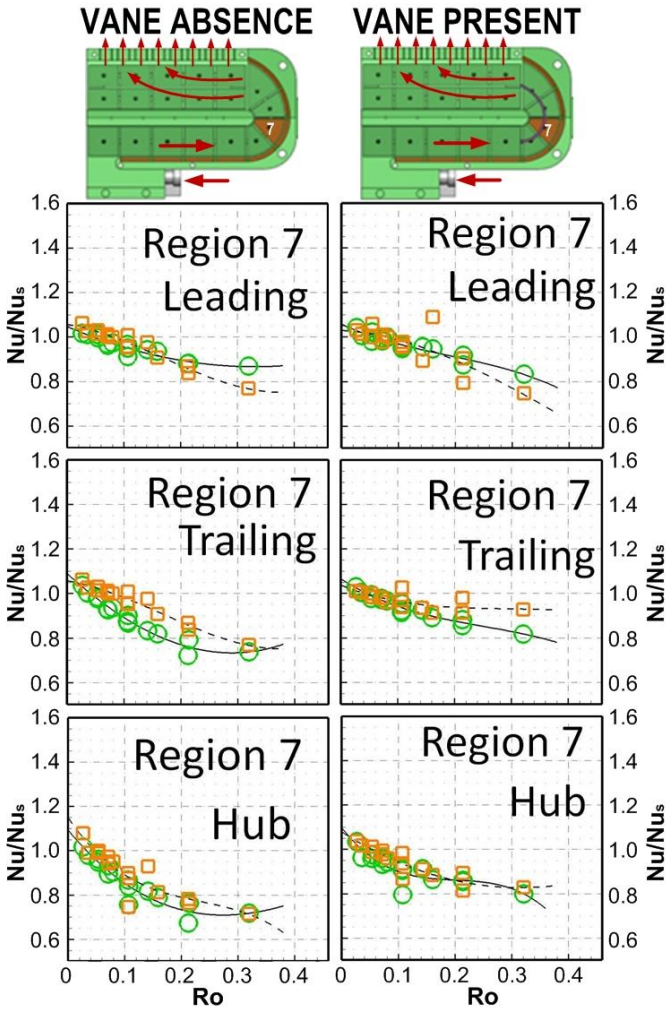

Figure 18 Nu ratio (Nu/Nu_s) distribution as a function of rotation number (Ro) on all surfaces for β=90° (○) and 45° (□) at regions #7 for cases (a) without vane (b) with vane

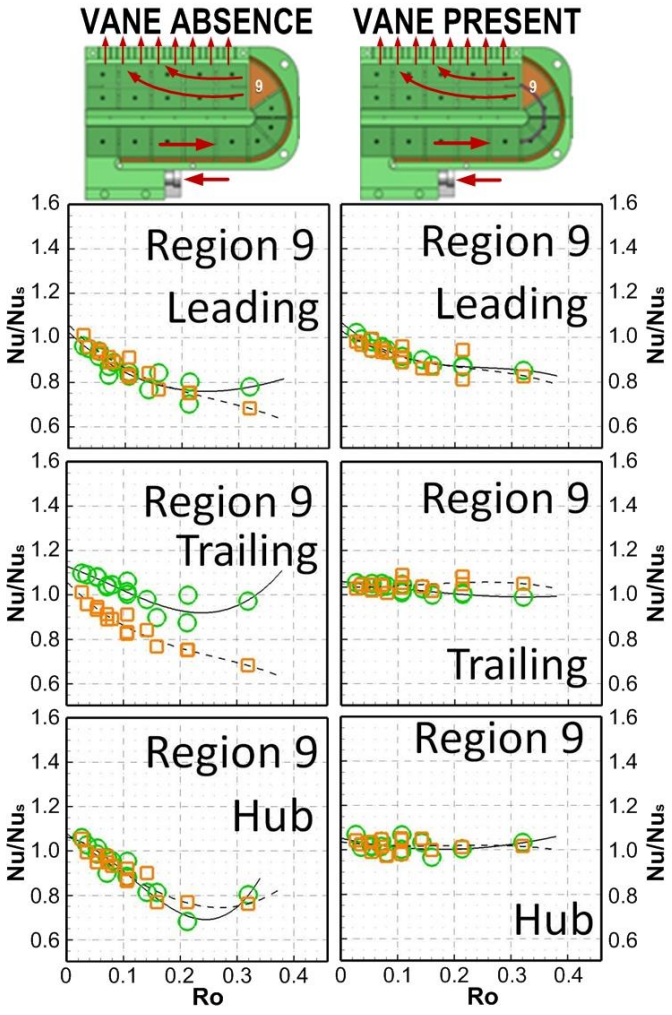

Figure 19 Nu ratio (Nu/Nu_s) distribution as a function of rotation number (Ro) on all surfaces for β=90° (○) and 45° (□) at regions #9 for cases (a) without vane (b) with vane

2.4.7 75~100% of Hub Turn Zone

Region 9 represents the data recorded at near hub turn exit. Consider both ($\beta=45^o$ and 90^o) turning vane absent cases, rotation exerts a negative overall effect on HT on all interested surfaces. The Ro-HT trends on leading and hub wall surfaces are highly coincident to each other, and the reduced value is as significant as 22% as the Ro rises. Only on the trailing surface, the HT distribution is more diverse. The HT decreasing trend is more severe in $\beta=45^o$ than in $\beta= 90^o$ case. The HT cut back is as significant as 10% and 30% respectively. The difference between the two cases proliferates as the rotation number increases, and is as large as 25% at Ro equals 0.32.

It is evident that the turning vane is favorable to HT in both channel orientation cases. On trailing and hub wall surfaces, the Ro-HT trends are almost horizontal and maintain a constant value around unity. The negative Ro-HT trend experienced on leading surface (both $\beta=45^o$ and 90^o) in vane absence case is also alleviated when adding the turning vane into hub turn regions

2.4.8 3RD Passage Mid-Region Inner Wall Adjacent Zone

Consider the 90^o channel orientation cases, HTE on both leading and trailing surfaces monotonically increase with rotation. The increments are as large as 50% and 100% (compares with stationary) at Ro equals 0.32 for leading and trailing surfaces respectively. On the inner wall surface, the expanding trend is steeper in Ro range from 0 to 0.1. After Ro equals 0.1, the trend becomes horizontal. The overall gain in HTE is as significant as 150% as Ro equals 0.32. The impact of turning vane existence is very

limited, and the effect is constrained on inner wall surface only. The HTE intensifies with rotation continuously.

Regardless of turning vane presence, altering channel orientation angle to 45^{o} introduces a drastic effect in terms of HTE on all three interested surfaces. HT-Ro correlations and level on leading and inner wall surfaces become constant and close to unity. On the trailing surface, the HTE diminishes with rotation. The HTE reaches its rock bottom (25% decrease compares with stationary) at Ro equals 0.21. For all three surfaces, the HT difference between both $\beta=90^{o}$ and 45^{o} propagates as rotation number increases.

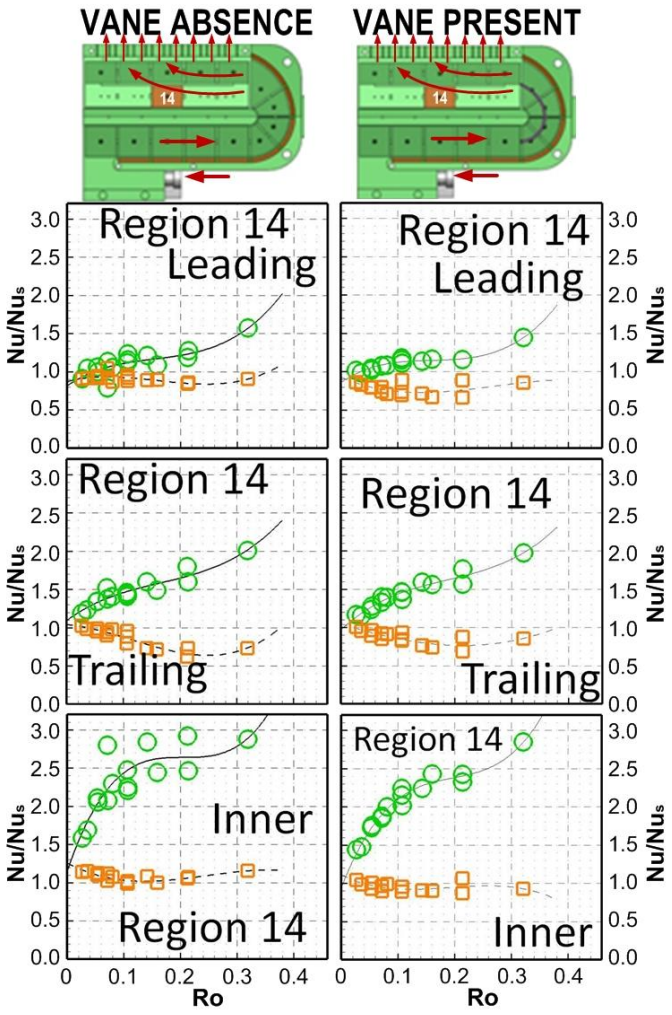

Figure 20 Nu ratio (Nu/Nu_s) distribution as a function of rotation number (Ro) on all surfaces β=90° (○) and 45° (□) at regions #14 for cases (a) without vane (b) with vane

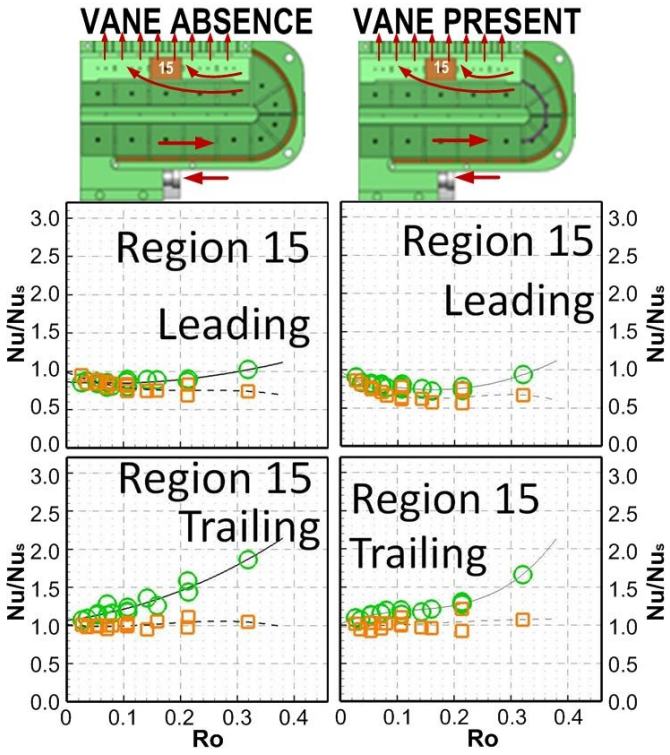

Figure 21 Nu ratio (Nu/Nu_s) distribution as a function of rotation number (Ro) on all surfaces for β=90° (○) and 45° (□) at regions #15 for cases (a) without vane (b) with vane

2.4.9 3RD Passage Mid-Region Ejection Slot Adjacent Zone

Region 15 HT information (Nu/Nus) is plotted verses rotation number as shown in **Figure21**. The HTE behavior in this region is similar compared with its adjacent region 14. In $\beta=90^{o}$ vane absent case, the Ro introduced HT enhancement dwindles compares with region 14. The leading surface HT-Ro correlation falls into horizontal close to 0.9.

On the trailing surface, HTE builds up with rotation monotonically, and the level is doubled as Ro reaches 0.32. The turning vane slightly hinders HTE in $\beta= 90^{o}$ case. On leading surface, the HT first shrinks with rotation and reaches it floor (about 15% cut back compares with stationary) around Ro equals 0.16 neighborhood. Beyond such Ro value, the trend reverses and again reaches unity at Ro equal 0.32. The HT-Ro trend on trailing surface is similar compared with vane presence case, only the gain in HT is marginally cut down.

Disregarding the turning vane existence, changing the channel orientation angle to 45^{o} again negatively impacts HTE, especially on trailing surface. Instead of positive rotation effect concluded with $\beta=90^{o}$, HT-Ro correlation become inert with rotation in $\beta=45^{o}$. On leading surface, HT in $\beta=45^{o}$ cases are constantly slightly lower than those of $\beta=90^{o}$. Consistence with the concluded from region 14, the HTE difference between $\beta=90^{o}$ and 45^{o} propagates as rotation intensifies. This phenomenon is due to the combine effect of rotation and the slot ejection. In $\beta=45^{o}$ cases, the HT reduction is even worse since the rotation introduced secondary flow tends to push the mainstream core towards side wall and consequentially reinforce ejection flow.

2.4.10 Conclusions – Smooth Surface

This study experimentally investigates the heat transfer performance in a smooth surface three passage turbine internal cooling channel. The effects of rotation number (Ro=0~0.32), turning vane, and channel orientation angle (β=45° and 90°) on heat transfer are studied. Build on the experiment results, the conclusions is summarized as the following:

1. Stationary case study: In the before turn portion, the effect due to turning presence is marginal. In the hub turn section, turning vane substantially impedes heat transfer at outer side wall (up to15%). Meanwhile it helps leading surface heat transfer; however the enhanced level decreases as the flow travels along the turn. Heat transfer in after-turn regions is boosted remarkably with turning vane (up to 20%) on both leading and trailing surface. The elevated level again fades as low travels downstream. Similar trend also concludes at the inner divider wall only the gain is marginal.
2. Rotation case study: Before the turn, rotation benefits and impedes HT on the leading and trailing surfaces respectively. A reverse trend is concluded for after turn portion. The effect of turning vane is diverse before and after the turn. It slightly reduces and increases HT on all interested surfaces before and after the turn respectively. Before the turn, the cut down is clearer (up to 12%) as the flow travels downstream. Rotation suppresses HT in the turn portion. The effect is most severe (near to 11%) at the hub turn side wall. The turning vane effect is diluted in the hub turn area under rotation.

3. Channel orientation case study: In radial inward flow, a small HT reduce results from changing channel orientation from 90° to 45° on all surfaces excepts outer side wall. The HT difference between leading and trailing surfaces slightly propagates as the flow travels towards the turn. Meanwhile, the outer side wall HT experiences a small gain. The rotation-induced secondary flow impinges onto both leading and side wall surface rather than leading surface alone (for β=90°). The similar reason also leads to dramatically reduced HT on all surfaces at after turn portion. The significant HT setback is as large as 50%, 33%, and 40% in the leading, trailing and inner divider wall surfaces respectively.

4. Nusselt Ratio Distribution in the Third Passage: HT phenomena in the third passage are studied by dividing the passage into inner (wall adjacent) and outer (slot adjacent) halves. The results show that the HT distribution in inner and outer halves are highly different and is dominated by the slot ejection configuration. This is contributed by the pressure gradient across each discharge slots. The pressure gradient causes circulating flow to discharge from the slots and culminates in fewer and fewer mass remain in the passage as it travels downstream. Adding a turning vane helps diminishing the HT gap between the passage inner and outer halves; however, vane effect fades as the flow travels along the channel. In rotating scheme, HT levels in β=45° is significant lower then β=90°, and it degrades to around 70% (without vane) ~80% (with vane) of the values observed in β=90°.

5. Nu/Nu_s ~ Ro Correlation- Rotation Effect: The Nu/Nu_s ratio is correlated as a function of rotation number that clearly illustrates the rotation number effect on HT.

Despite the channel orientation angle and turning vane, before the turn, the general trend shows that with Ro propagates, the Nu/Nu_s increases on the leading and side wall surfaces while decreases the trailing and inner divider wall surfaces. During the hub turn, the HT undergoes a decreasing trend as the rotation number increases on all surfaces. HT behavior in after-turn regions is more diverse and sometimes differs from the well know rotation effect in a radial outward flow. Since it is heavily affected by the third passage discharge slot configurations. The rotation effect on HT around mid-pass inner wall adjacent neighborhood (region 14) undergoes a monotonically increasing trend on all surfaces as Ro propagates. However, in mid-pass slot adjacent neighborhood (region 15), on the trailing surface, HT intensifies with rotation. While the Ro effect is small on the leading surface.

6. $Nu/Nu_s \sim$ Ro Correlation- Turning Vane Effect: Regardless the channel orientation angle, in both radial inward and outward flow passages the turning vane effect on HT is minimal. Turning vane effect is more significant at the vane intrusion end neighborhood (region 9). It favors HT and changed the monotonic decreasing Ro-HT trend to horizontal (around unity) on all three surfaces. The turning vane also benefits HT in region 7 (vane intrusion starts), however gain on trailing and side wall surfaces are small.

7. $Nu/Nu_s \sim$ Ro Correlation- Channel Orientation Effect: The channel orientation angle effect is significant in radial outward flow (third passage). By switching β from 90° to 45°, due to the rotation introduced secondary flow, HT is reduced and the differences level builds up with rotation number. Especially in mid-pass inner wall

adjacent neighborhood (region 14), HT of β=45° case is substantially cut down to 60%, 50%, and 40% of the values observed in β=90°case (Ro=0.32, leading, trailing, and inner wall surfaces respectively). HT in region 15 (mid-pass inner slot adjacent) shows similar yet thinner trends. HT of β=45° case is reduced to 80%, and 60% of the levels observed in β=90° case (Ro=0.32, leading, and trailing surfaces respectively).

2.5 Discussion of Results – Roughened Surface

2.5.1 Streamwise Nu Ratio Distribution Results – Stationary

The Nu_s/Nu_0 ratio distributions in the stationary channel at Re=20,000 is presented in **Figure 22**. All regions are shown except region #1, region #18, and #19. Data in above three regions were biased because of different and more complex flow behavior in these regions. Data from region#10, #12, #14, and #16 were averaged with #11, #13, #15, and #17 from the same surface, respectively. Region #1 and #2 both encountered strong entrance effect, which is the dominate factor for the flow behavior at the entrance. Thus the other effects, such as rotating effect or effect of ribbed induced flow are small in these regions. Region #18 and #19 are at the end of the third passage. Due to the ejection and the flow towards the closed end of passage, the flow behaviors in these two regions are different from other regions. From **Fig 22(a)**, the heat transfer at hub turn region increased on the leading surface (LE) is about 10% with turning vane. As to trailing surface (TR) at hub turn, the heat transfer decreased with a maximum about 12% at the first half of turn, and then increased about 4% at the second half of turn with the

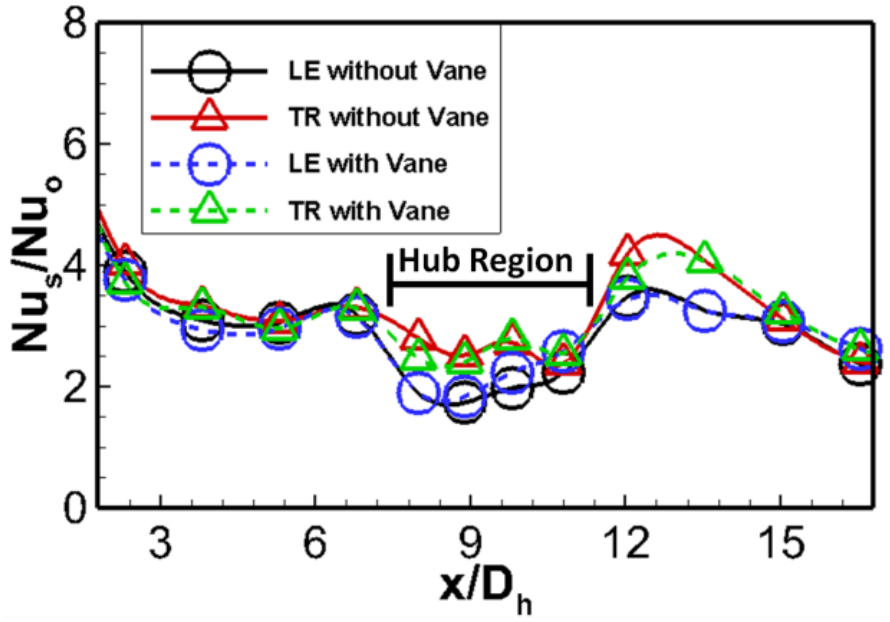

(a)

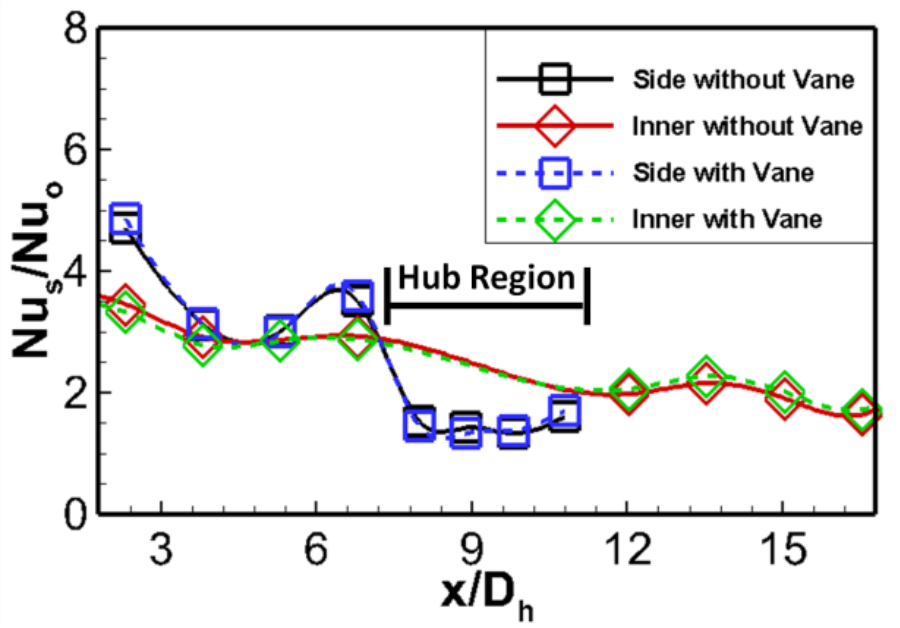

(b)

Figure 22 Effect of turning vane on stationary streamwise Nu ratio (Nu_s/Nu_0) distributions at Re=20k for (a) leading and trailing surfaces and (b) for side and inner walls

presence of turning vane. As shown in **Fig 22(b)**, heat transfer at hub side wall is very low. In **Fig 22(a)** & **(b)**, the presence of turning increased heat transfer in 3rd passage at Inner wall and TR slightly, but no effect on LE. On the side wall in **Figure 22(b)**, the heat transfer at the second passage was relatively higher compared to that of inner wall. This difference in heat transfer on two surfaces was due to the rib-induced vortices, which impinged the mainstream cold fluid on the side wall. In the hub turn portion, heat transfer dropped significantly. Nu_s/Nu_0 ratio in second passage for every surface is about 3, and then it dropped to about 2 for LE, 2.5 for TR and about 1.3 for Side wall. The absence of ribs would be the major reason for the dramatic heat transfer drop. Also, a difference between heat transfer of the leading surface and trailing surface was observed. This may be due to the staggered configuration of ribs at two surfaces, and the continuation of rib effect while flow enters the turn portion. On the leading and trailing surfaces of the third passage, Nu_s/Nu_0 restored to the level it was before the U-bend and went even higher. This enhancement may come from the combination of ribs, pin-fin array and slot ejection. However, heat transfer at Inner wall of 3rd passage is reduced compared to 2nd passage. This may result from the effect of ejection. The presence of turning vane slightly increased heat transfer at Inner wall in 3rd passage. Comparing the third passage with [7], The Nu/Nu_0 is considered at the same level except for the end of the channel. In [7], there is no pin-fin array or slot ejection. It is considered that pin-fin array and flow induced by ejections enhanced the heat transfer, while the mass loss from the ejection reduced heat transfer. These combined factors resulted in the similar level of Nu/Nu_0 for the start of the third in [7] and current study. At the end of the channel, heat

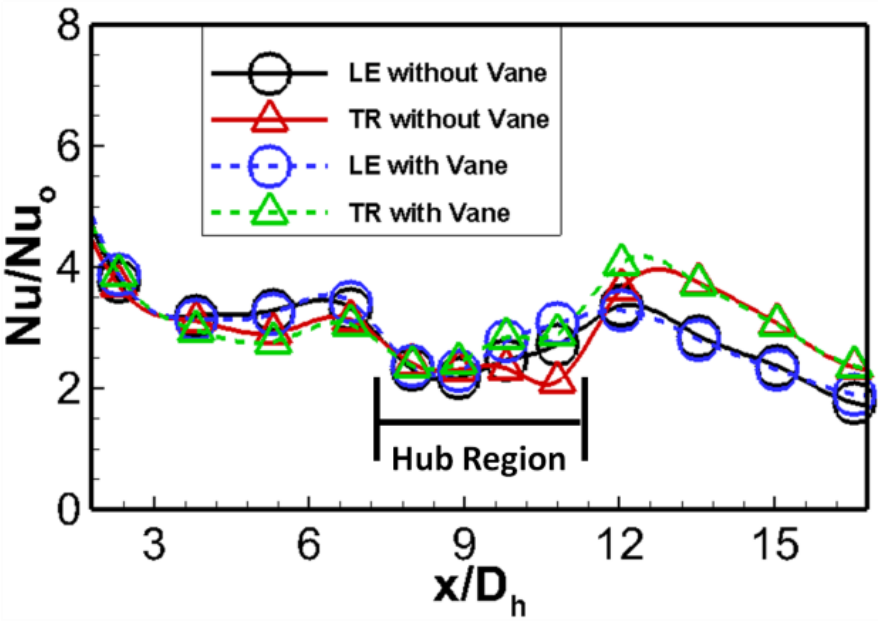

(a)

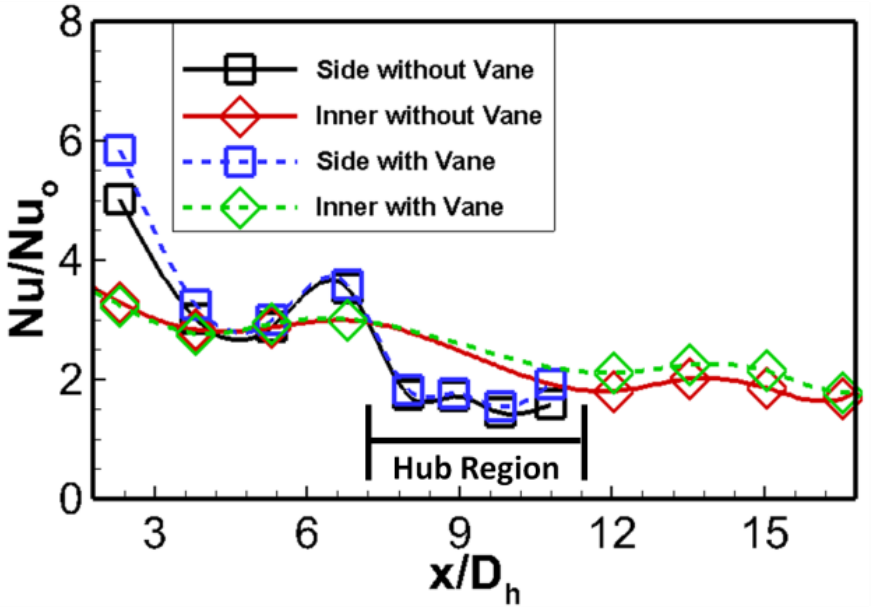

(b)

Figure 23 Effect of the turning vane on streamwise Nu ratio (Nu/Nu_0) distributions under rotating conditions (rpm=300, Ro=0.16) at Re=20k, and β=90° for (a) leading and trailing surfaces and (b) for side and inner walls

transfer eventually dropped due to mass loss of flow by ejection. These combined factors resulted in the similar level of Nu/Nu_0 for the beginning of the third in [7] and current study. At the end of the channel, heat transfer eventually dropped due to mass loss of flow. In the hub turn portion, heat transfer showed some difference between the two cases on the leading and trailing surfaces and on the hub wall. However, the increase was only about 10% after the vane was applied. In the third passage, on all surfaces, Nu_s/Nu_0 ratios increased about 10% after the application of turning vane.

2.5.2 Streamwise Nu Ratio Distribution Results –Rotating

Figure 23 illustrates the Nu/Nu_0 ratio distributions in the channel at Re=20,000 and RPM=300 for cases with and without turning vane at $\beta=90^o$. Similarly, all regions are shown in streamwise direction, except for region #1, region #18, and #19 because of different flow behavior. Comparing with **Figure 22 (a)**, in the second passage, which was with radially inward flow, heat transfer on the leading surface was elevated, while it was reduced on trailing surface. The rotating effect was reversed in the third passage, which had a radially outward flow. In the turn portion, heat transfer on the leading surface was increased, and the difference on heat transfer between the leading surface and trailing surface was reduced.

According to **Figure 23**, the turning vane did not affect the upstream flow and heat transfer behavior much, which was similar to the stationary channel shown in **Figure 22**. In the hub turn portion, heat transfer on the leading and trailing surfaces was

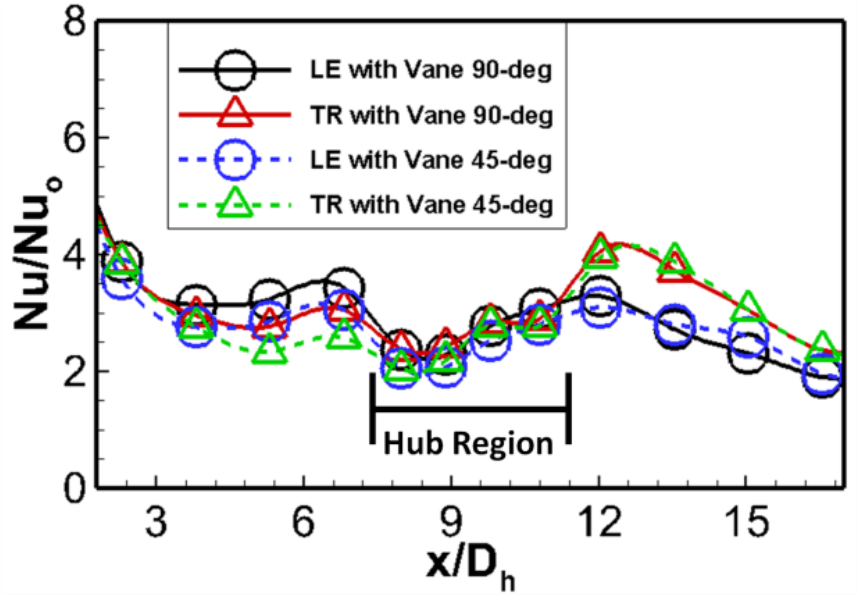

(a)

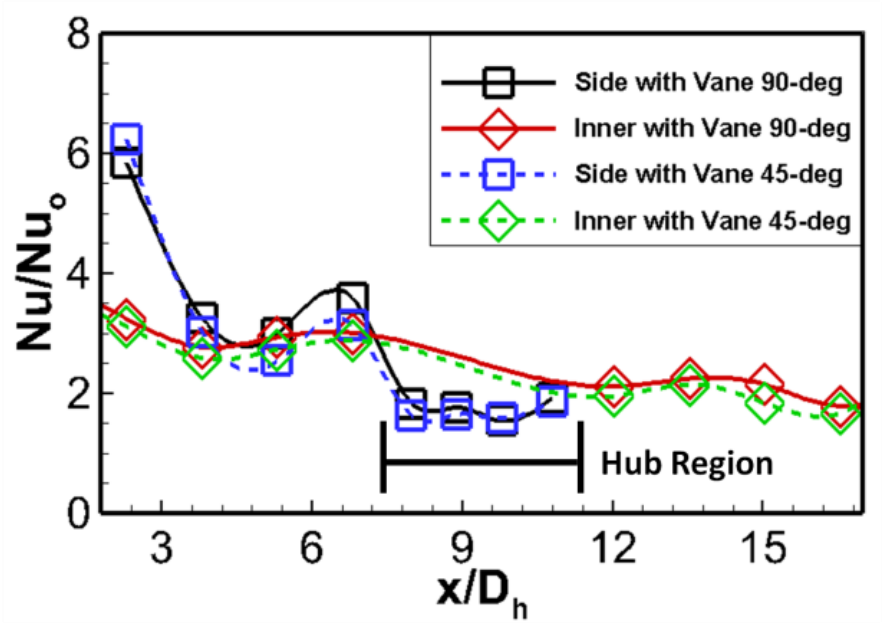

(b)

Figure 24 Effect of channel orientation (β=90° and 45°) on streamwise Nu ratio (Nu/Nu_0) distributions under rotating conditions (rpm=300, Ro=0.16) at Re=20k for (a) leading and trailing surfaces and (b) for side and inner walls

enhanced about 8% and 15% respectively with presence of turning vane, as well as on hub wall about 8%. It is shown that rotation enhanced the heat transfer at hub side wall by comparing **Fig 23 (b)** & **22 (b)**. In the third pass, Nu ratio was similar on the leading and trailing surfaces when the vane was applied, while it increased on the inner wall. Turning vane effect was small on leading and trailing surfaces under rotating condition at the third passage.

2.5.3 Streamwise Nu Ratio Distribution Results – Channel Orientation Angle

Figure 24 illustrated the effect of the channel orientation angle on streamwise Nu/Nu_0 distribution. Orientation angles of $\beta=90^o$ and 45^o were shown at Re=20,000 and RPM=300 for the case of with turning vane. It was shown that, compared to the heat transfer at $\beta=90^o$, streamwise Nu/Nu_0 at $\beta=45^o$ decreased on all surfaces in second passage. However, the differences between leading and trailing surfaces for two β angles were similar. The β effect on hub side wall on heat transfer is negligible, but heat transfer at leading and trailing surface were lower when β=45°. In the third passage, heat transfer slightly increased at LE and TR, but decreased at Inner wall. The difference on heat transfer between leading and trailing surface at the 3rd passage was larger when $\beta=90^o$ than that when $\beta=45^o$. The result suggested that rotation effect on heat transfer reduces when $\beta=45^o$.

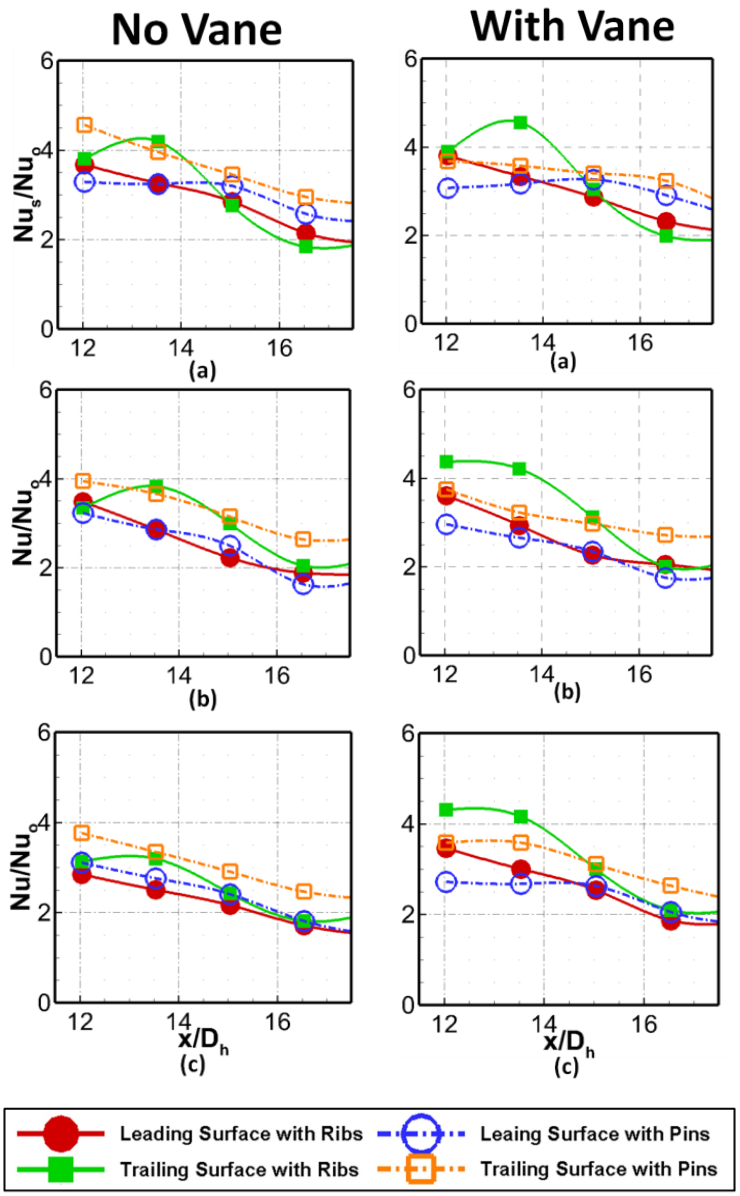

Figure 25 Nusselt number ratio distributions in the third passage for (a) Stationary at Re=20k, and β=90°; (b) Ro=0.16, Re=20k, and β=90°; (c) Ro=0.16, Re=20k, and β=45°

2.5.4 Nu Ratio Distribution Results in the Third Passage

Figure 25 showed the Nusselt number distributions in the third passage with rib and pin-fin roughened area respectively for (a) stationary Ro=0, at Re=20,000, and β=90°; (b) Ro=0.16 at Re=20,000, and β=90°; (c) Ro=0.16 at Re=20,000 and β=45°, for with and without turning vane cases. The difference on heat transfer between rib and pi-fin region at leading surface is smaller comparing to that at trailing surface. This may due to the staggered rib arrangement between leading and trailing surfaces resulting in different flow behaviors at two surfaces. Comparing (a) & (b) for both with and without turning vane cases, rotation slightly decreased heat transfer at leading surface for both rib and pin-fin region. Heat transfer at rib region on trailing surface slightly decreased and then increased along the passage at rotating condition comparing to stationary. Heat transfer is slightly lower at pin-fin region on trailing surface at Ro=0.16. Comparing between two channel orientation angles for without turning vane case, β=45° has slightly lower heat transfer in general. Comparing between two channel orientation angles for with turning vane case, difference on heat transfer is small. Turning vane affected on heat transfer more at lower x/D_h locations, where is closer to the turning vane. It enhanced heat transfer at ribbed regions on both surfaces, especially at β=45°. For pin-fin roughened area, turning vane decreased heat transfer at first two regions right after turn, and difference on heat transfer at large x/D_h locations for pin-fin region is small.

2.5.5 Nu/Nu_s ~ Ro Correlation – Rotation Effect

The rotation number (Ro) as defined in Eq. (7) indicates that different values of this number can be achieved by varying a combination of rotational speed and mainstream flow velocity. The rotation number in this study varied from 0 to 0.32 as shown in **Figure 11**. The effect of rotation on heat transfer (Nu/Nu_s) is illustrated as a function of the rotation number from region #4 to #15 in **Figure 26** ~ 3**0**. The effects of rotation can be compared with the stationary Nusselt number (Nu_s) as the denominator. The effect of channel orientation and the Nu ratio change with rotation number at given surface and region are observed in the figures. By comparing with vane and without vane cases at given surface and region, the turning vane effect can be obtained. By comparing Nu ratio As shown in **Figure 26**, flow at the second passage was radially inward, and the rotation effect in this passage wasshown to increase Nu/Nu_s on the leading surface around 10% at Ro~0.2. Nu/Nu_s on trailing surface decreased at low Ro and then increased at larger Ro. It was decreased about 10% at Ro~0.2. Moreover, heat transfer on the side wall decreased and then increased with Ro. Nu/Nu_s decreased with increasing Ro. Compared to the $\beta=90^o$, a lower Nu/Nu_s is found for $\beta=45^o$ at all surfaces. Effect of turning vane is negligible. at leading surface and trailing surface, rotation effect to radial inward or outward flow can be obtained.

Figure 27 shows the correlation between Nu/Nu_s and Ro in regions #7, i.e. the first half of the U-bend. For the case without vane, rotation increased the heat transfer on the

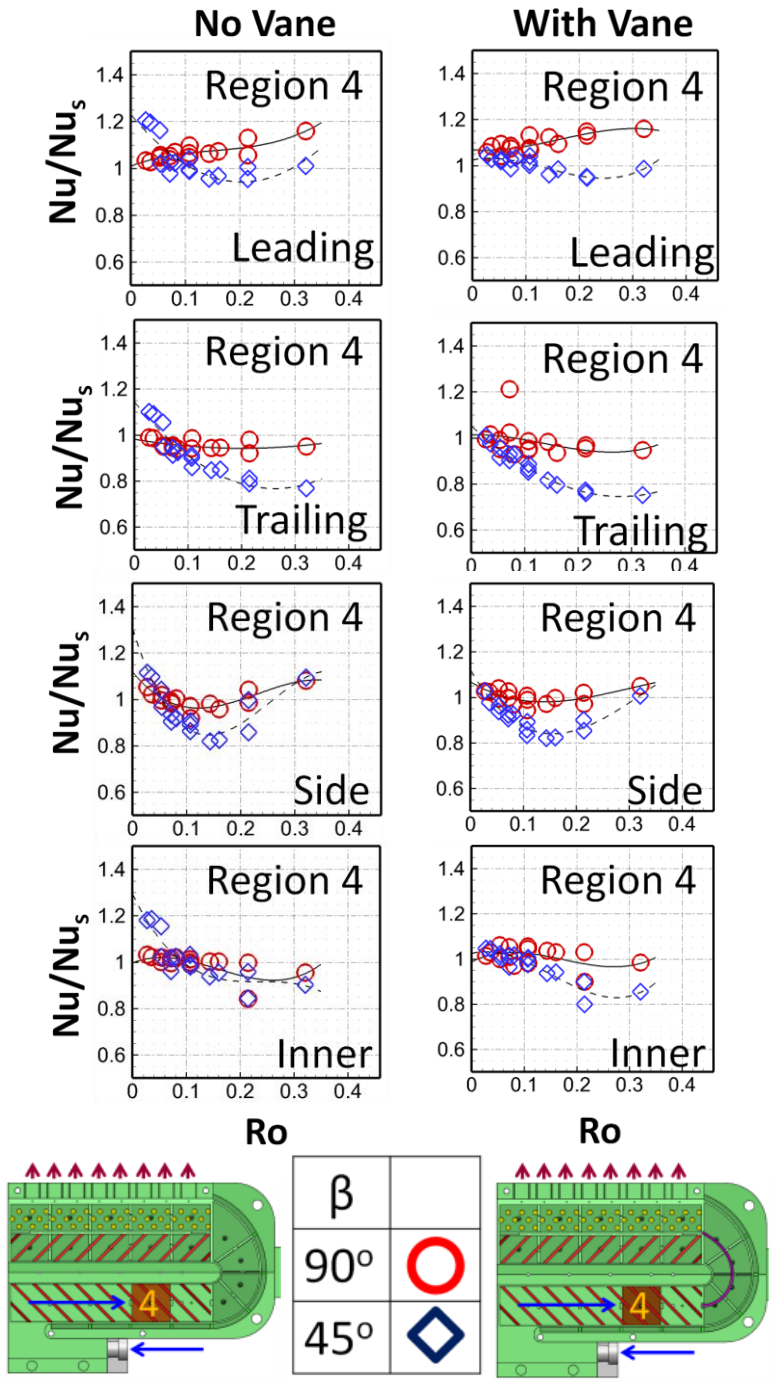

Figure 26 Nu ratio (Nu/Nu_s) distribution as a function of rotation number (Ro) on all surfaces for β=90° and 45° at regions #4 for cases (a) without vane (b) with vane

leading surface about 35% at Ro~0.2; and it decreased the heat transfer on trailing surface for about 15% at Ro=0.32. On the hub sidewall, heat transfer first decreased and then increased with Ro, and it increased up to 20% when Ro~0.2. For the case with turning vane, it was seen that the effect of rotation on heat transfer was reduced by the turning vane on leading surface. Nu/Nu_s only increased up to 30% at Ro~0.2. On trailing surface, heat transfer is enhanced by turning vane. It decreased only 5% at Ro=0.32. The effect of rotation on heat transfer was large on the hub side wall. It decreased and then increased around 30% at Ro~0.2. $\beta=45^o$ has lower heat transfer than $\beta=90^o$ on all surfaces for both with and without turning vane cases.

Figure 28 presents the correlations between Nu/Nu_s and Ro in regions #9, i.e. the second half of the U-bend. For the case without turning vane, rotation increased the heat transfer on the leading surface. Nu/Nu_s ratio is about 30% at Ro~0.2. For the trailing surface, heat transfer decreased and then increased with increasing Ro. Nu/Nu_s ratio on trailing edge is about 1 at Ro=0.32. On hub side wall, heat transfer also decreased first at low Ro, and then increased. For with turning vane case, heat transfer at TR is enhanced by turning vane. It is also observed that rotation effect on the heat trans fer was reduced since the difference on heat transfer between LE and TR is reduced with presence of turning vane. Turning vane helped to increase heat transfer at hub side wall.

Compared to $\beta=90^o$, the $\beta=45^o$ had lower heat transfer. Correlations between Nu/Nu_s and Ro at region #14 in the third passage are shown in **Figure 29**, and correlations at region #15 are shown in **Figure 30**. Rotation effect at region #14 increased the heat transfer on the trailing surface. Heat transfer decreased and then

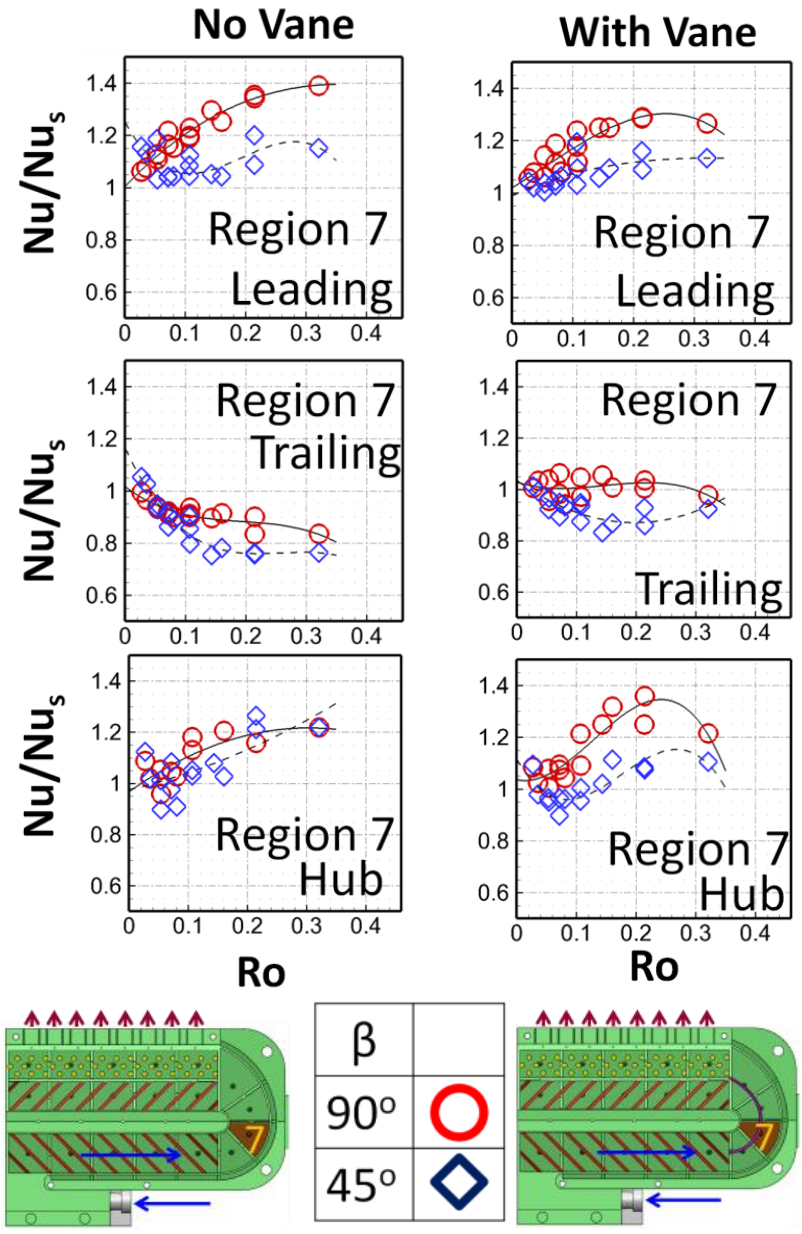

Figure 27 Nu ratio (Nu/Nu_s) distribution as a function of rotation number (Ro) on all surfaces for β=90° and 45° at regions #7 for cases (a) without vane (b) with vane

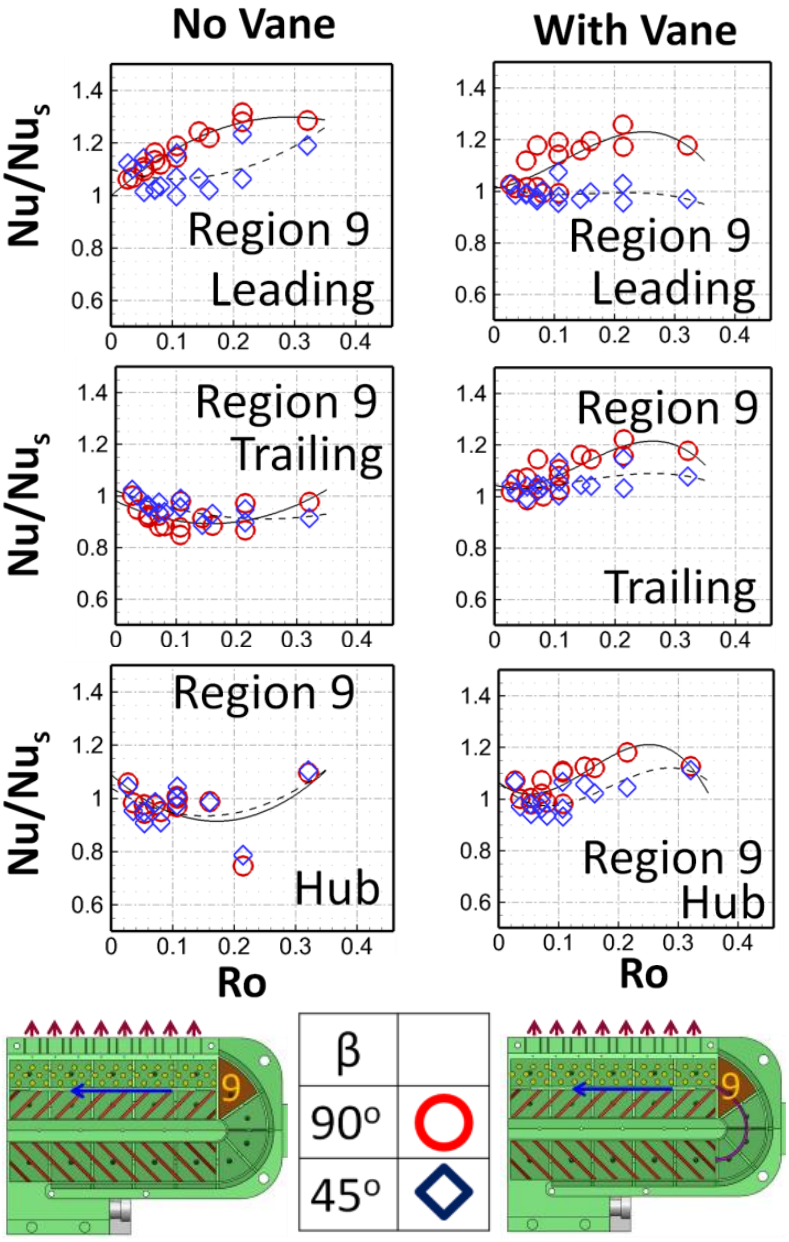

Figure 28 Nu ratio (Nu/Nu_s) distribution as a function of rotation number (Ro) on all surfaces for β=90° and 45° at regions #9 for cases (a) without vane (b) with vane

increased on the leading surface. The rotation effect was just opposite to regions #4 due to different flow direction in passages. Heat transfer at Inner wall increased with Ro, and the Nu/Nu_s ratio is about 1.4 at Ro = 0.32. Effect of turning vane is negligible in this region. Comparing with $\beta=90^o$ case, $\beta=45^o$ has lower Nu/Nu_s ratio at trailing surface and inner wall, especially at inner wall. Nu/Nu_s ratio decreased with Ro when $\beta=45^o$, while it increased when $\beta=90^o$.

In region #15, heat transfer on the leading surface shows large decrement with increasing Ro. Nu/Nu_s ratio dropped significantly to 0.6 at Ro~0.2. Nu/Nu_s ratio at trailing surface was decreased and then increased. Turning vane effect was negligible for leading surface. Presence of turning vane decreased heat transfer at TR when $\beta=90^o$, but increased it when $\beta=45^o$. For without turning vane case, lower heat transfer enhancement is found at TR for $\beta=45^o$ comparing with $\beta=90^o$ case, while it is higher for with turning vane case. Difference on Nu/Nu_s ratio between two β angles is small at LE.

2.5.6 Conclusion – Roughened Surface

Heat transfer in a rib and pin-fin roughened two-pass rotating channel with trailing edge slot ejection was studied for two orientation angles ($\beta=90^o$ and 45^o). Reynolds numbers change from 10,000 to 40,000, and Rotation numbers are from 0 to 0.32. Based on the result, it was concluded as following:

1. For the stationary roughened channel (Re=20,000), with presence of the turning vane, in the hub turn portion, Nu_s/Nu_0 ratio on leading surfaces was elevated by 10%, while that on trailing surface decreased. Heat transfer at side wall was low.

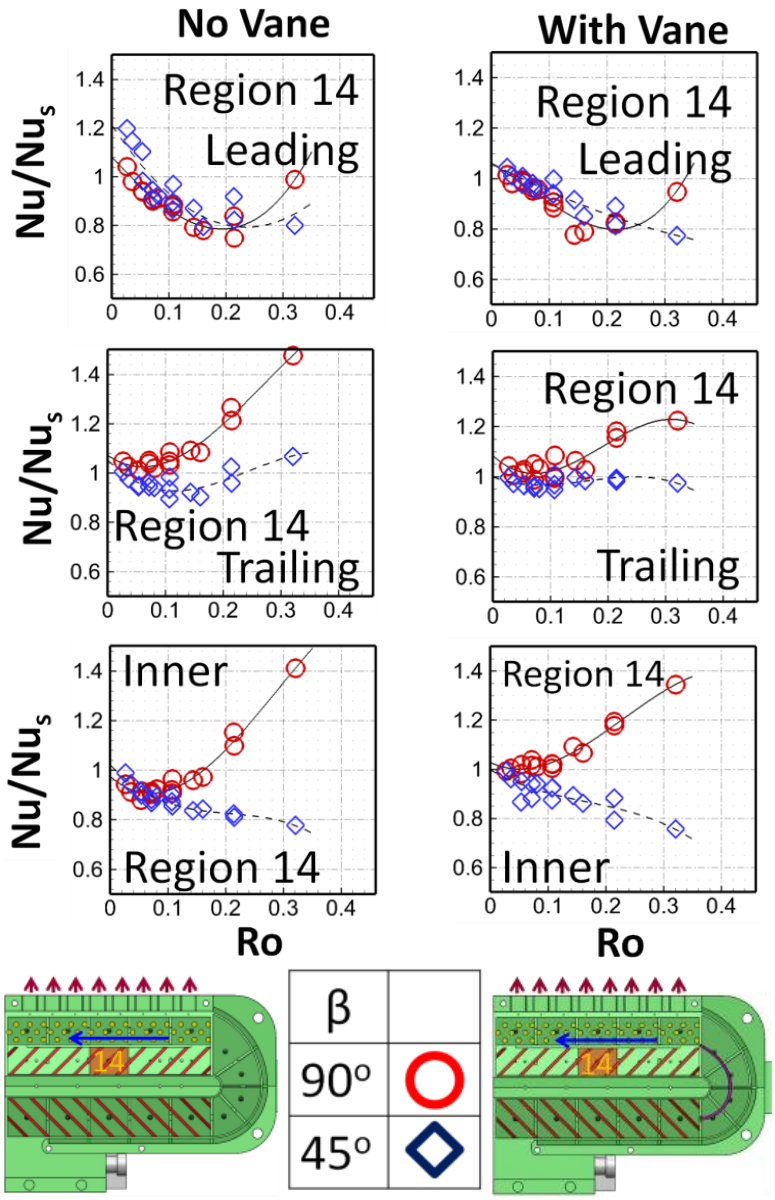

Figure 29 Nu ratio (Nu/Nu_s) distribution as a function of rotation number (Ro) on all surfaces for β=90° and 45° at regions #14 for cases (a) without vane (b) with vane

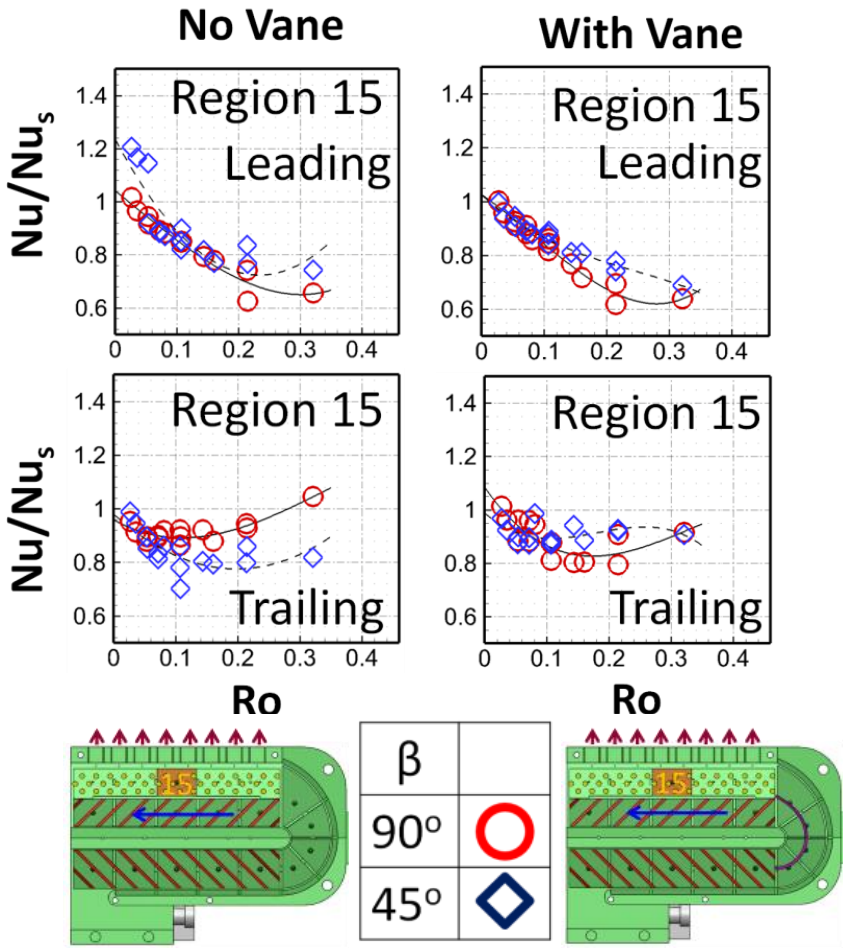

Figure 30 Nu ratio (Nu/Nu_s) distribution as a function of rotation number (Ro) on all surfaces for β=90° and 45° at regions #15 for cases (a) without vane (b) with vane

In the third passage, Nu_s/Nu_0 ratio increased up to 10% on leading trailing surfaces as well as on inner wall.

2. From stationary streamwise Nu_s/Nu_0, it is observed that pin-fin array, flow induced by ejection, and loss of air have a combined effect. Nu_s/Nu_0 ratio in the third passage gradually decreased toward the end of the channel.
3. For rotating condition, presence of turning vane reduced the difference on heat transfer between LE and TR surfaces, and enhanced heat transfer on the trailing surface and hub side wall in the turn region.
4. Nu/Nu_s ~ Ro correlation existed on all surfaces in the second passage, hub turn, and third passage of the roughened channel. In the second passage with radially inward flow, Nu/Nu_s ratio increased on the leading surface and decreased on the trailing surface. In the third passage with radially outward flow, on the contrary, Nu/Nu_s decreased on the leading surface and increased on the trailing surface. In the hub turn region, the Nu/Nu_s difference between leading and trailing surface was small.
5. From Nu/Nu_s ~ Ro correlation, channel orientation $\beta=45^o$ reduced heat transfer when comparing with $\beta=90^o$ in general, particularly the inner surface in the third passage at region 14.
6. From **Figure 25**, turning vane had more effect at the areas closer to the turn. Generally, turning vane enhanced heat transfer at ribbed regions on both leading and trailing surfaces, while decreased heat transfer at pin-fin region on both surfaces. However, the increment at ribbed region due to turning vane was larger at $\beta=45^o$ compared with $\beta=90^o$.

3. TIP TURN CHANNEL

3.1 Experimental Setup

3.1.1 Rotating Facility - Tip Turn Channel

The rotating rig for the tip turn channel is shown in **Figure 31** [12], which is very similar to the rig for the hub turn channel. The only difference is the way of connection between the base plate of the pressure vessel and test section. Tip turn channel is directly attached to the base plate with passages covering the inlet and exit of the coolant air on the base plate. The hub turn channel attached on the base plate with a connecting joint. There are fittings at the coolant inlet and exit on the base plate, and the air inlet of the test section is connected to the inlet fitting on the base plate with a rubber hose.

3.2 Test Section Geometry

Figure 32 shows the two-passage test section with tip turn. The flow in the first passage is radially outward, while the flow in the second pass is radially inward. Passages are divided by copper plates. The test section is divided into twelve regions in total in streamwise direction as shown in **Figure 32(c)**. Each surface consists of six regions, except for inner walls, which have 5 regions as shown. The hydraulic diameter of each passage is 16.9 mm, the same as the hydraulic diameter of the second passage of the hub turn test section. The overall length of test section is 203.0 mm and the distance between rotation axis and center of test section is 660.4 mm. There is 46.0 mm in length unheated area at inlet and exit of test section, and the heated length of both passages is

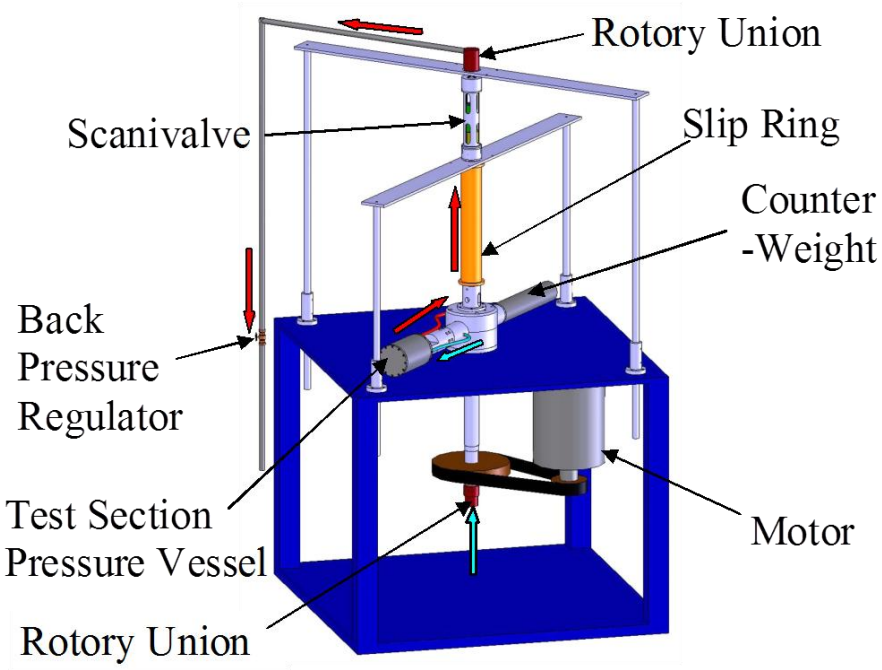

Figure 31 Rotating facility for the tip turn channel [12]

157.0 mm. There is one thermocouple placed at the inlet and exit of test section respectively to measure the air temperature.

The roughened configuration is the same as the rib configuration of the second passage of the hub turn test section. Straight squared copper ribs with P/e = 8, e/D_h = 0.1, and $\alpha = 45^o$ are attached on leading and trailing surfaces of the first and second passages by a very thin layer of super glue. The ribs are parallel to each other, and in stagger arrangement between leading and trailing surfaces.

The thickness of all copper plates is 3.175 mm. Dimensions of copper plates along the passages at leading and trailing surfaces are square and measured 23.81 mm x 23.81 mm. Copper plates in the turn regions (#6 & #7) on both leading and trailing surfaces are measured 28.58 mm x 28.58 mm, and with fillet 6.35 mm at the inner corner. Copper plates on outer and inner wall are rectangular and are measured 23.81 mm x 12.70 mm. Copper plates at tip region (tip cap #6 & #7) are measured 29.37 mm x 12.70 mm. Blind holes, with a diameter of 1.59 mm, are drilled 1.59 mm deep on the backside of each copper plate. Thermocouples are placed inside of the blind holes, which are with a diameter of 1.59 mm and 1.59 mm deep, on the bottom of copper plates and are affixed to the copper plates using highly conductive epoxy. The channel orientation angle (β) in the study is 90^o as shown in **Figure 32 (b)**. The range of Reynolds numbers tested is from 10,000 to 40,000, rotating speed is from 0 to 400 rpm, and the corresponding rotation number is from 0 to 0.42.

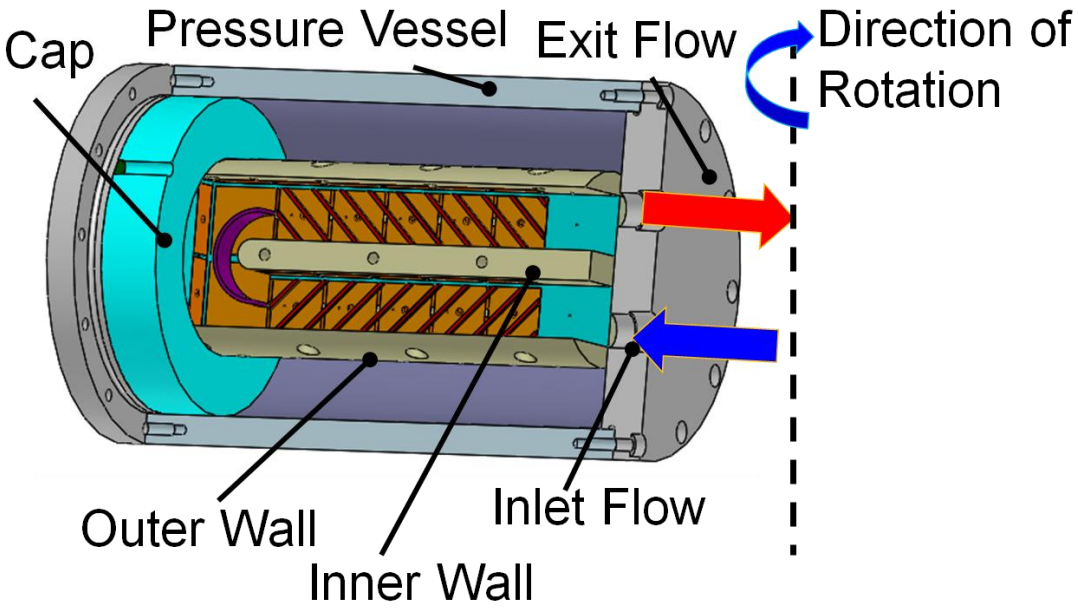

(a)

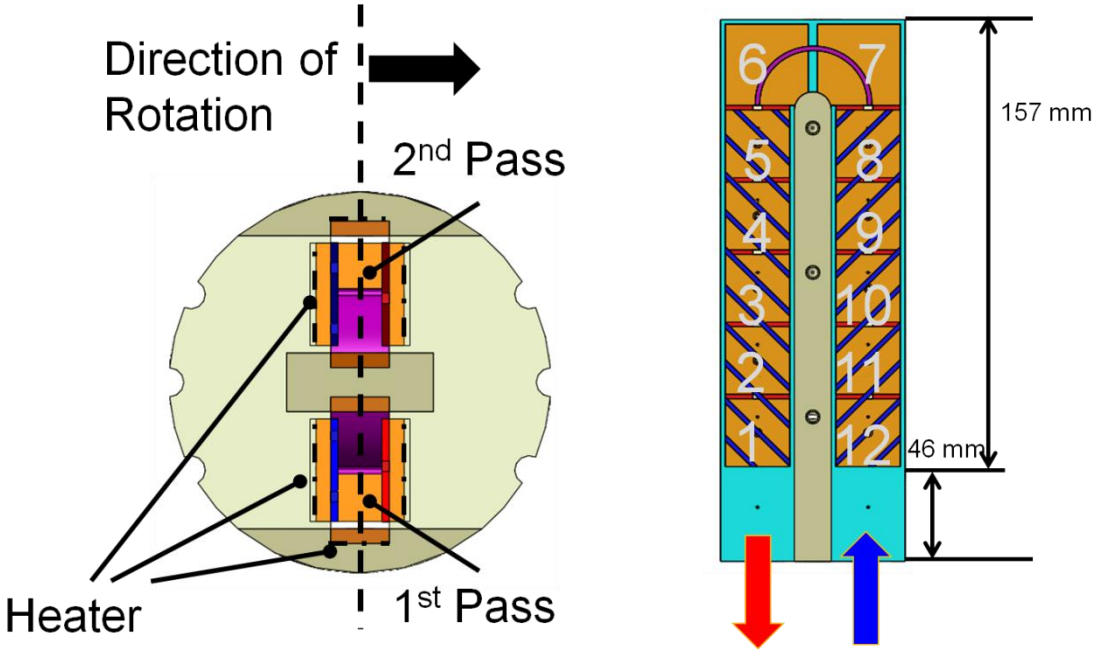

(b) (c)

Figure 32 Test section inside pressure vessel

3.3 Data Reduction

Only heat transfer measurement with roughened surface is performed under both with vane and without vane conditions. Methodology and governing equations are the same with the heat transfer measurement of hub turn test section as described in Ch 2.3..

3.4 Discussion of Results

3.4.1 Streamwise Nu Ratio Distribution Results -Stationary

Since the inlet of the test section is rectangular, and the inlet on pressure vessel base plate is circular with a diameter of the height of passage, the flow will expand after entering the passage before heating. Entrance effect may play a role at the first few regions near entrance. Although there is no Coriolis and the rotational buoyancy forces while the test section is stationary, the rib effects, such as mainstream flow separation, recirculation and reattachment, turbulent mixing, and angled rib-induced secondary flow still exist.

The Nusselt ratio distributions in the stationary channel at Re=20,000 is shown in **Figure 33**. The Nu_s/Nu_o ratio experiences a decrease and increase on leading and trailing surfaces in the first passage. The decrease on heat transfer may be a result from the entrance effect, while the increase after it maybe result from the rib induced secondary flow. Heat transfer drops significantly at the turn portion on leading and trailing surfaces due to lack of ribs at the turn area. For without turning van case, heat transfer at tip side wall is even lower. With presence of turning vane, heat transfer on both leading and trailing surface at the second half of the turn (region 7) are lower compared to without

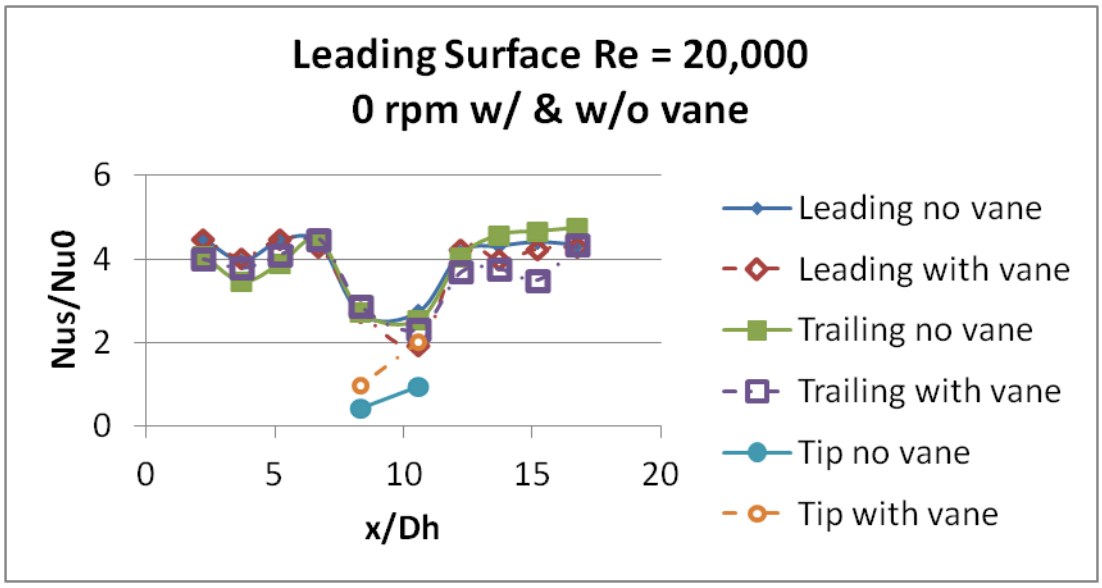

Figure 33 The Nusselt ratio distributions in the stationary channel at *Re*=20,000 for with and without turning vane cases

vane case. Heat transfers at the third passage on leading and trailing surfaces are also reduced with the presence of turning vane. Heat transfer at tip side wall (region 6 & 7) are significantly increased with turning vane.

3.4.2 Streamwise Nu Ratio Distribution Results -Rotating

Streamwise Nu/Nu_o ratio distribution on leading and trailing surfaces at Reynolds number of 20,000 and 400 rpm are presented in **Figure 34**. At turn portion, rotation enhanced the heat transfer on trailing surface, as well as on tip side wall when comparing **Figure 33** and **34**. On leading and trailing surfaces at turn portion, the Nu/Nu_o ratio increased at thr first half of turn (region 6), while decreased at the second half of the turn (region 7) with the presence of turning vane, like the stationary case. Tip side wall at the second half of the turn (region 7) is significantly enhanced with turning vane. Heat transfers on both leading and trailing surfaces at the second passage are highly elevated with turning vane.

3.4.3 Effect Of Rotation Number

The rotation number (*Ro*) as defined in Eq. (7) can be achieved by different combinations of rotational speeds and Reynolds numbers. The range of rotation number in this study is from 0 to 0.42. **Figure 35** is the correlation between the effect of rotation on heat transfer (Nu/Nu_s) and rotation number at region #3 and #5, which are in the first passage. The stationary Nusselt number (Nu_s) is the denominator for the ease of comparing the rotation effect.

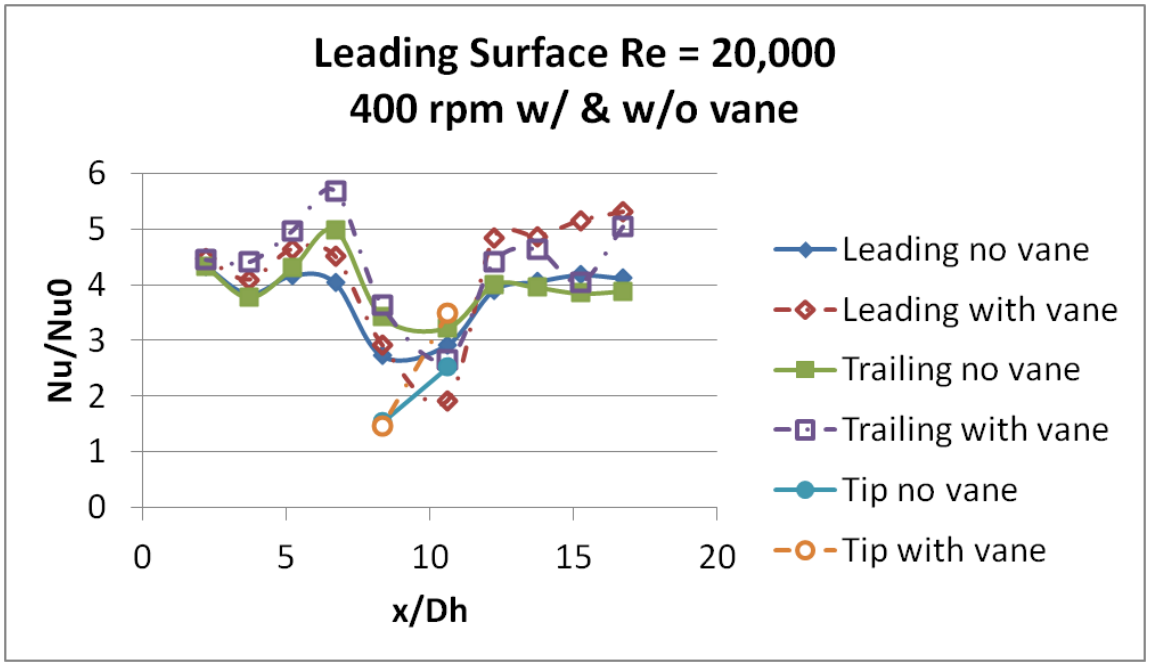

Figure 34 The Nusselt ratio distributions in the stationary channel at *Re*=20,000, 400 rpm for with and without turning vane cases

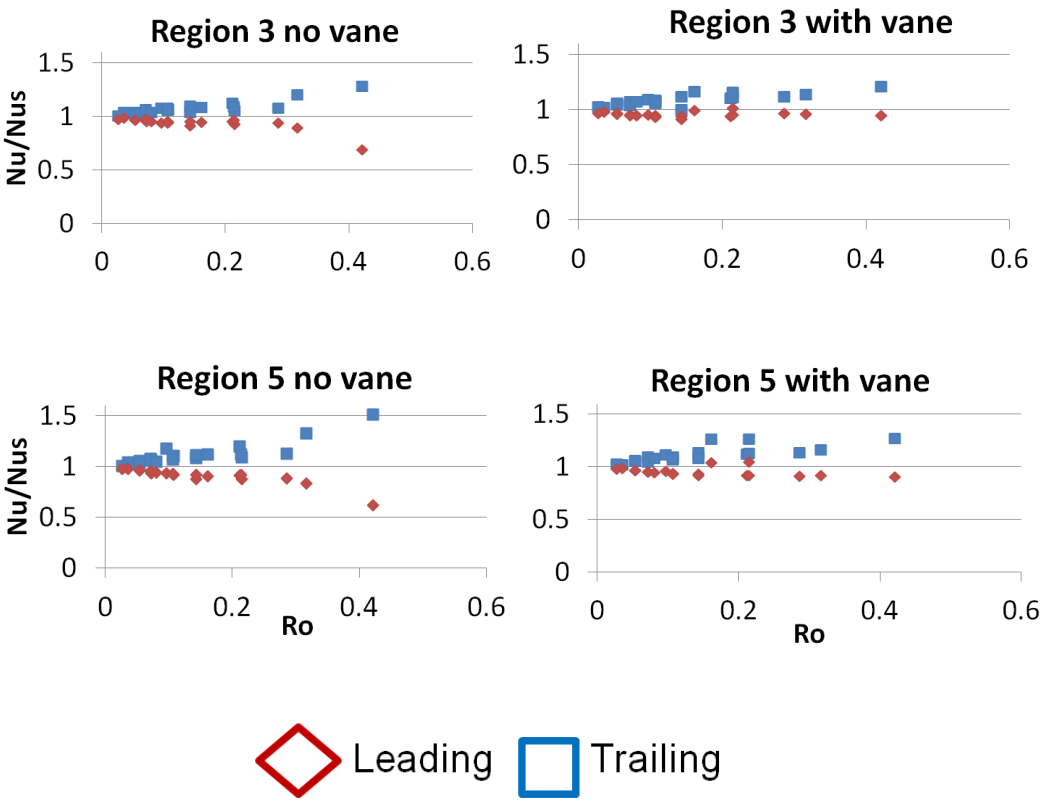

Figure 35 Nu/Nus distribution vs rotation number on all surfaces at region #3 & 5

In the first passage, which is the radially outward flow, the Nu/Nu_s ratio on the trailing surface increases up to 25% with increasing rotation numbers, while the Nu/Nu_s ratio on leading surface decreases up to 35% with increasing rotation numbers. This result is consist with conclusions of previous studies on the rotation effects. Although the regions are upstream of the turning vane, it seems that turning vane has some effect on the heat transfer enhancement by rotation, especially when the rotation number is high. More studies are needed for the phenomenon here.

Figure 36 shows the correlation between the effect of rotation on heat transfer (Nu/Nu_s) and rotation number on leading and trailing surfaces at tip turn regions, while **Figure 37** shows the correlation at tip side wall. For without vane case, rotation effect on leading surface, trailing surface, and tip side wall all increases with rotation numbers, especially the enhancement on the tip side wall. The presence of turning vane decreased the difference of rotating effect between leading and trailing surfaces. Turning vane also decreased the rotating effect at tip side wall. However, the difference on heat transfer enhancement by rotation at each rotation number between tip side wall 6 and tip side wall 7 is smaller with presence of turning vane. Region 8 and region 10 are at the second passage, which is the radially inward flow. From the Nu/Nus and rotation number correlation shows in **Figure 38**, rotation effect on trailing decreases with increasing rotation number. Effect of turning vane is small.

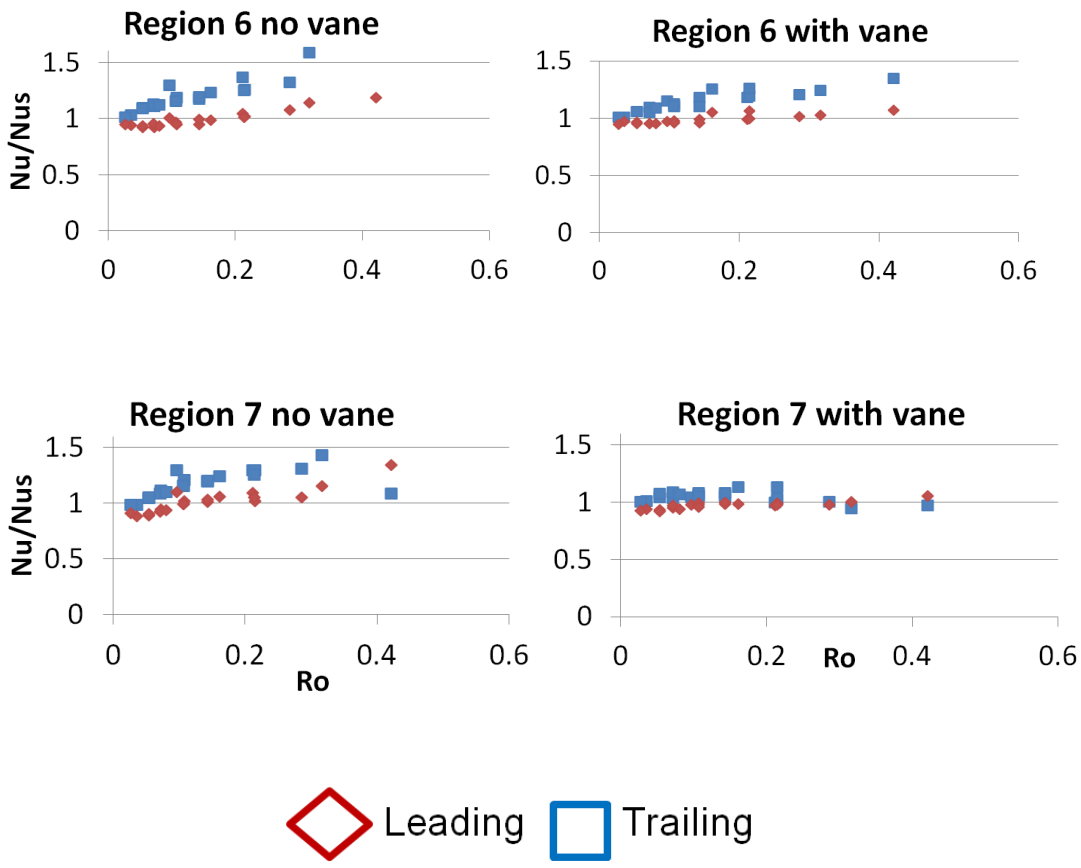

Figure 36 Nu/Nus distribution vs rotation number on all surfaces at region #6 & 7

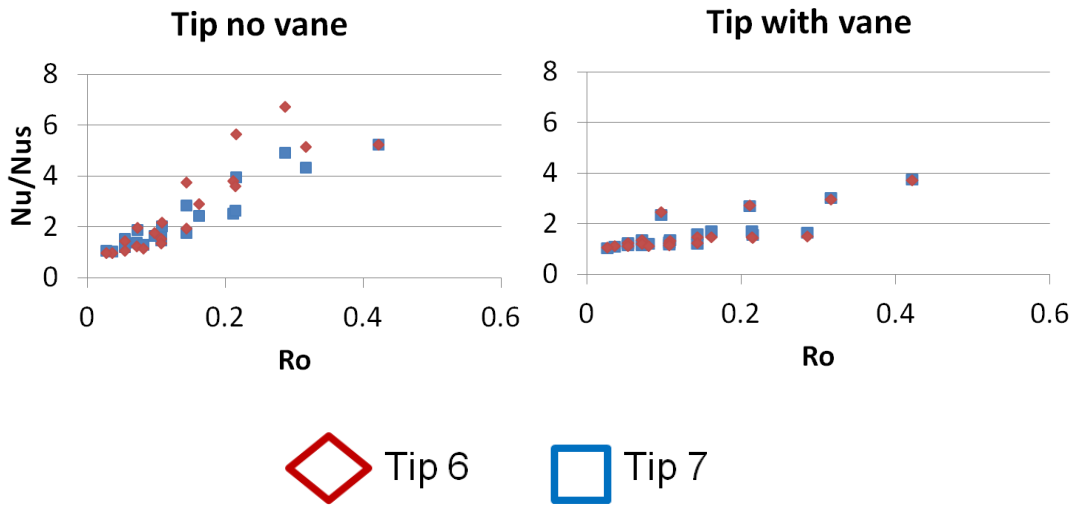

Figure 37 Nu/Nus distribution vs rotation number on all surfaces at tip #6 & 7

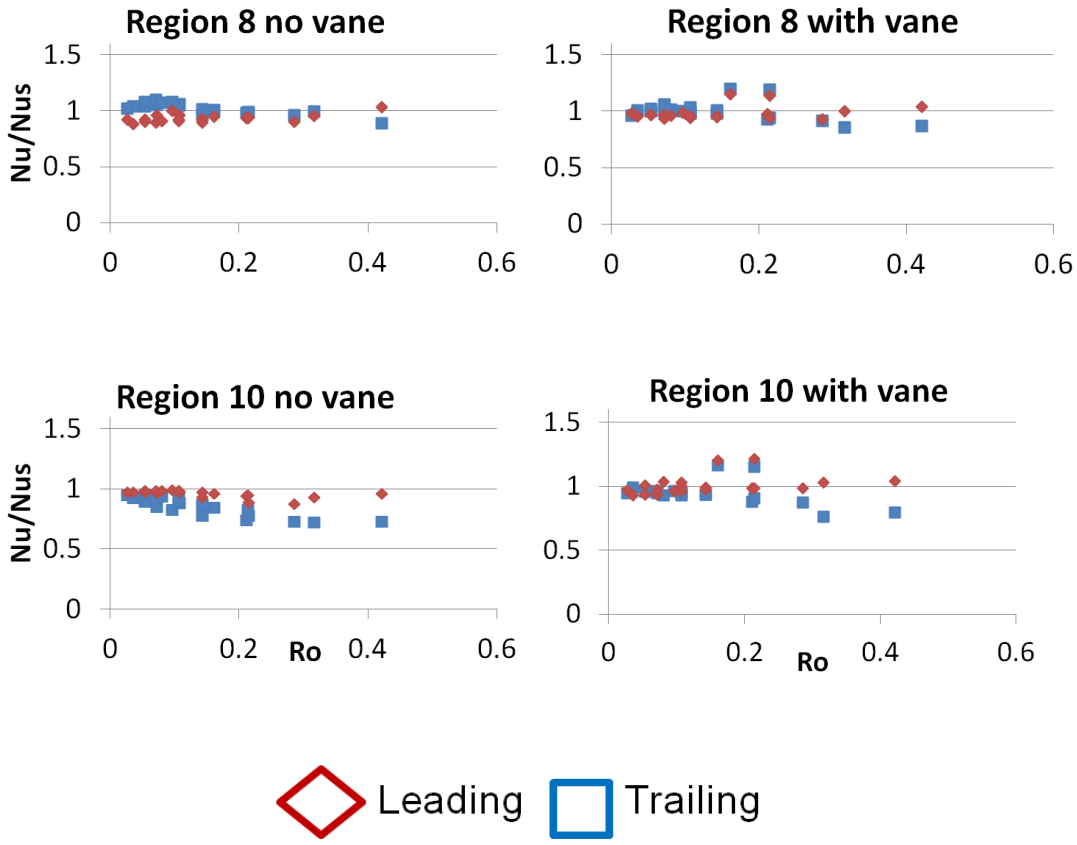

Figure 38 Nu/Nus distribution vs rotation number on all surfaces at tip #8 & 10

3.5 Conclusion – Tip Turn Channel

Current study investigated the effect of rotation in a 2:1 aspect ratio rotating channel with and without turning vane. According to the result reported, the following conclusions can be made:

1. The streamwise Nu_s/Nu_o ratios on leading and trailing surfaces at tip turn regions decrease significantly due to absence of ribs. Nu_s/Nu_o ratio at tip side wall is low.
2. For the stationary case (Re=20,000), presence of turning vane decreases the heat transfer enhancement on leading and trailing surfaces at the second half of turn, as well as that on leading and trailing surfaces at the second passage. However, turning vane increases the heat transfer enhancement on the tip side walls at turn regions.
3. For the rotating case (Re=20,000, 400 rpm), the heat transfer enhancement at tip side wall increases with presenting of turning vane, as well as that on leading and trailing surfaces at the second passage.
4. The effect of rotation is much larger at tip side wall comparing with other surfaces. The increment on rotation effect with respect to rotation numbers is decreased by the presence of on turning vane.
5. For rotating cases, turning vane reduced the difference on rotation effect between leading and trailing surfaces.

4. REAL SCALE ROTATING SERPENTINE CHANNEL

4.1 Experimental Setup

4.1.1 Rotating Facility for Serpentine Channel

The facility for the serpentine channel is a real scale rotating rig. The length of the rotating arm is 100 cm, and the rotating axis is horizontal. The rotating arms are covered inside a steel case, as shown in **Figure 39** [32, 33]. Rotating speed is up to 500 rpm. Instead of air, the working fluid is refrigerant R-134a, which has higher density than air. With higher density and being pressurized, the high rotation numbers can be achieved even with high Reynolds numbers. **Figure 40** [32] shows the R-143a recirculation loop.

4.1.2 Refrigerant R-134a Recirculation Loop

The working fluid of this facility is Freon R134a vapor. The benefit of using R134a vapor as the working fluid is due to its relatively high density. At test condition, which is 4.5 atmospheres, its density is 18kg/m3, comparable to that of air at gas turbine operating conditions. When compressed to same pressure, Freon R-134a can better meet our experimental conditions since its molecular weight is almost four times larger than air. Higher density means lower velocity at given Reynolds number. Calculated maximum Mach number (corresponding with the maximum measured Reynolds number

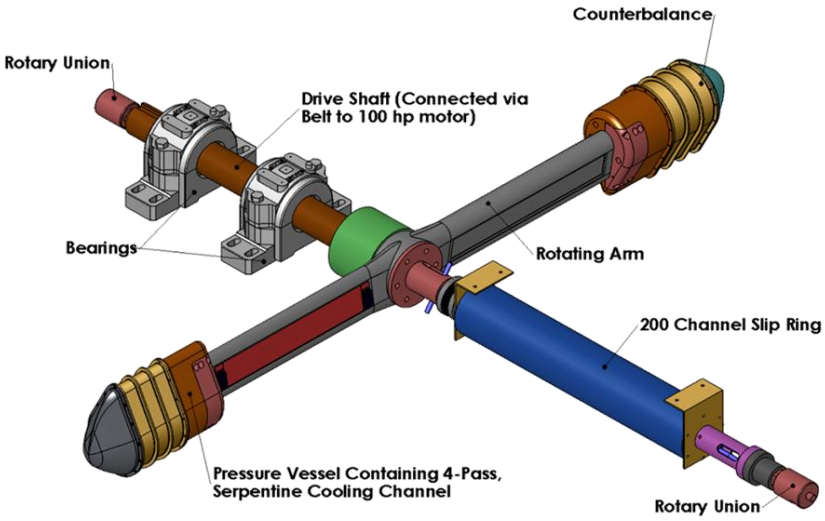

(a) [32]

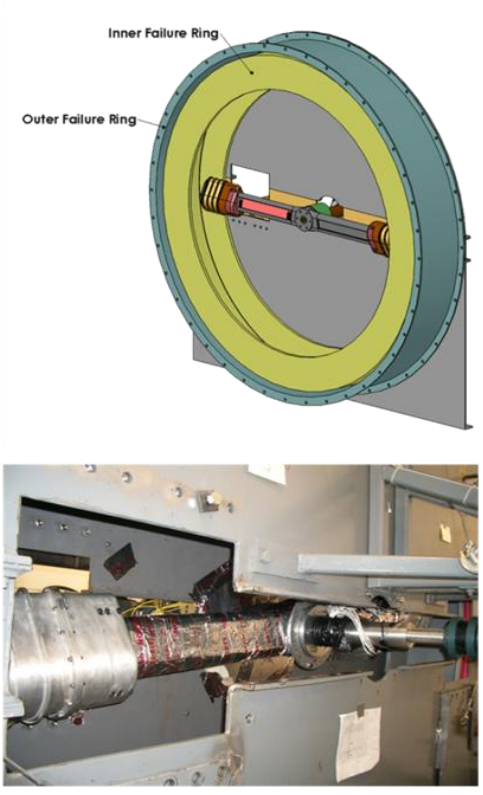

Figure 4 Rotating Rig Assembly -- CAD and Photographic Views

(b) [33]

Figure 39 Real scale rotating facility for serpentine channel.

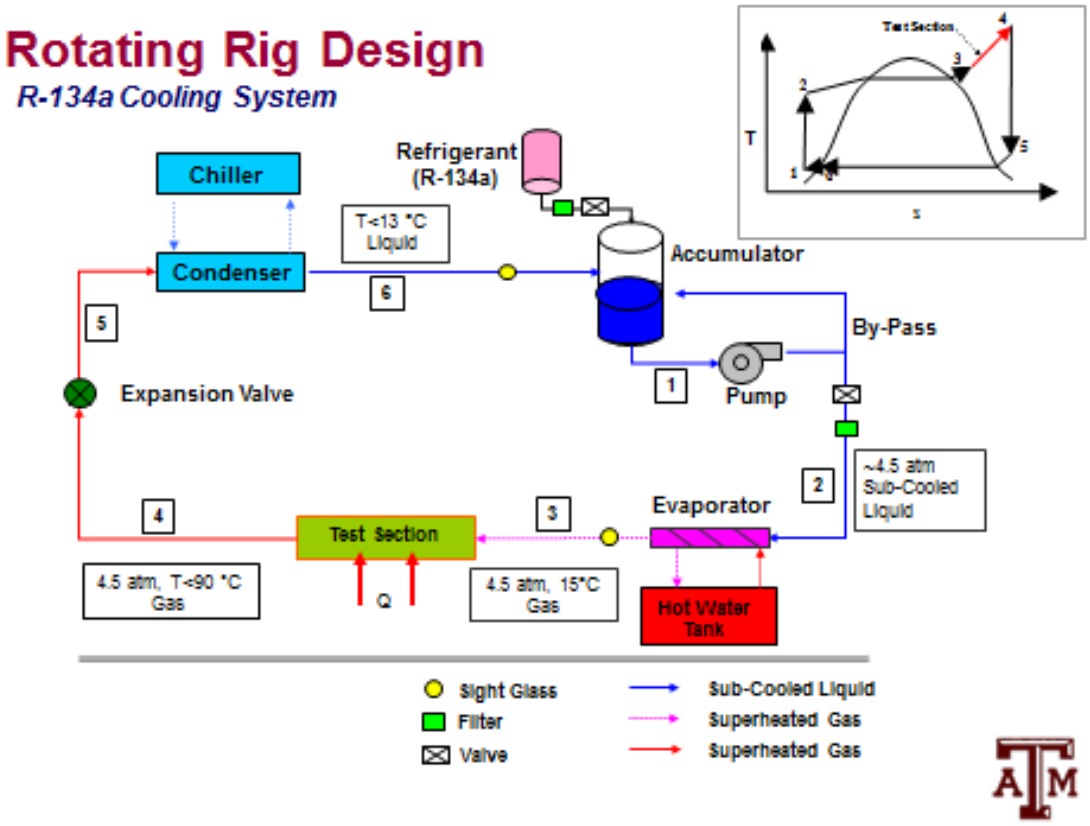

Figure 40 R-134a recirculation loop

of 190,000) is < 0.2, so the flow regime is incompressible. With a Prandtl number of 0.8 at test conditions, it is considered very close to that of air, which is 0.7.

R134a vapor flow is generated using two flow-loops as shown in **Figure 40**. First is the primary boiler loop, which supplies the R134a vapor for the tests. After the vapor returned from test section, it then passes through the condenser where heat is extracted from the vapor through a non-contact heat exchanger. The heat exchanger is cooled with a secondary loop, which is a conventional vapor compression refrigeration system. The working fluid (which absorbs heat from the primary R134a) is also R134a.

Flow rate of R-134a vapor though the test section is metered by a Coriolis flow-meter. The reported flow rate by the Coriolis flow-meter is also double-checked by a rotameter. Vapor pressure of the refrigerant is controlled to 4.5bar (abs) using a PID controller. To avoid ambient external water-vapor condensation on fluid pipe-related issues, vapor temperature is controlled to 15℃ using a PID controlled super-heater downstream of the boiler. A PID activated needle value of range from 1.65kg/min to 2.4 kg/min is used to control the flow rate. The corresponding range of Reynolds numbers is from 75,000 to 165,000. Rotating speeds is up to 600 rpm and rotation numbers is up to 0.4.

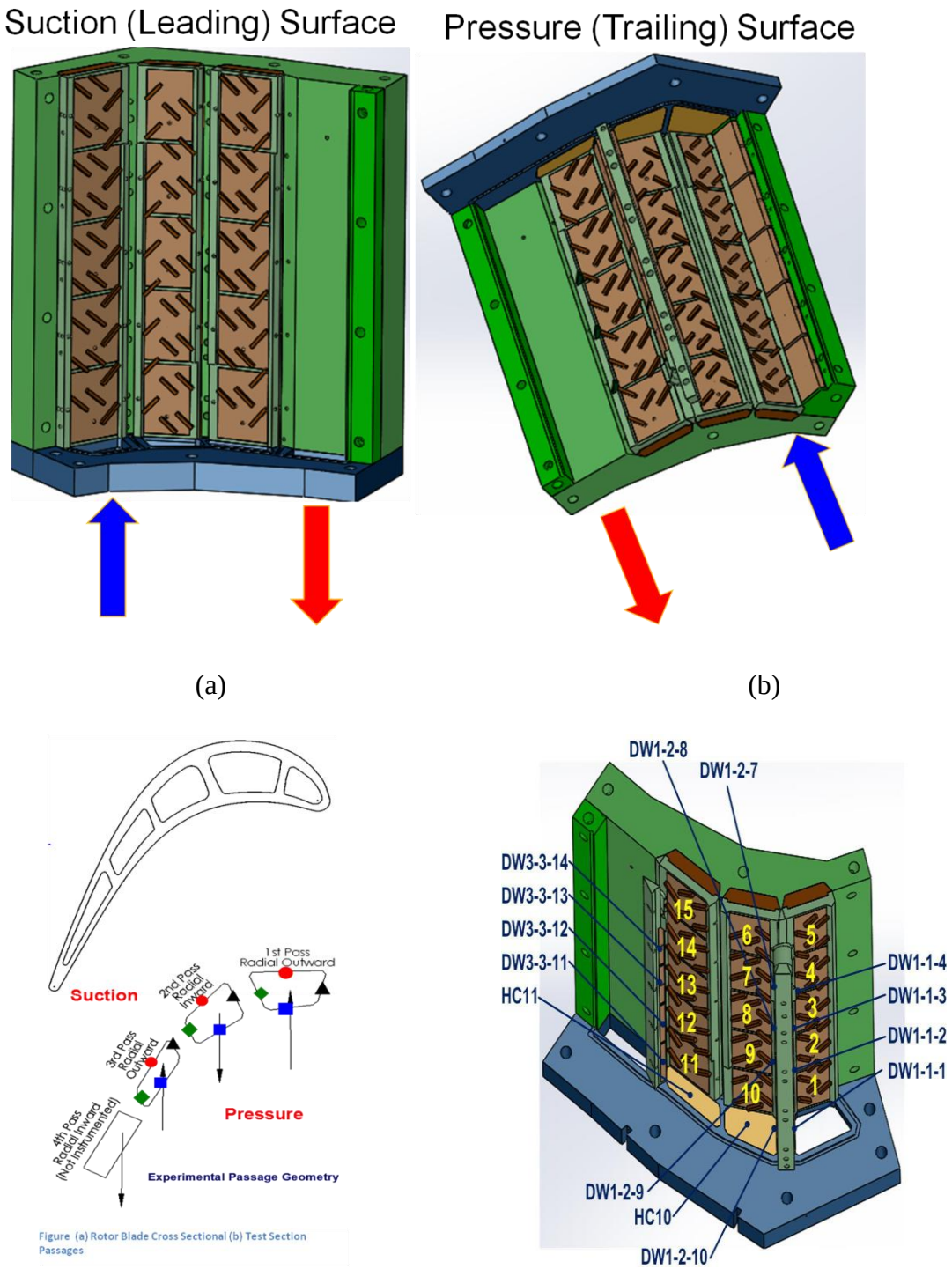

Figure 41 Serpentine channel (a) Suction (b) Pressure surface; (c) Channel cross section view (d) Region numbering

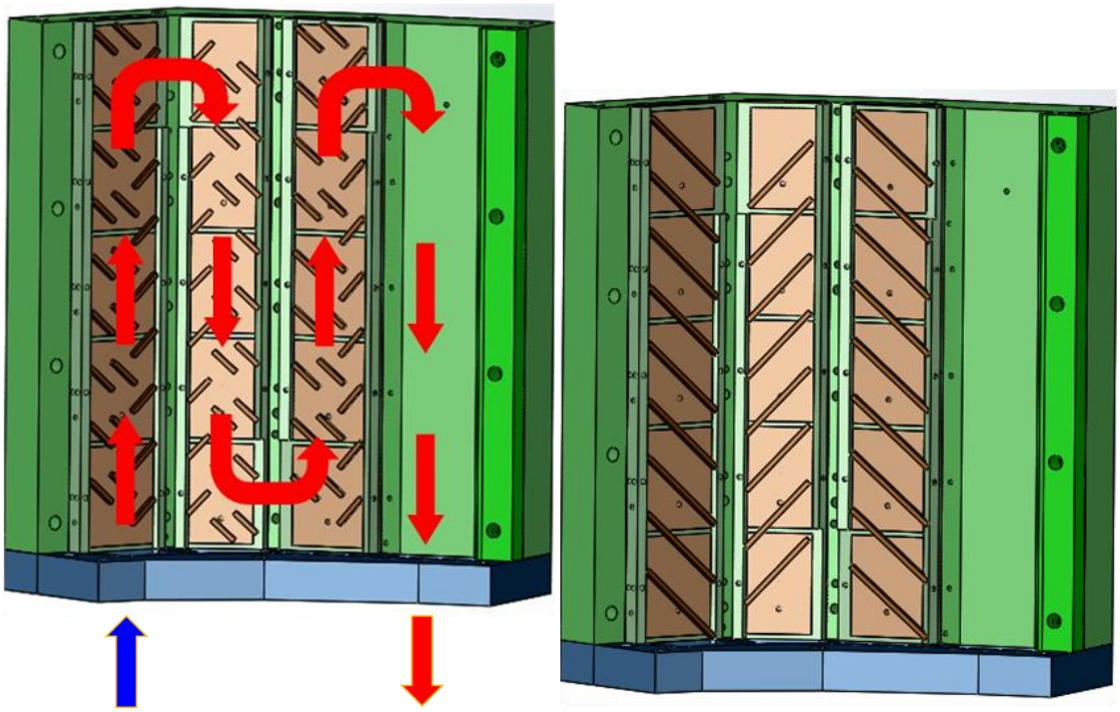

(a) (b)

Figure 42 (a) Flow direction in test section (b) Rib geometry of previous study

4.2 Test Section Geometry

A test section with four-pass serpentine geometry is used for the study, as shown in **Figure 41**. The test section is divided into15 sequential regions in total. Each region composed of either 3 (regions 5, 6, 10, 11 and 15) or 4 (all other regions) copper plates. Passages are all trapezoidal shaped, which changes in hydraulic diameter from the first to the third passes.

Each copper plates is thermally insulated from each other by using a garolite insert, which is designed to hold the copper plates onto the test section surface without requiring any nuts and bolts.

Four silicone heaters are used in each pass: one at 'suction' or 'leading', another at 'pressure or 'trailing', another at 'divider', and the other at 'leading edge' or 'trailing edge'. Each silicon heater contacts either 4 or 5 copper plates.

The test section is made of green garolite, which has good structural strength and resistance to test temperatures (~80℃). The test section is inside an aluminum pressure vessel when performing tests. A compression plate secured by two large 1" diameter (2.54cm) stainless steel bolts is used to hold test section in place.

The first pass has a hydraulic diameter of 0.75" [19.05mm], the second pass is 0.67" [17.02mm], and the third pass has a hydraulic diameter of 0.46" [11.68mm]. The fourth pass is not heated and only serves as a flow exit. A plenum (4 times in cross-section area to the first pass) is provided at upstream of the first pass to simulate the developing of thermal and momentum boundary layers in the first pass. In [33], a ribbed geometry with

an e/D of 0.081 for the first pass; 0.091 for the second pass and 0.133 for the third pass is studied. Straight squared ribs are placed parallel to each other on both pressure and suction walls with a staggered pattern and α of 45^{o}, and p/e (pitch to height ratio) of 10. In the current study, same geometry but broken, instead of straight, ribs are used. Test result is compared with results from [33]. Data from tip and hub regions are not reported in [33] due to broken heaters. Data from tip and hub regions are provided in the current study.

One T type (copper-constantan) thermocouple is embedded in the bottom of each copper plate. Biot number of each copper plate is calculated and with a value less than 0.1.

4.3 Results and Discussion

4.3.1 Stationary Channel Results

The Reynolds numbers studied are from 80,000 to 19,000 refers to 1^{st} passage. **Figure 43** shows the heat transfer enhancement and comparison of stationary data of the middle region of each passage. Region 8 is not available due to broken thermocouples, and thus data from region 9 is showing instead. **Figure 44** shows the tip turn regions, and **Figure 45** shows the hub turn regions.

As the figures illustrated, broken rib geometry has better heat transfer enhancement at every region in general. This may due to more secondary flow induced by the broken rib geometry. Comparing tip and hub regions, heat transfer enhancement is higher at tip

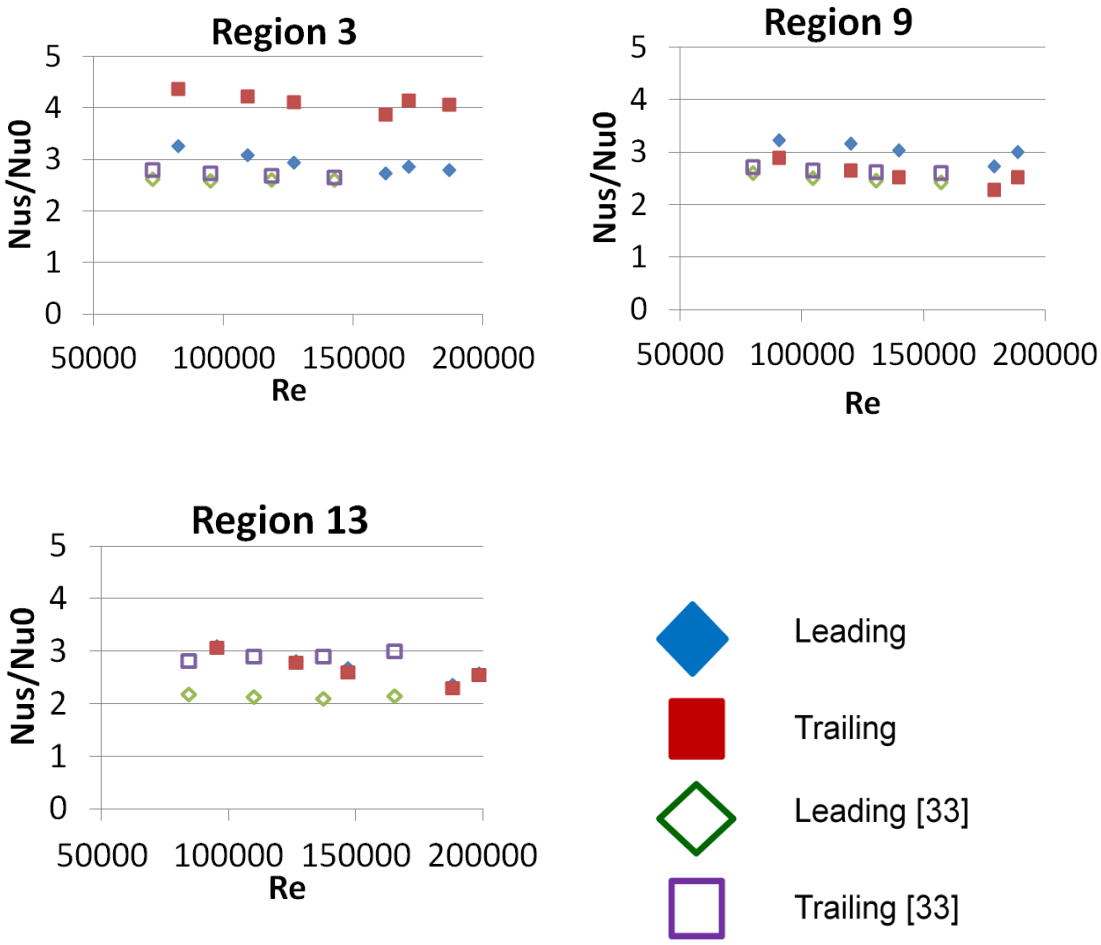

Figure 43 Heat transfer enhancement comparison at middle of passages at stationary

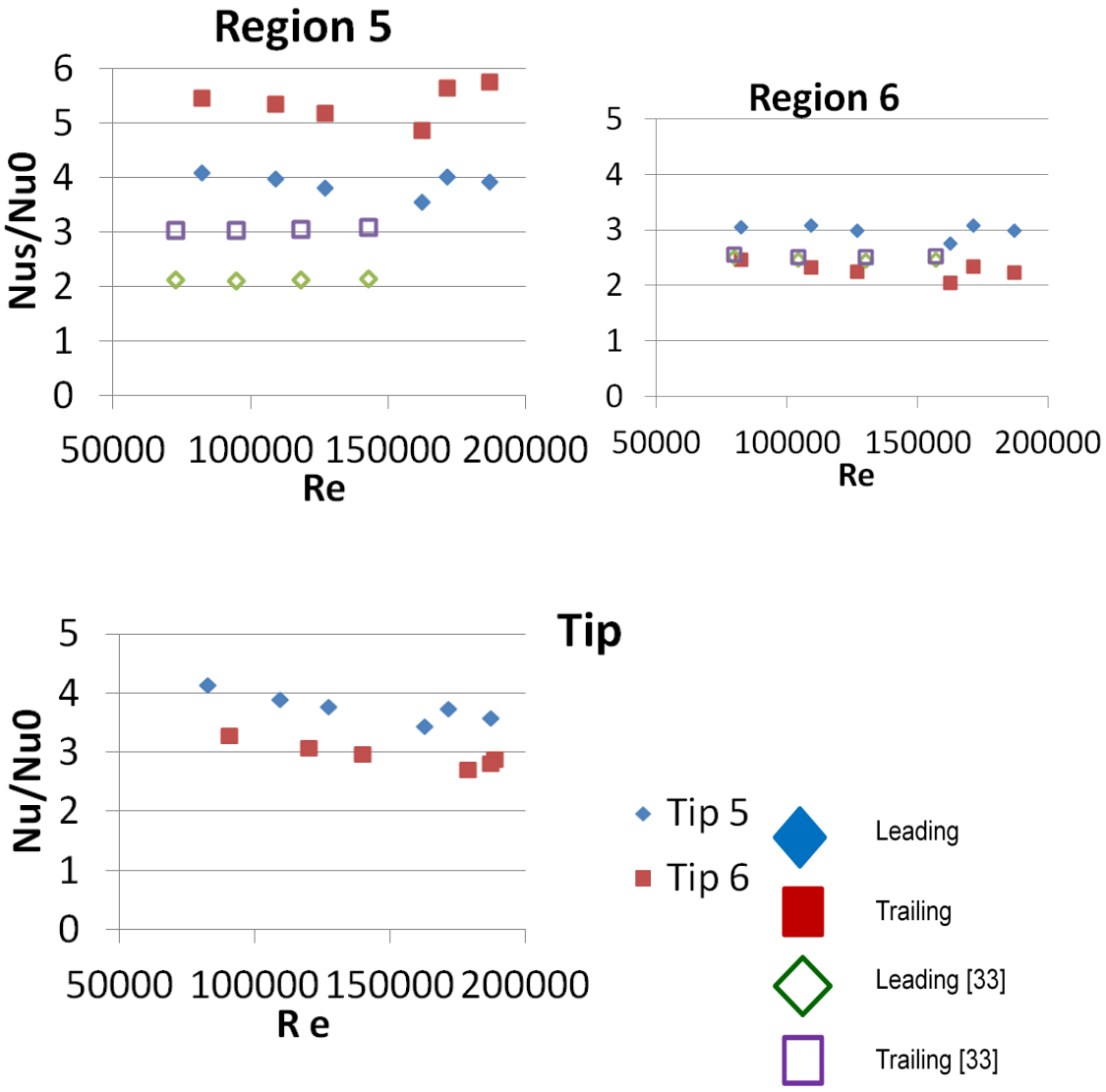

Figure 44 Heat transfer enhancement comparison at tip regions at stationary

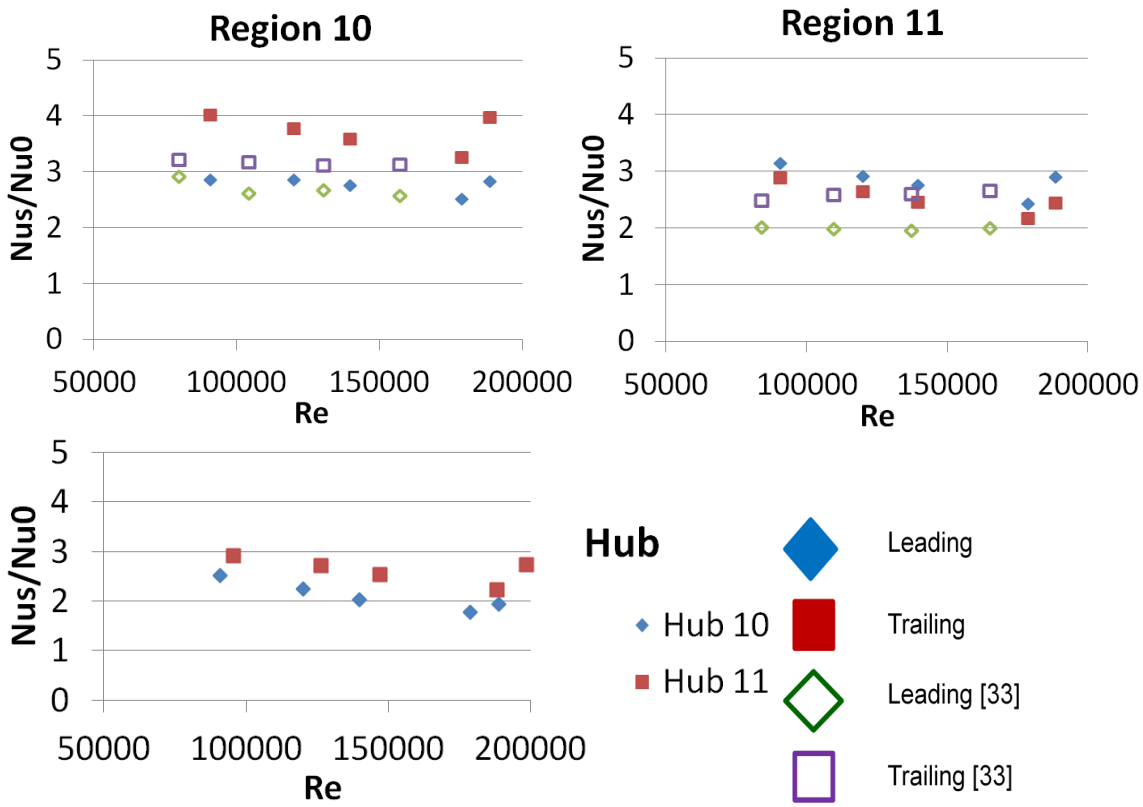

Figure 45 Heat transfer enhancement comparison at hub regions at stationary

turn regions. It is also noticed that heat transfer enhancement in the first passage is higher than that in the second, and than that in the third passages; before the turn (#5, #10) is higher than after the turn (#6, #11). This is may be caused by the combining effects of rib angle and 180-sharp turn, as well as channel cross-section and orientation between passages. It is also noted that the Nu/Nu_0 ratio between the pressure and suction sides is asymmetry. It can be resulted from the trapezoidal passage cross section design causing a asymmetry from the square/rectangular channel case. Staggered rib arrangement is also a potential reason. Or it may be due to the vorticity induced by relative angularity and change in cross section between the first, second and third passes.

4.3.2 Rotation Channel Result

Figure 46 shows the effect of rotation and comparison at the middle of each passage under rotating condition. The rotating speed performed is 300 rpm and corresponding rotation number is 0.23.

It is radially outward flow at the first and the third passage, while the second is radially inward flow. It is noted that the rotation number is smaller at the second and the third passage, because the hydraulic diameters are smaller at the second and third passage. Thus the rotation effect is not obvious at the third passage.

Comparing tip and hub regions, rotating effect is increasing with rotation number at tip, while heat transfer is smaller at hub under rotating.

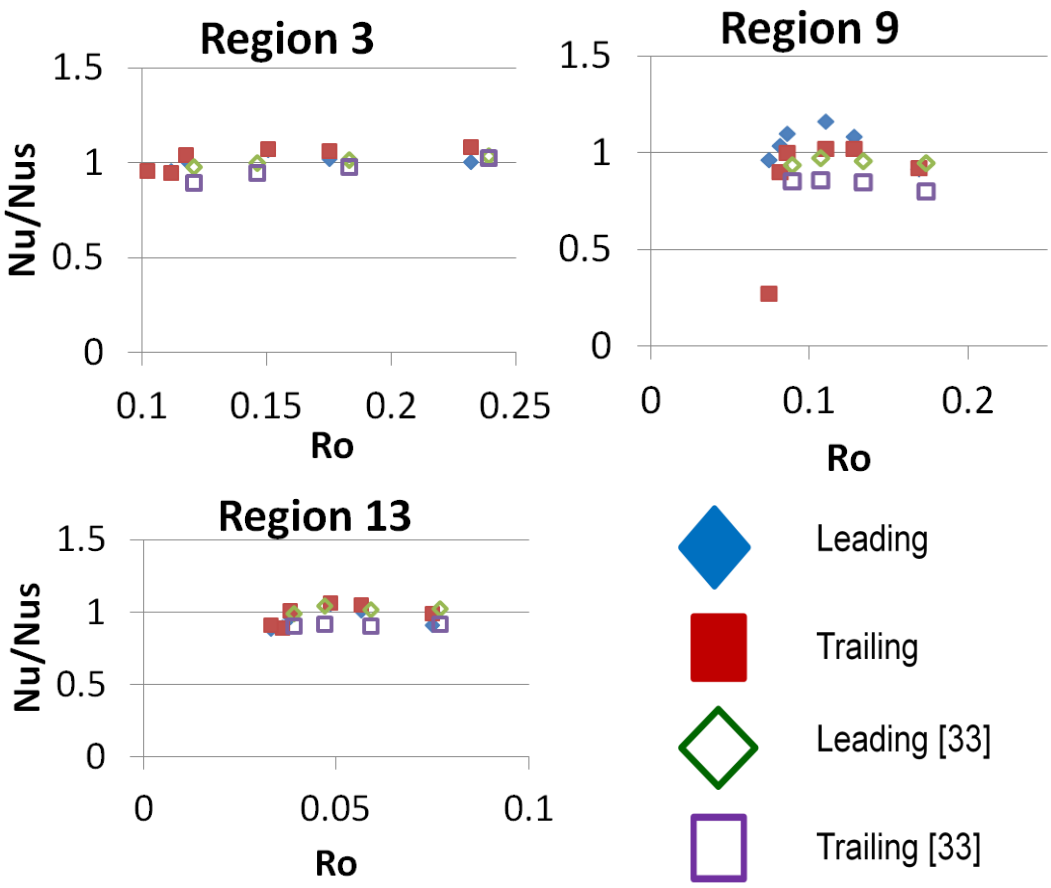

Figure 46 Effect of rotation and comparison at the middle of each passage

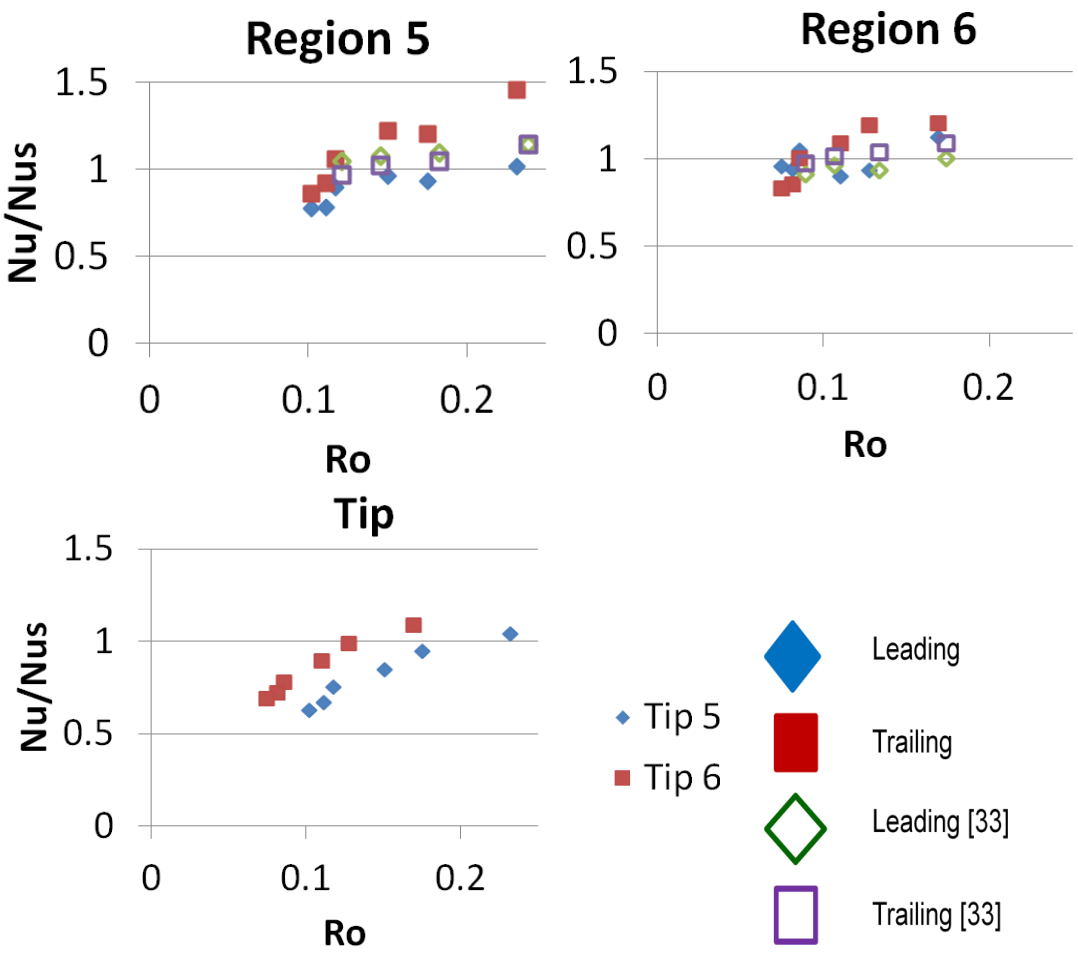

Figure 47 Effect of rotation and comparison at tip regions

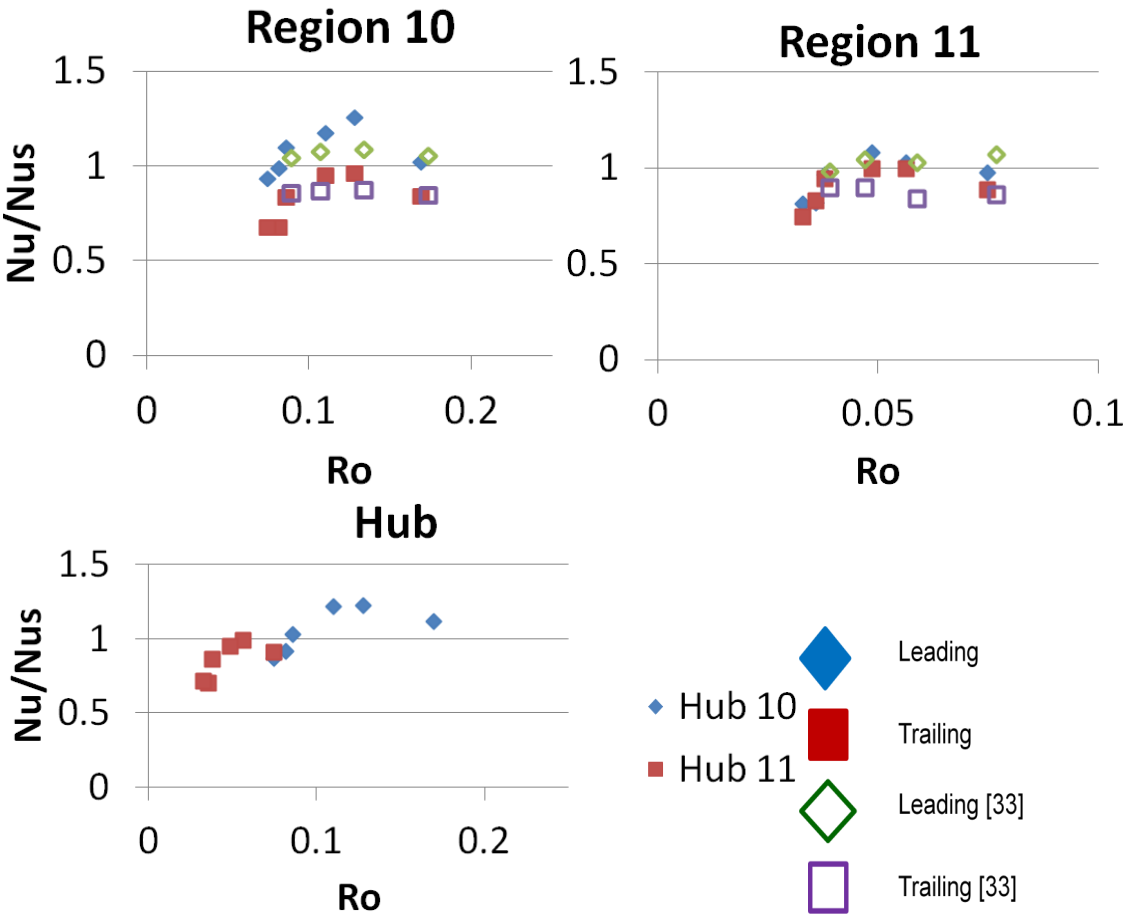

Figure 48 Effect of rotation and comparison at hub regions

4.4 Conclusion – Serpentine Channel

Heat transfer measurement is performed on a 1:1 scaled turbine blade replica in the laboratory environment with simulated engine conditions, for high Reynolds numbers from 80,000 to 190,000, high rotation numbers up to 0.23. The effects of rotation are studied. Results are obtained and compared with previous rib geometry.

1. R134a can be used as a working fluid. With its high density, non dimensional numbers corresponding to actual engine conditions (high Reynolds numbers and high rotation numbers) can be more easily achieved.
2. Broken rib geometry are found to be better in increasing the heat transfer coefficient than straight ribs. The Nu_S/Nu_0 values with Reynolds numbers are higher for thr broken rib geometry at all surfaces.
3. For the high Reynolds numbers studied, the rotation effect is higher at tip turn regions comparing with hub turn regions.
4. Heat transfer is shown to decrease in the hub region pressure side for up to 25%. This reduction in heat transfer under rotating is critical for turbine cooling designs.

5. CONCLUSIONS

Heat transfer at turn portions of internal cooling channel of gas turbine blades is investigated experimentally in this research under high rotation numbers. Three test sections are used for the investigations, which include a test section with hub turn and trailing edge ejection slots, a test section with tip turn, and a serpentine channel with tip and hub turn. Turning vane effect on heat transfer is also studied, as well as rotation effect. The rage of rotation number studied is from 0 to 0.42.

Correlations between Nu ratios (Nu/Nus) and rotation numbers (Ro) are found on all surfaces for all test sections. For radially inward flow, heat transfer (Nu/Nus) increased on the leading surface and decreased on the trailing surface. As to radially outward flow, on the contrary, Nu/Nus decreased on the leading surface and increased on the trailing surface.

Generally, heat transfer enhancement is higher at tip turn than in hub turn. Adding a turning does not pay the penalty of heat transfer at turn portion. With trailing edge ejection and β angle of 45^o, rotation reduced heat transfer significantly at the region near ejections. This reduction of heat transfer causes a great concern when designing gas turbine blades.

In general, heat transfer at channel orientation angle $\beta = 45°$ is smaller when compared with $\beta = 90°$.

REFERENCES

[1] Han, J.C., Dutta, S., Ekkad, S.V., 2012, "Gas Turbine Heat Transfer and Cooling Technology", 2nd ed., Taylor and Francis.

[2] Wagner, J.H., Johnson, B.V., Hajek, T.J., 1991, "Heat Transfer in Rotating Passages with Smooth Walls and Radial Outward Flow", ASME J. Turbomachinery, Vol. 113, pp. 42-51.

[3] Wagner, J.H., Johnson, B.V., Kooper, F.C., 1991, "Heat Transfer in Rotating Passage with Smooth Walls", ASME J. Turbomachinery, Vol. 113, pp. 321-330.

[4] Han, J.C., Zhang, Y.M., Kalkuehler, K., 1993, "Uneven Wall Temperature Effect on Local Heat Transfer in a Rotating Two-Pass Square Channel with Smooth Walls", ASME J. Heat Transfer, Vol. 115, pp. 912-920.

[5] Taslim, M.E., Rahman, A., and Spring, S.D., 1991, "An Experimental Investigation of Heat Transfer Coefficients in a Spanwise Rotating Channel With Two Opposite Rib-Roughened Walls", ASME J. Turbomachinery, Vol.113, pp. 75-82.

[6] Dutta, S., Andrews M. J., and Han, J.C., 1996, "Prediction of Turbulent Heat Transfer in Rotating Smooth Square Ducts", Int. J. Heat Mass Transfer. Vol. 39, No. 12, pp. 2505-2514.

[7] Lei, J., Li, S.J., Han, J.C., Zhang, L., and Moon, H.K., 2012, "Heat Transfer in Rotating Multi-Pass Rectangular Ribbed Channel with and Without a Turing Vane", ASME, J. Heat Transfer, Vol. 135, pp. 041903-1~041903-10

[8] Lei, J., Li, S.J., Han, J.C., Zhang, L., and Moon, H.K., 2014, “Effect of a Turning Vane on Heat Transfer in Rotating Multipass Rectangular Smooth Channel”, J Thermophys Heat Tr., Vol. 28(3), pp. 417-427.

[9] Rallabandi, A., Lei, J., Han, J.C., Azad, S., and Lee, C.P., 2014, “Heat Transfer Measurement in Rotating Blade-Shape Serpentine Coolant Passage With Ribbed Walls at High Reynolds Numbers”, ASME, J. Turbomachinery, Vol. 136, pp. 091004-1~091004-9.

[10] Parsons, J.A., Han, J.C., Zhang, Y., 1995, “Effect of Model Orientation and Wall Heating Condition on Local Heat Transfer in a Rotating Two-Pass Square Channel with rib turbulators”, Int. J. Heat Mass Transfer, Vol. 38, pp. 1151-1159.

[11] Johnson, B.V., Wagner, J.H., Steuber, G.D., and Yeh, F.C., 1994, “Heat Transfer in Rotating Serpentine Passages with Selected Model Orientations for Smooth or Skewed Trip Walls”, ASME J. Turbomachinery, Vol. 116, pp. 738-744.

[12] Huh, M., Lei, J., and Han, J.C., 2012, “Influence of Channel Orientation on Heat Transfer in a Two-Pass Smooth and Ribbed Rectangular Channel (AR=2:1) Under Large Rotation Numbers”, ASME, J. Turbomachinery, Vol. 134, 011022-1~011022-14.

[13] Qiu, L., Deng, H., and Tao, Z., 2013, “Effect of Channel Orientation in a Rotating Smooth Wedge-Shaped Cooling Channel With Lateral Ejection”, ASME Paper No. GT2013-94758

[14] Li, Y., Deng, H., Xu, G., Lu, Q., and Tian, S., 2014, "Effect Of Channel Orientation On Heat Transfer In Rotating Smooth Square U-Duct At High Rotation Number", ASME Paper No. GT2014-25188.

[15]Srinivasan, B., Dhamarla, A., Jayamurugan, C., and Rajan, A.B., 2014, "Numerical Studies On Effect Of Channel Orientation In a Rotating Smooth Wedge-Shaped Cooling Channel", ASME Paper No. GT2014-26560.

[16] Han, J.C., Chandra, P.R., Lau, S.C., 1988, "Local Heat/Mass Transfer Distributions Around Sharp 180 Deg. Turns in Two-Pass Smooth and Rib-Roughened Channels", ASME J. Heat Transfer, Vol. 110 pp. 91-98.

[17] Schabacker, J., Bolcs, A., and Johnson, B.V., 1998, "PIV Investigation of the Flow Characteristics in an Internal Coolant Passage with Two Ducts Connected by a Sharp 180 Deg Bend," ASME Paper No. 98-GT-544.

[18] Son., S.Y., Kihm, K.D., and Han, J.C., 2002, "PIV Flow Measurements for Heat Transfer Characterization in Two-Pass Square Channels with Smooth and 90^{o} Ribbed Walls," Int. J. Heat Mass Transfer, 45, pp. 4809-4822.

[19] Saha, K., and Acharya S., 2013, "Bend Geometries in Internal Cooling Channels For Improved Thermal Performance", ASME, J. Turbomachinery, Vol. 135, pp. 031028-1~031028-10.

[20] Luo, J., and Razinsky, E.H., 2009, "Analysis of Turbulent Flow in 180 deg Turning Ducts with and without Guide Vanes," ASME J. Turbomachinery, Vol. 131, pp, 021011-1~021011-10.

[21] Schüler, M., Zehnder, F., Weigand, B., Wolfersdorf, J., and Neumann, N.O. 2011, "The Effect of Turning Vanes on Pressure Loss and Heat Transfer of a Ribbed Rectangular Two-Pass Internal Cooling Channel," ASME, J. Turbomachinery, Vol. 133, pp. 021017-1~021017-10.

[22] Chu, H.C., Chen, H.C., and Han, J.C., 2013, "Numerical Simulation of Flow and Heat Transfer in Rotating Cooling Passage With Turning Vane in Hub Region", ASME Paper No. GT2013-94289.

[23] Taslim, M. E., Li, T., and Spring, S. D., 1995, "Experimental Study of the Effects of Bleed Holes on Heat Transfer and Pressure Drop in Trapezoidal Passages with Tapered Turbulators", Journal of Turbomachinery, Vol. 117, No. 2, 1995, pp. 281–289

[24] Hwang, J. J., and Lu, C. C., 2001, "Lateral-Flow Effect on Endwall Heat Transfer and Pressure Drop in a Pin Fin Trapezoidal Duct with Various Pin Shapes", Journal of Turbomachinery, Vol. 123, No. 1, 2001, pp. 133–139. doi:10.1115/1.1333093

[25] Rallabandi, A., Liu, Y. H., Han, J. C., 2011, "Heat Transfer in Trailing Edge Wedge-Shaped Pin-Fin Channels With Slot Ejection Under High Rotation Numbers", Journal of Thermal Science and Engineering Applications, Vol. 3, pp. 021007-1 – 021007-9.

[26] Krueckels, J., Naik, S., and Lerch, A., 2014, "Heat Transfer in a Vane Trailing Edge Passage with Conical Pins and Pin-Turbulator Integrated Configurations", ASME Paper No. GT2014-25522.

[27] Liu, Y.H., Huh, M., and Han, J.C., 2012, "High Rotation Number Effect on Heat Transfer in a Trailing Edge Channel with Tapered Ribs", Int J Heat Fluid Flow, Vol. 33(1), pp, 182-192.

[28] Wright L. M., Fu W. L., and Han, J. C., 2005, "Influence of Entrance Geometry on Heat Transfer in Rotating Rectangular Cooling Channels (AR=4:1) With Angled Ribs" Journal of Heat Transfer, April 2005, Vol 127, pp 378 – 387.

[29] Kline, S.J., McClintock, F.A., 1953, "Describing Uncertainty in Single-Sample Experiments", Mechanical Engineering, Vol.75, pp.3-8.

[30] Coletti, F., and Arts, T., 2011, "Aerodynamic Investigation of a Rotating Rib-Roughened Channel By Time-Resolved Particle Image Velocimetry", Journal of Power and Energy, Vol. 255(7), pp, 975-984.

[31] Coletti, F., Maurer, T., and Arts, T., 2012, "Flow Field Investigation in Rotating Rib-Roughened Channel by Means of Particle Image Velocimetry", Experiments in fluids, Vol. 52(4), pp.1043-1061.

[32] Yang, S. F., Han, J. C., Azad, S., and Lee, C. P., 2013, "Heat Transfer in Rotating Serpentine Coolant Passage with Ribbed Walls at Low Mach Numbers", ASME Turbo Expo 2013, GT2013-94288.

[33] Rallabandi, A., Lei, J., Han, J. C., Azad, S., and Lee, C. P., 2014, " Heat Transfer Measurements in Rotating Blade–Shape Serpentine Coolant Passage With Ribbed Walls at High Reynolds Numbers" ASME Journal of Turbomachinery, SEPTEMBER 2014, Vol. 136 / 091004-1 - 091004-9